Appendix C

Precipitation, Runoff and
Natural Groundwater Recharge

Antelope Valley Area of Adjudication

APPENDIX C

Natural Groundwater Recharge
Antelope Valley, California

Prepared by:

Timothy J. Durbin
West Yost Associates
2020 Research Park Drive, Suite 100
Davis CA 95618

July 12, 2010

WEST YOST
ASSOCIATES
Consulting Engineers

371-00-10-02

CONTENTS

Figures

Tables

Appendix C
Natural Groundwater Recharge
Antelope Valley, California

C.1.0   Introduction

The precipitation within the Antelope Valley watershed is the source of natural recharge to the underlying groundwater basin. As shown on Figure C.1, the precipitation not consumed by evapotranspiration or evaporation becomes groundwater recharge. During rainfall or snowmelt events, streamflow runoff or soil infiltration is produced. The streamflow, in turn, produces streambed infiltration and sometimes produces streamflow discharges onto playa surfaces, such as those represented by Rosamond, Rogers, and other dry lakes. The streambed infiltration is removed, in part, by evaporation from the streambed surface, but the remaining infiltration produces groundwater recharge by deep percolation of the infiltrated water to the groundwater table. Streamflow discharges onto playa surfaces evaporate and do not produce recharge. The soil infiltration is removed, in part, by evapotranspiration, but the remaining infiltration produces groundwater recharge, again, by the deep percolation of the infiltrated water to the groundwater table.

Based on this conceptual model, groundwater recharge within the Antelope Valley occurs by either streambed infiltration or soil infiltration. While these processes occur throughout the watershed, soil infiltration is probably more important within the mountain-block areas, and streambed infiltration is probably more important within the valley-floor areas. Within the valley-floor areas, recharge most likely does not occur from soil infiltration where the average annual precipitation is less than about 8 inches (Maxey and Eakin, 1949; Dettinger, 1989; Avon and Durbin, 1992; Tyler and others, 1992; Tyler and others, 1996; and Russell and Minor, 2002), which represents the entire valley-floor area except for the higher parts of the alluvial fans.

Within the mountain-block areas, such as those represented by the San Gabriel and Tehachapi mountains, significant runoff is generated from rainfall and snowmelt. However, much of the runoff is discharged from the mountain canyons onto the alluvial fans comprising the valley-floor areas. Therefore, to the extent that groundwater recharge occurs within the mountain-block areas, recharge is probably produced mostly by the deep percolation of soil infiltration. The mountain-block recharge, in turn, produces either groundwater flows directly from the mountain-block into the valley-floor areas or perennial streamflows from mountain canyons into valley-floor areas.

Within the valley-floor areas, little runoff is generated by either rainfall or snowmelt. Correspondingly, the precipitation is almost entirely disposed to soil infiltration. However, essentially all of the soil infiltration is consumed by the evapotranspiration processes, and little groundwater recharge occurs. Nevertheless, runoff and stream baseflow generated within the mountain-block areas do produce significant groundwater recharge within the

valley-floor areas. Streamflows on the alluvial fans produce streambed infiltration and, subsequently, groundwater recharge.

The processes described above are quantified below in terms of long-term average values and annual values. The precipitation and streamflow within Antelope Valley are described and the translation of those quantities into recharge is described.

C.2.0   Assembly of Basic Data

The estimation of the natural recharge to the Antelope Valley groundwater basin required the compilation and assembly of basic data. Those data include information on topography, precipitation, streamflow, evapotranspiration, and water chemistry as described below. Topographic data were compiled to analyze the relation of precipitation and evapotranspiration to altitude. Precipitation data were compiled to analyze its relation to groundwater recharge. Streamflow data were compiled to analyze its relations to precipitation and, ultimately, to groundwater recharge. Evapotranspiration data were compiled to analyze its relations to water yield and, ultimately, to groundwater recharge. Chloride data were compiled to analyze its relation to groundwater recharge.

C.2.1   Quantification of Topography

Topographic information was assembled as a digital elevation model (DEM) and as graphs representing the cumulative distribution of altitude for subareas of the Antelope Valley watershed.

The Antelope Valley watershed, which is about 1.7 million acres in size, includes both the mountain-block and valley-floor areas. As shown on Figure C.2, the watershed is bordered on the south by the San Gabriel Mountains and on the north by the Tehachapi Mountains. The San Gabriel Mountains have a maximum altitude within the watershed of about 9,000 ft, and they rise about 7,000 ft above Rogers Lake, which represents the lowest land-surface altitude within Antelope Valley. The altitude on the Rogers Lake playa surface is about 2,200 ft. The Tehachapi Mountains have a maximum altitude of about 8,000 ft, and they rise about 6,000 ft above Rogers Lake.

A DEM was downloaded from the U. S. Geological Survey (2007a). The downloaded DEM has 30-meter cells, but it was resampled using ArcGIS into 100-meter cells. The DEM was resampled to facilitate computationally efficient GIS analyses involving altitude. The 100-meter DEM was used for most of the analyses described in this report. However, a smoothed 100-meter DEM was created to represent a 2,000-meter moving average of the local topography. The smoothed DEM was used in the analysis of topographic effects on precipitation, evapotranspiration, and other climatic variables.

The cumulative distribution of altitude derived from the DEM is shown on Figure C.3. The horizontal axis represents the cumulative acreage, and the vertical axis represents the maximum altitude within the cumulative acreage. The altitude corresponding with zero acres is the minimum altitude within the watershed, and the altitude corresponding to the maximum acreage is the maximum altitude. Summary statistics for altitude can be extracted from the cumulative distribution. Firstly, the altitude corresponding to one-half the maximum acreage is the median altitude, which from Figure C.3 is 2,800 ft. Secondly, the area-weighted average altitude (which corresponds to the integrated area under the cumulative-distribution graph) is 3,100 ft. While altitudes within the watershed range from 2,200 to 9,000 ft, 80 percent of the watershed has an altitude less than 3,500 ft.

Figure C.2 shows the principal sub-watersheds within the overall Antelope Valley watershed, and Figures C.4a-e and C.5a-d show the respective cumulative distributions of altitude within the delineated watersheds. Figures C.4a-e show graphs for Big Rock, Little Rock, Mescal, Pallett, and Santiago Canyon creeks, which are the principal sub-watersheds within the San Gabriel Mountains. Figures C.5a-d show graphs for Cottonwood, Joshua, Mojave, and Oak creeks, which are the principal sub-watersheds within the Tehachapi Mountains.

C.2.2 Quantification of Precipitation

Precipitation data were assembled for the analysis in the form of monthly precipitation for selected gaged sites within or near the Antelope Valley watershed and in the form of a map showing average annual precipitation. Data were assembled for the period 61-year period 1949-2009. However, only precipitation data for the 57-year period 1949-2005 were used for the analysis.

C.2.2.1   General Approach

The geographic distribution of precipitation within the Antelope Valley watershed is significantly dependent on altitude. Both annual and average-annual precipitation tend to increase with altitude. While the average annual precipitation ranges from 5 to 8 inches/yr easterly across the valley-floor area, the average annual precipitation ranges from 25 to 40 inches/yr along the crest of the San Gabriel Mountains and from 15 to 30 inches/yr along the crest of the Tehachapi Mountains. This altitude dependence was used to quantify the geographic distribution of average annual precipitation based on the relation

$$\overline{P}(x, y) = \overline{p}(z(x, y)) \text{ (C.1)}$$

where

$\overline{P}(x, y)$ is the average annual precipitation at point (x, y),

z is the altitude at point (x, y), and

$\overline{p}(z)$ is the average annual precipitation at altitude z.

The application of this relation involves using precipitation data to identify a precipitation-altitude relation $\overline{p}(z)$ and subsequently combining the precipitation-altitude relation with the DEM for Antelope Valley to estimate the geographic distribution of precipitation $\overline{P}(x, y)$.

C.2.2.2   Precipitation Data

Data Sources. Precipitation data are available for sites within and near the Antelope Valley watershed. The earliest and latest years represented by the data are 1949 and 2009. Monthly data for 23 sites were downloaded from the Western Regional Climatic Center (2009). The downloaded sites are shown on Figure C.6 and are listed in Table C.1. The period of record for individual sites is variable. As indicated in Table C.1, the earliest

and latest years represented by the sites are 1949 and 2009, but only nine sites have continuous measurement records for that 61-year period. However, the additional 14 sites have records within that period ranging from 5 to 51 years in length. The monthly precipitations for the overall 23 sites are listed in Tables C.2a-w. The average annual precipitation for the sites ranges from 5 to 40 inches for the 57-year period 1949-2005 used in the analysis, and the site altitudes range from 1,400 to 6,800 ft.

To screen the records for temporal consistency, a double-mass graph was prepared for each site as shown on Figures C.7a-w. The horizontal axis on the graph is the cumulative annual precipitation for selected base stations, where the base stations comprise the nine sites with continuous records for 1949-2009. The vertical axis is the cumulative annual precipitation for the site of interest. For a site with a consistent record, the plotted points approximately follow a straight line. For a site impacted adversely by relocation or other factors, the slope of the straight line will be different during different record subperiods. The double-mass graphs suggest that each of the sites listed in Tables C.2a-w has a consistent record, except for the site at Big Bear Lake.

The double-mass relation for Big Bear Lake exhibits a slope break in 1977. The slope is flatter after 1977 than before. While the slope before 1977 is 1.18, the slope after is 0.83. Correspondingly, the average precipitation before 1977 was higher relative to the nine base stations than after 1977. While the double-mass relation suggests the rejection of the Big Bear Lake record, the entire available 1961-2005 record, nevertheless, was used because of the paucity of higher-altitude precipitation data.

Data Adjustments for Missing Measurements. Before using the available data, the data were adjusted for days with missing observations. All of the precipitation records contain at least a few days with no observation. All of the reported monthly totals omit those days with no observation, which biases downward the reported precipitation from the actual precipitation. This bias was removed by adding for each missing day the long-term average daily precipitation for the month according to the relation

$$p(m, y) = p_R(m, y) + \overline{p}_d(m) \cdot n_m(y, m) \text{ (C} \tag{.2}$$

where

$p(m, y)$ is the estimate of the actual monthly precipitation for the month m and year y,

$p_R(m, y)$ is the reported monthly precipitation for the month and year,

$\overline{p}_d(m)$ is the average daily precipitation over all years for the month, and

$n_m(y, m)$ is the number of days with missing observations.

Equation C.2 has the properties so that the estimate of the actual average monthly precipitation overall all years is unbiased.

Data Adjustments for Partial Record. The data were adjusted for missing years during 1966-2005. In particular, the average annual precipitation for a site with a partial record was adjusted to account for the fact the climatic conditions during the period of record may not be the same as the conditions during 1966-2005. The adjustment is based on the precipitation for sites with a complete record, where the adjustment is given by the relation (Linsley, 1982)

$$\overline{P}\Big|_a = \frac{\overline{P}\Big|_b}{\overline{P_B}\Big|_b} \cdot \overline{P_B}\Big|_a \tag{C.3}$$

where

      a represents the period 1966-2005,

      b represents the years contained within the record for the site to be adjusted,

      $\overline{P}\Big|_a$ is the adjusted average annual precipitation for the partial-record site for

              period a,

      $\overline{P}\Big|_b$ is average annual precipitation for the partial-record site for period b,

      $\overline{P_B}\Big|_a$ is the average annual precipitation for the complete-record site for

              period a, and

      $\overline{P_B}\Big|_b$ is the average annual precipitation for the complete-record site for period b.

Equation C.3 has the desirable property that, as the completeness of the record for the partial-record site increases, the adjusted average equals the record average.

      The adjusted average annual precipitation is listed in Table C.3. The adjustment factors, which are the adjusted mean divided by the unadjusted mean, range from 0.75 to 1.16. The sites with a factor less than unity represent those with a record period during which climatic conditions were wetter than during 1949-2005, and the record average was adjusted downward to correspond with normal conditions. Likewise, the sites with a factor greater than unity represent those with a record period during which climatic conditions were dryer than during 1949-2005, and the record average was adjusted upward.

      The adjustment of average annual precipitation to the 1949-2005 base period depends on the existence of a correlation between the base stations and the site to be adjusted. To identify the underlying correlations, the correlation of the annual precipitation was calculated for 15 sites, which represent those sites having a continuous record during the 36-year period 1961-1996. The resulting correlations are listed in Table C.4. The correlations range from 0.43 to 0.96, with most values larger than 0.7. The correlation structure expressed in Table C.4 suggests a generally high degree of spatial correlation throughout the Antelope Valley watershed. Paired nearby sites appear to be just as correlated as pair distant sites.

C.2.2.3 Precipitation-Altitude Relation

The adjusted average annual precipitation values were used to identify a precipitation-altitude relation for the Antelope Valley watershed. Five forms for the relation were considered: geographically constant slope and intercept, constant slope and linear geographically varying intercept, constant slope and quadratic geographically varying intercept, constant slope and cubic geographically varying intercept, and constant slope and contoured geographically varying intercept. The five relations each incorporate a geographically invariant slope. That relational structure was selected because orographic effects tend to have moderately large scales (Dettinger and others, 2004; Pandey and others, 1999; and Pierrehumbert, 1984). Furthermore, the processes controlling orographic precipitation tend worldwide to be characterized by precipitation-altitude relations having similar slopes (Barry, 1981).

The first form used was a linear relation with a geographically constant slope and intercept. The relation has the form

$$\overline{p}(z) = a_0 + a_1 z(x, y) \text{ (C} \tag{.4}$$

where

$\overline{p}(z)$ is the average annual precipitation for elevation z,
a_0 is the intercept for the relation,
a_1 is the slope of the relation, and
$z(x, y)$ is the altitude at a point.

The second was a linear relation with a geographically linear intercept but a geographically constant slope. The geographic variation of the intercept has the two-dimensional linear form

$$a_0 = b_0 + b_1 x + b_2 y \tag{C.5}$$

where $b_0, \ldots, b_2$ are the coefficients of the relation. The third form was a linear relation with a geographically quadratic intercept but a geographically constant slope. The geographic variation of the intercept has the two-dimensional quadratic form

$$a_1 = c_0 + c_1 x + c_2 y + c_3 x^2 + c_4 y^2 + c_5 xy \tag{C.6}$$

where $c_0, \ldots, c_5$ are the coefficients of the relation. The fourth was a linear relation with a geographically cubic intercept but a geographically constant slope. The geographic variation of the intercept has the two-dimensional cubic form

$$a_1 = d_0 + d_1 x + d_2 y + d_3 x^2 + d_4 y^2 + d_5 xy + d_6 x^3 + d_7 y^3 + d_8 x^2 y + d_9 xy^2 \tag{C.7}$$

where $d_0, \ldots, d_9$ are the coefficients of the relation.

The fifth, and final form, was a linear relation with a geographically varying intercept and invariant slope, but the shape of the surface representing the intercept was created by using the Spatial Analysis extension of ArcGIS, where the surface is based on fitting splines to the data points (ESRI, 2001). The data points were derived by applying Equation C.4 to individual precipitation sites: Firstly, the geographically global slope of the precipitation-altitude relation was identified by fitting Equation C.4 to the set of average annual precipitations listed in Tables C.2a-w. This step yields a value for a_1. Secondly, an individual intercept was computed for each site based on Equation C.4 in the form

$$a_{0i} = \bar{p}_i - a_1 z(x_i, y_i) \quad \text{(C.8)}$$

where

$\quad a_{0i}$ is the intercept for site i,

$\quad \bar{p}_i$ is the average annual precipitation for the site derived from the measurement for the site,

$\quad a_1$ is a specified slope for the relation,

$\quad z$ is the altitude of the site,

$\quad x_i$ is a geographic coordinate for the site, and

$\quad y_i$ is a geographic coordinate for the site.

Thirdly, the intercepts were plotted on a map and contoured. The contouring was accomplished using the spline interpolation within the Spatial Analyst extension to ArcGIS (ERSI, 2001).

The results for the five forms of the precipitation-altitude relation are shown on Figures C.8a-e and C.9 and are listed in Table C.5. Figures C.8a-e show scatter diagrams comparing the fit of the relation to the observation for the respective relational forms. The horizontal axis for each graph represents the average annual precipitation derived from the observations. The vertical axis represents the average annual precipitation computed from the precipitation-altitude relation. Figure C.9 shows the geographic variation of the contoured intercepts, where the contours represent an underlying ArcGIS raster file (ESRI, 2001). Table C.5 lists the regression results for each form of the precipitation-altitude relation, including the coefficient of determination (r^2) and the standard error (s_e).

The coefficient of determination (r^2) values listed in Table C.5 increase progressively for the relations represented respectively by Equations C.4 through C.7. The different forms of the precipitation-altitude relation have a respectively larger number of parameters, and r^2 is inversely related to the number of parameters. The relation based on Equation C.4 has two parameters, and the r^2 is 0.53. The relation based on Equation C.5 has four parameters, and the r^2 is 0.60. The relation based on Equation C.6 has six parameters, and the r^2 is 0.71. The relation based on Equation C.7 has ten parameters, and the r^2 is 0.85. The r^2 for the contoured intercept equals one because the contouring of the intercept was performed such that the computed precipitation exactly matches the measured precipitation at the precipitation gages.

The standard errors (s_e) listed in Table C.5 decrease progressively for the relations represented respectively by Equations C.4 through C.7. The relation based on Equation C.4 again has two parameters, and the s_e is 6.7 inches. The relation based on Equation C.5 has four parameters, and the s_e is 6.6 inches. The relation based on Equation C.6 has six parameters, and the s_e is 6.1 inches. The relation based on Equation C.7 has ten parameters, and the s_e is 5.0 inches. The s_e for the contoured intercept is not listed in Table C.5 because the effective number of parameters corresponding to the contouring is unknown. However, the standard error probably is less than 5 inches, based on the regression statistics for the cubic form of the intercept.

C.2.2.4 Geographic Distribution of Precipitation

Among the five forms of the precipitation-altitude relation, the relation based on the contoured intercept is probably the best predictor of average annual precipitation within the Antelope Valley watershed, and that relation was used in this work to characterize the precipitation. Figure C.10 shows the corresponding geographic distribution of average annual precipitation, where the contours represent an underlying ArcGIS raster file. That raster file was constructed using the map calculator within the Spatial Analyst (ESRI, 2001) extension of ArcGIS. The inputs to the calculator were the DEM (the quantity $z(x, y)$ in Equation C.4), the contoured intercept raster file underlying Figure C.9 (the quantity a_0 in Equation C.4), the global slope of the precipitation-altitude relation (the quantity a_1 in Equation C.4, which is listed in Table C.5), and Equation C.4.

Based on Figure C.10, the average annual precipitation within the Antelope Valley watershed ranges from 4 to 47 inches, and the area-weighted geographic average is 8.3 inches. Considering the non-valley-floor areas identified on Figure C.11, which are defined as those areas where the average annual precipitation exceeds 8 inches, the respective area-weighted averages are 15.4 inches within the San Gabriel Mountains area, 13.1 inches within the Tehachapi Mountains area, 8.7 inches within the eastern buttes area, and 9.2 inches within the northern buttes area. A summary of precipitation statistics is listed in Table C.6.

The geographic distribution of precipitation shown on Figure C.10 represents higher precipitation than that estimated by the Oregon Climate Service using PRISM (Parameter-elevation Regressions on Independent Slopes Model). PRISM (Daly and others, 1994) is an expert system that uses point data and a digital elevation model to generate estimates of climate parameters. The PRISM map of average annual precipitation for California was downloaded from the Oregon Climatic Center (2007), and Figure C.12 shows the precipitation contours covering the Antelope Valley watershed. The contours represent a precipitation range of 5 to 38 inches. Nevertheless, Figure C.10 represents a precipitation range of 4 to 47 inches, which is about 20 percent higher than PRISM at the upper range. However, that comparison result is not unexpected because such comparisons involving other semiarid areas have been similar (Donovan and Katzer, 2000).

C.2.3   Quantification of Streamflow

Streamflow data were assembled in terms of monthly streamflows for selected streamgaging sites within the Antelope Valley watershed. Data were assembled for the 61-year period 1949-2009. Additionally, channel-geometry characteristics were measured at gaged and ungaged sites within the Antelope Valley watershed, and those measurements were translated into the estimates of average annual streamflow.

C.2.3.1   Streamflow Data

Data Sources. Streamflow data are available for sites within the Antelope Valley watershed. The earliest and latest years represented by the sites are 1924 and 2009, however data prior to 1949 and later than 2005 are not used in the analysis. Daily data for 18 sites were downloaded from the U. S. Geological Survey (2007b). These sites are listed in Table C.7, and they are shown on Figure C.13, along with a delineation of corresponding watershed. The monthly streamflows are listed in Tables C.8a-r. Only Big Rock Creek near Valyermo has continuous measurements for 1949-2009, which is the 61-year period used in the development of a precipitation-altitude relation. However, among the 18 sites, 17 have partial records during 1949-2005 ranging from 3 to 49 years in length. As indicated in Table C.7 for the 18 sites, the average annual streamflows range from 2 to 13,000 acre-ft, the watershed areas range from 200 to 31,000 acres, and the area-weighted average annual precipitation ranges from 4 to 45 inches.

Data Adjustments for Partial Records. Before using the downloaded streamflow data, the data were adjusted for missing years during 1949-2005. In particular, the average annual streamflow for a site with a partial record was adjusted to account for the fact the streamflow conditions during the period of record may not be the same as the conditions during 1949-2005. The adjustment is based on the complete record for Big Rock Creek near Valyermo, where the adjustment is given by the relation (Linsley, 1981)

$$\left.\overline{Q}\right|_a = \frac{\left.\overline{Q}\right|_b}{\left.\overline{Q_B}\right|_b} \cdot \left.\overline{Q_B}\right|_a \tag{C.9}$$

where

    a represents the period 1949-2005,

    b represents the years contained within the record for site to be adjusted,

    $\left.\overline{Q}\right|_a$ is the adjusted average annual streamflow for the partial-record site for period a,

    $\left.\overline{Q}\right|_b$ is the average annual streamflow for the partial-record site for period b,

    $\left.\overline{Q_B}\right|_a$ is the average annual streamflow for the Big Rock Creek for period a, and

    $\left.\overline{Q_B}\right|_b$ is the average annual streamflow for Big Rock Creek for period b.

Like Equation C.3 for the adjustment of precipitation records, Equation C.9 has the desirable property that, as the completeness of the streamflow record for a partial-record site increases, the adjusted average equals the record average.

The adjusted average annual streamflow is listed in Table C.9. The adjustment factors, which are the adjusted average divided by the unadjusted average, range from 0.50 to 1.54. The sites with a factor less than unity represent those with a record period during which climatic conditions were wetter than during 1949-2005. Likewise, the sites with a factor greater than unity represent those with a record period during which climatic conditions were dryer than during 1949-2005.

The adjustment of average annual streamflow to the 1949-2005 base period depends on the existence of a correlation between the base stations and the site to be adjusted. To identify the underlying correlations, the correlation of the annual streamflow was calculated for two groups of sites. The first group includes three sites with continuous streamflow measurements during the 22-year period 1958-1979, and the second group includes nine sites with measurements during the 5-year period 1990-1994. The resulting correlations are listed in Tables C.10a-b. For the first group (Table C.10a), which represents a 22-year period, the correlation values range from 0.75 to 0.98. For the second group (Table C.10b), which represents a 5-year period, the correlation values range from -0.74 to 0.98. The correlation structures expressed in Tables C.10a-b suggest a generally high correlation between nearby sites but a generally moderate correlation between more distant sites. This conclusion relies mostly on the correlation estimates based on the 22-year record period, because the correlation estimates based on the 5-year period are significantly uncertain.

C.2.3.2   Streamflow Estimates from Channel-Geometry Data

To supplement the streamflow data from the U. S. Geological Survey streamgaging sites, channel-geometry measurements (Hedman and Osterkamp, 1982) were collected to estimate the average annual streamflow at additional sites. The average annual streamflow is related to the active-channel width, bed material, bank material, and streamflow patterns. Hedman and others (1972), Hedman (1970), Osterkamp and others (1982), Osterkamp and Hedman (1982), and Leopold and Maddock (1953) developed relations for estimating average annual streamflow within the intermountain western United States based on these metrics. Antelope Valley is marginally within the study area evaluated by Hedman and Osterkamp (1982), however the valley is sufficiently similar to the study area to apply the channel-geometry relations.

The general form for the relations are (Hedman and Osterkamp, 1982)

$$\overline{Q} = \alpha w^{n} \quad \text{(C.10)}$$

where

$\overline{Q}$ is the average annual streamflow,
α is a coefficient,
w is the active channel width, and
n is an exponent.

The coefficient and exponent depend on whether the bed and bank materials are fine or coarse grained. The coefficient and exponent also depend on whether the streamflow is ephemeral, seasonal, or perennial. Hedman and Osterkamp (1982) developed separate parameter pairs for various combinations of bank material, bed material, and streamflow pattern.

Channel-geom   etry measurements were made at about 25 gaged and ungaged sites throughout the Antelope Valley watershed during spring 2007, but only 16 sites yielded useful results. The latter sites are listed in Table C.11, and the locations are shown on Figure C.14. The sites include seven gaged streams and four ungaged streams draining the San Gabriel Mountains, one gaged stream and three ungaged streams draining the Tehachapi Mountains, and one gaged stream draining the Edwards AFB area. For the channel-geometry measurements at gaged sites, the adjusted average annual streamflow based on the streamflow measurements are listed in Table C.12.

The average annual streamflows estimated from channel-geometry measurements are listed in Table C.12. For the gaged sites, the average annual streamflows derived from the discharge measurements also are listed. Figure C.15 shows a comparison of the estimated and measured streamflows at gaged channel-geometry sites. The horizontal axis represents the adjusted average annual streamflow determined from the streamflow measurements. The vertical axis represents the estimated streamflow based on the channel-geometry measurements. Based on the scatter of the plotted points about the match line, the standard error (s_e) is about 2,700 acre-ft/yr, the corresponding coefficient of variation (C_V) is 0.79, and the coefficient of determination (r^2) is 0.78. However, the plotted point for Big Rock Creek near Valyermo appears to represent a statistical outlier. If Big Rock Creek is omitted in calculating the relational statistics, the standard error is 280 acre-ft/yr, the coefficient of variation is 0.12, and the coefficient of determination is 0.99.

Big Rock Creek plots as an outlier most likely because of artificial disturbances to the channel. The streamgaging site is on a reach used for wading and swimming, and the recreational visitors have constructed many small rock dams to create deeper water. Even though the channel-geometry measurements were made at locations between the dams, the dams have probably altered the natural channel regimen.

C.2.3.3   Streamflow-Duration Relations

The temporal streamflow pattern was characterized by developing generalized dimensionless flow-duration relations. Three relations were developed to represent, respectively, the general streamflow classes of perennial, seasonal, and ephemeral streams. A flow-duration relation has the exceedance probability as the independent variable and the corresponding streamflow discharge as the dependent variable. A dimensionless relation replaces the discharge by a normalized discharge, where the average streamflow is the normalizing factor.

For a particular streamflow class, the generalized relation was developed by a two-step process. Firstly, dimensionless flow-duration relations were developed from the daily discharges for each gaged site within the class. For a particular gaged site within the class, the probability for a normalized discharge is calculated from the expression (Benson, 1962a; Benson, 1962b)

$$p(r) = \frac{r}{N+1} \quad \text{(C.11)}$$

and the normalized discharge is given by the expression

$$q(r) = \frac{Q(r)}{\overline{Q}} \quad \text{(C.12)}$$

where

p	is the exceedance probability,
N	is the number of daily-discharge values,
r	is the rank for a particular value,
q	is the normalized discharge,
Q	is the measured discharge, and
$\overline{Q}$	is the average of the measured discharges.

The discharge values are ranked from highest ($r = 1$) to lowest ($r = N$). Secondly, a generalized flow-duration relation was constructed for the class by fitting a single relation to the collective of relations.

The individual relations and the fitted generalized relations are shown on Figures C.16a-c and C.17a-c. Figure C.16a shows the individual relations for the perennial streams, Figure C.16b shows the relations for the seasonal streams, and Figure C.16c shows the relations for the ephemeral streams. Figure C.17a-c respectively shows the normalized relation for perennial, seasonal, and ephemeral streams. A non-normalized flow-duration relation can be created for any ungaged site simply by scaling the appropriate normalized relation by the estimated average discharge for the site.

C.2.4   Quantification of Evapotranspiration

Evapotranspiration data were assembled for the Antelope Valley watershed and adjacent areas in terms of potential evapotranspiration, temperature, and satellite images. Potential evaporation data were compiled for the available records, which cover 1995-2007 or shorter periods. Temperature data were compiled for the 57-year period 1949-2005. Satellite images were obtained for water years 1986 and 2005. The potential evapotranspiration and temperature data were then used to calculate potential evapotranspiration for the 57-year period 1949-2005. The satellite images were used to estimate vegetation coefficients for water years 1986 and 2005.

C.2.4.1 General Approach

The geographic distribution of natural evapotranspiration within the Antelope Valley watershed depends on the potential evapotranspiration, vegetation cover, and precipitation. However, the effects of vegetation coverage and precipitation can be described in terms of the vegetation coefficient in the relation (Doorenbos and Pruitt, 1977)

$$ET = k_c PET \quad \text{(C.13)}$$

where

  ET is the actual evapotranspiration,
  k_c is the vegetation coefficient, and
  PET is the potential evapotranspiration.

The vegetation coefficient accounts for the density and growth stage of the vegetation. Equation C.13 was used to estimate evapotranspiration within the Antelope Valley watershed. The application of this relation, in turn, involved compiling information on potential evapotranspiration and the vegetation coefficient.

C.2.4.2 Potential Evapotranspiration

C.2.4.2.1 Evapotranspiration Data

Data Sources. Evapotranspiration data are available for the Antelope Valley watershed and adjacent areas from the California Department of Water Resources (2007). Data are also available for four CIMIS (California Irrigation Management Information System) stations. The stations are listed in Table C.13, and their locations are shown on Figure C.18. As indicated in Table C.13, the station altitudes range from 2,500 to 6,900 ft. The monthly CIMIS data for Palmdale are listed in Tables C.14a-b.

Adjustment for Partial Records. The record periods represented by the sites include 1995-2006 for a site near Victorville, 2005-2006 for a site at Lake Arrowhead, and 2006 for sites at Big Bear Lake and Palmdale. The station at Victorville was used to adjust the other station averages to a 1995-2006 base period. The adjustment is based on the same approach as described for the adjustment of precipitation and streamflow records. The adjusted potential evaporations are listed in Table C.15.

C.2.4.2.2 Evapotranspiration-Altitude Relation

Developing PET-Altitude Relation. The geographic distribution of evapotranspiration within the Antelope Valley watershed is related mostly to altitude. Figure C.19 shows *PET*-altitude relation derived from the CIMIS data. However, the dependent variable is expressed in terms of the relative *PET*, which is *PET* normalized to the *PET* at the Palmdale station. The independent variable is expressed in terms of the altitude difference, which is the altitude minus the altitude at the Palmdale station. Figure C.19 shows

14

a linear relation, where the intercept for the relation is 1 and the slope is 0.0000635 ft^{-1}. The relation has the form

$$\frac{PET}{PET_P} = 1 - 0.0000635(z - z_P) \quad \text{(C.14a)}$$

or

$$PET = \left[1 - 0.0000635(z - z_P)\right]PET_P \quad \text{(C.14b)}$$

where

z is the altitude,
z_P is the altitude at Palmdale,
PET is the potential evapotranspiration at altitude z, and
PET_P is the potential evapotranspiration at Palmdale.

The standard error (s_e) for the relation is 0.078, the corresponding coefficient of variation (C_V) is 0.078, and the coefficient of determination (r^2) is 0.85.

Estimating PET at Palmdale. While Equation C.14a or C.14b can be used to estimate the geographic distribution of PET given the DEM for the Antelope Valley watershed and the PET at Palmdale, CIMIS data are available at Palmdale only for April 2005 through March 2007. For dates outside that period, the Blaney-Criddle method was used to estimate the PET at Palmdale. The Blaney-Criddle method is based on the equation (Doorenbos and Pruitt, 1977)

$$PET_i = c_i\left[p_i(0.46T_i + 8)\right] \quad \text{(C.15)}$$

where

T is the mean temperature over a month i in degrees Celsius,
p is the proportion of daylight hours, and
c is an adjustment factor dependent on wind, humidity, and cloud cover.

However, the coefficients p and c can be combined into a single coefficient C to yield the Blaney-Criddle equation in the form

$$PET_i = C_i(0.46T_i + 8) \quad \text{(C.16a)}$$

or

$$C_i = \frac{PET_i}{(0.46T_i + 8)} \quad \text{(C.16b)}$$

The coefficients $C_{Jan}, \ldots, C_{Dec}$ were estimated for each calendar month from the CIMIS data for Palmdale. Table C.14a lists the monthly average maximum temperature, average minimum temperature, the computed average temperature, the potential evapotranspiration, and the computed Blaney-Criddle coefficients for basic data (from Equation C.16b). For a particular month, a coefficient value was computed for both 2005 and 2006, and the computed values were averaged to obtain $C_{Jan}, \ldots, C_{Dec}$. Table C.14b lists those averages.

The comparison of the computed *PET* with the measured *PET* at Palmdale for 2005-2006 is shown on Figure C.20 as a scatter diagram. The horizontal axis represents the *PET* measured at the Palmdale CIMIS station. The vertical axis represents the *PET* calculated from the Blaney-Criddle relation. The plotted data are the monthly *PET* values for the 24-month period April 2005 through March 2007. The scatter of the plotted points about the match line represent a standard error (S_e) of 0.29 inches/mo, a coefficient of variation (C_v) of 0.047, and a coefficient of determination (r^2) of 0.99.

Using the estimates of $C_{Jan}, \ldots, C_{Dec}$, the *PET* at Palmdale can be calculated using Equation C.16a for any year and month from the mean temperature. Tables C.16a-c list the monthly average temperature at Palmdale for the 57-year period 1949-2005. The monthly average temperatures were computed from the average minimum and maximum temperatures, which were downloaded from the Western Regional Climatic Center (2007). Based on the monthly temperatures listed in Tables C.16a-c, Equation C.16a was used to calculate the monthly *PET* at Palmdale. The results are listed in Table C.17.

C.2.4.3　Vegetation Coefficient

Satellite imagery of the Antelope Valley watershed was analyzed to identify the geographical and temporal distributions of the vegetation coefficient. Satellite imagery contains information on the consumptive use of the native vegetation within Antelope Valley. In particular, the imagery can be related to consumptive use through the *NDVI* (Normalized Difference Vegetation Index) vegetation index (Kerr and others, 1989; Chong and others, 1993; Kustas and others, 1994; Seevers and Ottman, 1994; Szilagyi and others, 1998; and Szilagyi, 2002). This index is related to reflectances measurements acquired in the red and near-infrared spectral regions by the expression (Rouse and others, 1974)

$$NDVI = \frac{\rho_{NIR} - \rho_R}{\rho_{NIR} + \rho_R} \quad (C.17)$$

where
$\quad \rho_R \quad$ is the red reflectance and
$\quad \rho_{NIR} \quad$ is the near-infrared reflectance.

NDVI is related directly to the energy adsorption of plant canopies and hence to transpiration.

By design (Rouse and others, 1974), *NDVI* values range from +1 (when $\rho_R = 0$) to -1 (when $\rho_{NIR} = $). However, the *NDVI* calculated from a particular satellite image and for a particular vegetative condition depends on the atmospheric opacity when the image was acquired. The *NDVI** index corrects for atmospheric and other factors (Huete and Liu, 1994; Liu and Huete, 1995), which has the form

$$NDVI^* = \max\left[\min\left(\frac{NDVI - NDVI_0}{NDVI_S - NDVI_0}, 1\right), 0\right] \quad \text{(C.18)}$$

where
      $NDVI_0$ is the *NDVI* representing bare soil and
      $NDVI_S$ is the *NDVI* representing saturation.

Saturation occurs in areas with the most verdant vegetation, such as irrigated crops. The $NDVI^*$ index has a range of 0 (for bare soil) to 1 (for verdant vegetation), and it enables the comparison of *NDVI* measured at different times with different atmospheric opacities.

The   *NDVI** index is related to actual evapotranspiration of the vegetative canopy by the relation (Baugh and Groeneveld, 2006)

$$ET = NDVI^* \cdot PET \quad \text{(C.19)}$$

where
      ET   is the actual evapotranspiration and
      PET   is the reference evapotranspiration.

Equation C.19 has the same form as Equation C.13, where $NDVI^*$ is the vegetation coefficient, which means the *NDVI** index is equivalent to the vegetation coefficient k_c.

Eleven LANDSAT TM images were analyzed representing the dates listed in Table C.18. Six images were analyzed for water year 1986 (September, January, February, June, August, and September). Five images were analyzed for water year 2005 (September, November, April, June, and September). Water year 1986 was selected for the analysis because the annual precipitation was near normal and some satellite images were available from Luhdorff & Scalmanini (Lisa Lavagnino, 2007, written communication). Water year 2005 was selected for the analysis because the annual precipitation was substantially above normal. The precipitation during water year 1986 was 106 percent of the 1949-2005 average, and the precipitation during water year 2005 was 168 percent of the average. Each image represents a cloud-free instant over the entire Antelope Valley watershed. The images not obtained from Luhdorff & Scalmanini were obtained from the U. S. Geological Survey (2007c).

NDVI was calculated for the available images using the Leica image-analysis extension for ArcGIS, and the *NDVI* values representing bare soil and verdant vegetation were extracted as listed in Table C.18. The *NDVI*[*] index was then calculated using the map-calculator function within ArcGIS. Figures C.21a-k show the resulting geographic distribution of *NDVI*[*] within the Antelope Valley watershed for the months represented by the available satellite images. The statistics of the *NDVI** distributions are listed in Table C.19. As indicated in that table for 1986, the spatially averaged *NDVI** values range seasonally within the San Gabriel Mountains from 0.23 (June) to 0.42 (February). The spatially averaged *NDVI** values range seasonally within the Tehachapi Mountains from 0.21 (also June) to 0.37 (also February). For 2005, the spatially averaged *NDVI** values range seasonally within the San Gabriel Mountains from 0.22 (September) to 0.39 (April). The spatially averaged *NDVI** values range seasonally within the Tehachapi Mountains from 0.22 (also September) to 0.41 (also April). As discussed with respect to Equation C.19 above, these *NDVI** values are numerically equivalent to the vegetation coefficients applicable to the San Gabriel and Tehachapi mountains.

Figures C.22a-b and C.23a-b show the temporal variation of *NDVI** respectively during water years 1986 and 2005. Each figure includes separate graphs for the San Gabriel and Tehachapi mountains. For 1986, which was a year of nearly average precipitation, the *NDVI** peaks in February for both mountain ranges. For 2005, which was a year of above average precipitation, the *NDVI** peaks in April.

C.2.5 Quantification of Water Chemistry

Chloride data were compiled for precipitation and groundwater for selected sites within and nearby the Antelope Valley watershed. The compiled data on precipitation chloride represents the 10-year period 1994-2003. The compiled data on groundwater chloride represents the 12-year period 1995-2006.

The precipitation and groundwater chloride data were obtained from the U. S. Geological Survey. The data on precipitation chloride were provided by the U. S. Geological Survey (John Izbicki, 2007, written communication), and the data on groundwater chloride were downloaded from the U. S. Geological Survey national database (U. S. Geological Survey, 2007d). The precipitation data represent bulk samples collected over periods of at least several months. Correspondingly, the data represent the accumulative wetfall and dryfall during the sampling interval. The monitoring sites are shown on Figure C.24. The sites are described in Table C.20, and the compiled data are listed in Table C.21. The groundwater monitoring sites are shown on Figure C.25. The sites are described in Table C.22, and the compiled data are listed in Table C.23.

C.3.0   Estimation of Natural Recharge

Three independent methods were used to estimate groundwater recharge. Firstly, evapotranspiration and precipitation data were used to estimate the water yield from the mountain-block areas and to translate that yield into groundwater recharge. Secondly, the chloride data were used to apply the chloride method for estimating groundwater recharge. Thirdly, the precipitation and streamflow data were used to develop a streamflow-precipitation relation that was used to estimate streamflow from ungaged watersheds and, subsequently, to estimate the recharge from gaged and ungaged streamflow.

Each of the three methods requires identifying the regions within the Antelope Valley watershed where the infiltration of precipitation produces groundwater recharge. Little recharge occurs where the average annual precipitation is less than some small amount. Russell and Minor (2002) studied 35 sites within southern Nevada where the average annual precipitation ranged from 6 to 10 inches, and they concluded that insignificant recharge occurs within interfluvial areas for that range. Izbicki and others (2000) concluded from a study area within the western Mojave Desert that recharge does not occur where the average annual precipitation is about 7 inches. Dettinger (1989) studied regional groundwater recharge within eastern Nevada, and he assumed for his work that recharge does not occur within interfluvial areas where the average annual precipitation is less than 8 inches, based on work by Maxey and Eakin (1949). Maxey and Eakin (1949) developed a method for estimating recharge from precipitation that has been used extensively throughout Nevada (Avon and Durbin, 1992). That method is based, in part, on the assumption that recharge does not occur within interfluvial areas where the average annual precipitation is less than 8 inches. A review by Avon and Durbin (1992) suggests that the Maxey-Eakin approach reasonably represents recharge from precipitation, and their assumption is used here.

C.3.1 Evapotranspiration Method

The water yield of a watershed is the precipitation less the evapotranspiration. The yield over a particular period and geographic location is given by the relation

$$Y(x, y) = \max[P(x, y) - ET(x, y), 0] \quad \text{(C.20)}$$

where
> Y is the water yield for the period at point (x, y),
> P is the precipitation at the point, and
> ET is the actual evapotranspiration.

The maximum is taken to eliminate the occurrence of a negative yield, which is most likely just an artifact of the noise in the estimates of precipitation and evapotranspiration. The effect of taking the maximum is to increase the calculated water yield for the period.

The actual evapotranspiration was obtained by combining the geographic distribution of $NDVI^*$ (Figure C.21a-k) with the PET-altitude relation (Equation C.14) and the monthly PET at Palmdale (Table C.17). Based on these inputs, the geographic distribution of ET was calculated using the map-calculator function within ArcGIS (ESRI, 2001). The applied function was

$$ET(x, y) = [1 - 0.0000635(z(x, y) - z_P)] \cdot PET_P \cdot NDVI * (x, y) \quad \text{(C.21)}$$

where

ET	is the actual evapotranspiration at point (x, y),
z	is the land-surface altitude,
z_P	is the land-surface altitude at Lancaster,
PET_P	is the potential evapotranspiration at Palmdale, and
$NDVI^*$	is the geographic distribution of that index.

The altitude at Lancaster is 2,550 ft, and the land-surface altitude is derived from the smoothed DEM. The map calculator within the Spatial Analyst extension of ArcGIS was used to implement Equation C.21. The resulting maps for the months represented by the satellite images are shown on Figures C.26a-k. The statistics for ET distributions are listed in Table C.24, where the statistics represent those regions where the average annual precipitation is greater than 8 inches.

Figures C.27a-b shows the geographic distributions of annual ET for water years 1986 and 2005. The annual ET is the sum of monthly evapotranspiration. For the months with a satellite image, the monthly ET shown on the appropriate map within Figures C.26a-k was used. For the months without a satellite image, a map of $NDVI^*$ was created by a linear interpolation based on the adjacent months within a satellite image. Equation C.21 was then used to generate the corresponding map of ET. The map calculator within the Spatial Analyst extension of ArcGIS was used to generate the intermediate $NDVI^*$ maps and to implement Equation C.21. For water year 1986, the spatially averaged annual ET is 1.62 ft/yr for the San Gabriel Mountains and 1.43 ft/yr for the Tehachapi Mountains, where the statistics represent the regions where the average annual precipitation is greater than 8 inches. For water year 2005, the spatially averaged annual ET is 1.65 ft/yr for the San Gabriel Mountains and 1.60 ft/yr for the Tehachapi Mountains, which is similar to that of water year 1986. The actual ET is similar even though the annual precipitations were nearly normal in 1986 and much above normal in 2005.

The similarity in actual ET suggests that, for normal and above normal years with respect to precipitation, the actual ET is mostly independent of precipitation. Correspondingly, the average of the geographic distributions of annual ET for water years 1986 and 2005 was assumed to characterize the actual ET for years of normal and above normal precipitation, and that average distribution is shown on Figure C.28. The spatially averaged annual ET from Figure C.28 is 1.63 ft/yr for the San Gabriel Mountains and 1.52 ft/yr for the Tehachapi Mountains. The rates are the area-weighted average within the region where the average annual precipitation is greater than 8 inches.

The average annual water yield is a function of the precipitation regimen and the actual evapotranspiration. Accordingly, the average annual water yield is the average of the water yields produced from the long-term collection of years with a variety of annual precipitation. The regimen of annual precipitation within the Antelope Valley watershed was characterized by the cumulative distribution of precipitation as shown on Figures C.29a-b. The graph represents precipitation at the nine gages with a continuous record for the 57-year period 1949-2005. However, to produce precipitation distributions for the San Gabriel and Tehachapi mountains, the distribution derived from the nine gages was scaled to represent the respective mountain ranges. For the San Gabriel Mountains, Figure C.29a represents an average annual precipitation of 15.4 inches. The maximum annual precipitation is 37.7 inches (which represents 240 percent of the average annual precipitation) and the minimum annual precipitation is 5.9 inches (which represents 38 percent of the average annual precipitation). For the Tehachapi Mountains, Figure C.29b represents an average annual precipitation of 13.1 inches. The maximum annual precipitation is 32.1 inches (which represents 240 percent of the average annual precipitation) and the minimum annual precipitation is 5.0 inches (which represents 38 percent of the average annual precipitation).

The corresponding cumulative distribution of water yield was developed using decile precipitation values derived from Figures C.29a-b. For each precipitation value, a water yield was calculated using Equation C.20. The precipitation in the equation was the geographic distribution of average annual precipitation (Figure C.10) multiplied by ratio of the decile precipitation over the average annual precipitation. The actual *ET* was the geographic distribution of the 1986 and 2005 average *ET* (Figure C.28). The resulting cumulative distribution of annual water yield is shown on Figures C.30a-b. The distribution corresponds to an average annual water yield of 52,000 acre-ft/yr from the San Gabriel Mountains and 12,000 acre-ft/yr for the Tehachapi Mountains. For the San Gabriel Mountains, the minimum annual yield is 700 acre-ft/yr (1 percent of the average) and the maximum annual yield is 190,000 acre-ft/yr (370 percent of the average). For the Tehachapi Mountains, the minimum annual yield is 50 acre-ft/yr (0.4 percent of the average) and the maximum annual yield is 80,000 acre-ft/yr (660 percent of the average).

However, the average annual water yield is not the average annual groundwater recharge. Part of the water yield produces flooding on the Rosamond Lake, Rogers Lake, and other playas, and those floodwaters do not produce groundwater recharge. French and others (2005) suggest that the floodwater volume can be large, where they estimated a volume of over 2 million acre-ft for the 100-year flood. Based on the runoff model described in Section 3.3 below, the cumulative distribution of playa flooding was constructed based on the decile precipitation values derived Figures C.29a-b. The resulting cumulative distribution of annual flood volumes is shown on Figures C.31a-b. The distribution corresponds to an average annual flood volume of 9,200 acre-ft, which can be partitioned as 6,100 acre-ft to the San Gabriel Mountains and 3,100 acre-ft to the Tehachapi Mountains. The minimum annual flood volume is zero and the maximum annual volume is 190,000 acre-ft/yr (2,100 percent of the average), where the volume equals zero for 32 percent of the years.

21

The average annual groundwater recharge is the difference between the average annual water yield and the average annual playa flood volume. Based on Figures C.30a-b, the average annual water yields are 52,000 acre-ft from the San Gabriel Mountains and 12,000 acre-ft from the Tehachapi Mountains. Based on Figure C.31a-b, the average annual playa flooding is 6,100 acre-ft from the San Gabriel Mountains and 3,100 acre-ft from the Tehachapi Mountains. Correspondingly, the average annual groundwater recharge is 46,000 acre-ft from the San Gabriel Mountains and 9,000 acre-ft from the Tehachapi Mountains. The total average annual recharge from both sources is 55,000 acre-ft.

C.3.2 Chloride Method

Groundwater recharge originating from precipitation can be estimated from the chloride in precipitation and groundwater (Claassen and others, 1986; Johnston, 1987; Vacher and Ayers, 1980; Mandel and Stiftan, 1981; Irving, 1982; and Dettinger, 1989). Within the Antelope Valley watershed, both streamflow and mountain-block underflow originate from precipitation. While the underflow is a direct recharge source, streamflow produces recharge by channel infiltration within the valley-floor areas. The recharge rate from these processes is the precipitation volume less the losses associated with native vegetation and channel processes. Because evapotranspiration and evaporation do not remove chloride mass from soil water, the chloride mass loading to the watershed surface due to precipitation equals the chloride mass loading to the groundwater system. Nevertheless, the losses associated with vegetation and channel processes result in higher groundwater chloride than the original precipitation chloride. Based on this enrichment, the recharge can be calculated from the relation (Dettinger, 1989)

$$\overline{R} = \left(\overline{P} - \overline{F}\right)\frac{C_p}{C_g} \quad \text{(C.22)}$$

where

$\overline{R}$	is the average annual recharge,
$\overline{P}$	is the average annual precipitation volume for a watershed,
$\overline{F}$	is the average annual playa flooding,
C_p	is the precipitation chloride, and
C_g	is the groundwater chloride.

The precipitation chloride was calculated from the bulk precipitation data, where the reported chloride is the dryfall and wetfall dissolved in the water collected during the sampling period. Only wet season sampling periods (approximately October through April of each water year from 1995 through 2003) were used, because dry season records showed unrealistically high chloride concentrations. These were interpreted to be biased due to redeposition and concentration of chloride carried by winds from Rosemont and other dry lakes. The effective precipitation chloride was, for each station, calculated from the relation

$$\overline{C}_P = \frac{\sum_{i=1}^{n} \left(\dfrac{C_{pi} P_i}{\Delta t_i} \right)}{\overline{P}} \quad \text{(C.23)}$$

where

$\overline{C}_p$ is the effective precipitation chloride concentration,

C_{pi} is the chloride concentration for a particular sampling interval i,

Δt_i is the duration of the sampling period,

P_i is the precipitation depth during the sampling interval, and

n is the number of sampling intervals.

The sampling-interval precipitation depth is in units of inches, the average annual precipitation is units of inches per year, and the duration of the sampling interval has units of years.

       The resulting effective precipitation chloride for individual sampling sites ranged from 0.46 to 32.3 mg/L (Figure C.24). However, four of the sites were located in areas where precipitation was less than approximately 8 inches per year. Areas with less than approximately 8 inches per year of precipitation are unlikely to undergo recharge (Dettinger, 1989). Also, three of the four sites had high chloride concentrations that may be impacted by the wind-driven resuspension of particles previously deposited on the land surface. Consequently, these four sites were not used in the estimation of recharge. Based on the remaining three stations, the geographically averaged precipitation chloride is 2.31 mg/L.

       The effective average annual precipitation volume is about 453,000 acre-ft on the San Gabriel Mountains and 143,000 acre-ft on the Tehachapi Mountains, which was derived from Figure C.10. This precipitation volume is that corresponding to the areas where the average annual precipitation is greater than 8 inches, which is identified on Figure C.11. For areas with lower precipitation, chloride tends to accumulate within the unsaturated zone because the deep percolation of precipitation does not occur (Russell and Minor, 2002; Izbicki and others, 2000). Correspondingly, the application of Equation C.22 requires the exclusion of the precipitation volume and the associated chloride mass loading where the average annual precipitation is less than 8 inches (Dettinger, 1989).

       The groundwater chloride is characterized by the temporal average groundwater chloride within the alluvial aquifer near the mountain fronts. The chloride in wells adjacent to mountain fronts were considered most representative of the effects of recharge, because the chloride in more downstream wells is more likely to be impacted by irrigation returns. Figure C.25 shows the temporal average groundwater chloride in wells located along the San Gabriel and Tehachapi mountain fronts. Among the wells adjacent to the San Gabriel Mountains, the temporal average groundwater chloride ranges geographically from 4 to 90 mg/L; the geographical average chloride is 30.5 mg/L. Among the wells adjacent to the Tehachapi Mountains, the average groundwater chloride ranges geographically from 3 to 35 mg/L; the geographical average chloride is 13.9 mg/L.

Based on the precipitation and groundwater characterization described above, the average annual recharge is about 34,000 acre-ft from the San Gabriel Mountains and 24,000 acre-ft from the Tehachapi Mountains. However, the recharge estimated for the Tehachapi Mountains does include the precipitation within the Mojave Creek watershed. While the runoff within that watershed is tributary to Antelope Valley, the upper part is underlain partly by the Fremont Valley groundwater basin (California Department of Water Resources, 2003). Precipitation on the Mojave Creek watershed most likely produces some deep percolation and corresponding groundwater recharge to the Fremont Valley basin. To the extent that such recharge occurs, the average annual recharge to the Antelope Valley groundwater basin from the Tehachapi Mountains is less than 24,000 acre-ft by that recharge. Neglecting that effect, the total average annual recharge estimated by the chloride method within Antelope Valley is 58,000 acre-ft.

Other uncertainties in the chloride method include potential bias in the chloride concentrations in precipitation and groundwater (Dettinger, 1989). Precipitation chloride results may be affected by resuspension of particulate matter containing chloride and deposition in precipitation chloride stations. This affect would increase the observed precipitation chloride concentrations and result in over-estimates of recharge. Groundwater chloride concentrations may be affected by dissolution of chloride along groundwater flow paths. This affect would increase the groundwater chloride concentrations above levels due solely to precipitation recharge and result in under-estimates of recharge.

C.3.3 Precipitation-Yield Method

The water yield within the Antelope Valley watershed depends on precipitation. This precipitation dependence was used to quantify the geographic distribution of average annual yield based on the relation

$$\overline{q}(x, y) = \overline{q}\left(\overline{P}(x, y)\right) \text{ (C.24)}$$

where

$\overline{q}(x, y)$ is the average annual water yield per unit area at point (x, y),

$\overline{P}(x, y)$ is the average annual precipitation at point (x, y), and

$\overline{q}(\overline{P})$ is the average annual yield for the particular average annual precipitation $\overline{P}$.

Following from Equation C.24, the water yield for a watershed is based in the integration of point processes over the watershed. Correspondingly, the translation of Equation C.24 to a watershed yield is given by the relation

$$\overline{Q} = \int_A \overline{q}\left(\overline{P}(x, y)\right) dy dx \text{ (C.25)}$$

where

$\overline{Q}$ is the average annual yield for the watershed and

A is the watershed area.

The overall approach to developing a watershed model based on Equation C.25 was to develop a generalized model form and then to calibrate the model to the available streamflow information.

C.3.3.1   Generalized Model Form

The generalized model form has two components, which include a runoff component and a mountain-groundwater component. The water yield from a watershed is the sum of the runoff and groundwater flow.

Runoff is a short term process resulting from rainfall and snowmelt. Runoff is comprised of water that follows either a surface-water path through the watershed or a short groundwater path. The average annual runoff is generated at a point in response to the physical characteristics of the land surface and average annual precipitation at the point. The average runoff is the integrated result of precipitation and soil processes that occur at small temporal and special scales. Nevertheless, the small-scale processes result in average annual runoff that tends to increase with increased average annual precipitation. For watersheds within the Antelope Valley, this dependence is represented in the runoff component by the nonlinear relations

$$\overline{q}_R = a_R \left(\overline{P} - P_0 \right)^{n_R} \qquad \text{for} \qquad \overline{P} \geq P_0 \quad \text{(C.26a)}$$

otherwise

$$\overline{q}_R = 0 \quad \text{(C.26b)}$$

where
$\overline{P}$ is the average annual precipitation,
P_0 is the threshold precipitation,
$\overline{q}_R$ is the average annual runoff,
a_R is the coefficient for the relation, and
n_R is the exponent.

Mountain groundwater represents longer-termed processes than runoff. Groundwater flow results from rainfall and snowmelt moving through groundwater paths, and the paths are longer than those considered as part of runoff. The paths are associated with hillslope processes, percolation through the mountain blocks, and underflow through channel alluvium. The source water for these paths is the deep percolation of rainfall or snowmelt below the root zone of the mountain vegetation. The local percolation rate equals local precipitation less the local runoff and consumptive use. These are processes controlled principally by the hydraulic characteristics of the materials comprising the root zone, the precipitation pattern, and the vegetation cover. However, prior research work with semiarid and arid regions suggests vegetation communities develop in response to the local climatic and soils conditions such that the infiltrated water is mostly consumed (Rodrigues-Itubre and Porprato, 2004; Eagleson, 2002; and Noy-Meir, 1973), and little deep percolation occurs. Furthermore, the hydrogeologic characteristics of the mountain block tend to have a minor role in this outcome.

Underflow is dependent on precipitation and evapotranspiration, and it tends to increase with increased average annual precipitation. The underflow comprises all groundwater flow from a watershed, including both groundwater flow within the mountain-block mass and channel deposits. For watersheds within Antelope Valley, this dependence is represented in the runoff component by the nonlinear relations

$$\overline{q}_U = a_U \left(\overline{P} - P_0 \right)^{n_U} \qquad \text{for} \qquad \overline{P} \geq P_0 \quad \text{(C.27a)}$$

otherwise

$$\overline{q}_U = 0 \quad \text{(C.27b)}$$

where

$\overline{P}$ is the average annual precipitation,
P_0 is the threshold precipitation,
$\overline{q}_U$ is the average annual underflow,
a_U is the coefficient for the relation, and
n_U is the exponent.

Nevertheless, the mountain-block topography and hydrogeologic characteristics do influence the groundwater-flow paths within the mountain block. If the mountain block is poorly permeable or if more permeable materials are limited to near-surface intervals, then the mountain-block groundwater discharges mostly as stream baseflow and mountain springs. This condition is exaggerated if the topography is characterized by long canyons and steep slopes. If highly permeable materials occur over large depth intervals, the mountain-block groundwater discharges mostly as subsurface flow into the adjacent valley-floor area.

C.3.3.2 Model Calibration

The water-yield model was calibrated to average annual streamflow derived from both streamflow and channel-geometry measurements. The watersheds used in the calibration are listed in Table C.25 and the watershed locations are shown on Figure C.32. Figures C.33a-z show the distribution of average annual precipitation for individual watersheds. For each watershed, the streamflow is computed according to the relation

$$\overline{Q}_i = \int_{A_i} R\left(a_R, n_R, \overline{P}_i(x,y)\right) dy dx + \int_A U\left(a_U, n_U, \overline{P}_i(x,y)\right) dx dy \quad \text{(C.28)}$$

where

i refers to a particular watershed,
$\overline{Q}_i$ is the average annual streamflow for the watershed,
R is the runoff function represented by Equation C.26,

U is the groundwater function represented by Equations C.27,
P_i is the average annual precipitation on the watershed, and
A_i is the watershed area.

The four model parameters a_R, n_R, a_U, and n_U are as defined for Equations C.26 and C.27.

The identification of the model parameters involved separate calibrations, respectively, for the runoff and the groundwater parameters. This is possible because ephemeral streamflow does not contain a groundwater component, and the second integral of Equation C.28 is absent. Correspondingly, the water-yield model has only the two parameters a_R and n_R, which can be identified by calibrating to the measured ephemeral average annual streamflows. The perennial and seasonal streamflows include both runoff and groundwater flows, and both the first and second integrals of Equation C.28 are present. However, assuming that the runoff parameters derived from the ephemeral streamflows apply to the perennial and ephemeral streamflows, the water-yield model has only two unidentified parameters a_U and n_U, which can be identified by calibrating to the measured perennial and seasonal average annual streamflows.

The runoff model was calibrated to the watersheds listed in Table C.25, except for Big Rock, Little Rock, and Oak creeks. The selected watersheds represent ephemeral and selected seasonal streams that lack significant baseflows. Calibration results are listed in Tables C.26 and C.27 and are shown on Figure C.34a. Table C.26 lists the values for a_R and n_R corresponding to a least-squares fit of the runoff model to the watersheds, where the Solver function within Microsoft Excel was used to identify the optimal parameter values. Table C.27 lists the computed streamflows. Figure C.34a is a scatter diagram comparing the measured and computed streamflows. The calibration is characterized by a coefficient of determination (r^2) of 0.90, a standard error (s_e) of 140 acre-ft/yr, and a coefficient of variation (C_v) of 0.53. Big Rock, Little Rock, and Oak creeks were not included in the calibration. Figure C.34b is similar to Figure C.34a except that it includes those creeks. With Big Rock, Little Rock, and Oak creeks included in the calibration statistics, the resulting coefficient of determination (r^2) is 0.99, the standard error (s_e) is 190 acre-ft/yr, and the coefficient of variation (C_v) is 0.20.

Table C.27 lists the "measured" runoff, groundwater, and yield for Big Rock, Little Rock, and Oak creeks. These were derived from the measured streamflows for those creeks as listed in Tables C.8a, C.8d, and C.8n with adjustments for the record period as listed in Table C.9. Based on the average monthly streamflows, the groundwater baseflows were separated from the runoff using a hydrograph of annual baseflow. The hydrograph has two components: An October – March part that increases linearly and a May – September part that decreases exponentially. The resulting baseflows are 7,000 acre-ft/yr for Big Rock Creek, 2,920 acre-ft/yr for Little Rock Creek, and 470 acre-ft/yr for Oak Creek. Based on the result from the groundwater model (Section C.3.3.5) that underflow component of the groundwater outflow equals 30 percent of the baseflow component, the groundwater outflows for Big Rock, Little Rock, and Oak creeks were derived as listed in Table C.27. Subsequently, the watershed yield was calculated as the measured streamflow (runoff plus

baseflow) plus the underflow. Finally, the runoff was calculated as the yield minus the groundwater (baseflow plus underflow).

Using the yields listed in Table C.27, the model was calibrated to the Big Rock, Little Rock, and Oak Creek watersheds. These watersheds represent perennial and seasonal streams that exhibit significant baseflows. Calibration results are listed in Tables C.26 and C.27 and are shown on Figure C.35. Table C.26 lists the values for a_U and n_U corresponding to a least-squares fit of the model to the watersheds. Table C.27 lists the computed water yield. Figure C.35 is a scatter diagram comparing the measured and computed water yields. The calibration is characterized by a coefficient of determination (r^2) of 0.74, a standard error (s_e) of 3,000 acre-ft/yr, and a coefficient of variation (C_V) of 0.33.

Table C.27 lists the runoff, groundwater flow, and total water yield for each of the watersheds used to calibrate either the runoff or yield models. Table C.27 includes these quantities also for the remainder of the Antelope Valley watershed. The measured, simulated, and best-estimate values of runoff, groundwater flow, and total water yield are listed in Table C.27 for each watershed. The measured values are those derived from streamflow or channel-geometry measurements. The simulated values are those derived from the runoff model or overall water-yield model. These best-estimate values represent either a measured or simulated value depending on which best represents the watershed. For the watersheds used to calibrate the runoff model (watersheds other than Big Rock, Little Rock, or Oak Creeks), the best-estimate runoff is the simulated streamflow, the best-estimate groundwater flow is the simulated groundwater flow, and the best-estimate water yield is the simulated yield. For the watersheds used to calibrate the yield model (Big Rock, Little Rock, and Oak Creeks), the best-estimate total water yield is the measured yield, the best-estimate runoff is the measured runoff, and the best-estimate groundwater flow is the measured groundwater.

As indicated in Table C.27, the best-estimate average annual water yield for the Antelope Valley is 68,000 acre-ft. The water yield expressed in the measured streamflow for Big Rock, Little Rock, and Oak creeks represents 40 percent of the Antelope Valley water yield. The runoff component of the water yield is 38,000 acre-ft/yr, and the groundwater-flow component is 30,000 acre-ft/yr. However, diversion from Little Rock Reservoir currently removes 4,000 acre-ft/yr of runoff from the Little Rock Creek watershed.

C.3.3.3 Streamflow Losses

Streamflow can be lost from a channel by percolation through the channel bed. This occurs where the channel bed is composed of permeable materials and the local groundwater table is below the channel bed. Where the groundwater table is sufficiently below the channel bed, the channel loss within a reach is proportional to the wetted streambed area, the infiltration rate per unit area, and the wetted duration.

C.3.3.3.1 Channel Loss Model Formulation

Channel losses can be described by the differential equation

$$\frac{dQ}{dx} = -w(I + E) \quad \text{(C.29)}$$

where

        Q is the streamflow,
        x   is the distance downstream,
        w is the wetted channel width for the discharge Q,
        I is the infiltration rate per unit area, and
        E is the evaporation rate per unit area.

The channel width in turn can be expressed by a relation in the form (Leopold and others, 1964)

$$w = a_W Q^c \quad \text{(C.30)}$$

where a_W is the coefficient for the relation and c is the exponent. However, Equations C.29 and C.30 can be combined such that

$$\frac{dQ}{dx} = -bQ^c \quad \text{(C.31)}$$

where b equals $a_W(I + E)$.

      Equation C.31 is a differential equation that describes the change in streamflow in the downstream direction due to channel infiltration through and evaporation from the wetted channel bed. The equation has the solution

$$Q = \left[Q_0^{1-c} - (1 - c)bx\right]^{\frac{1}{1-c}} \quad \text{(C.32)}$$

or

$$L = Q - Q_0 = \left[(1 - c)bx\right]^{\frac{1}{1-c}} \quad \text{(C.33)}$$

where

        Q_0 is the streamflow at the reach beginning,
        x   is the distance downstream from the beginning, and
        L is the streamflow loss from the reach beginning downstream to distance x along the reach.

Equations C.32 and C.33 apply along the reach until the channel is dry. That occurs at the distance

$$x_D = \frac{Q_0^{1-c}}{(1-c)b} \quad \text{(C.34)}$$

where x_D is the distance below which the channel is dry.

C.3.3.3.2   Channel Loss Model Calibration

Limited data are available for the Antelope Valley watershed to assess the parameters b and c in Equations C.32 or C.33. However, Leopold and others (1964) indicate the exponent *c* has a value of about 0.5 for ephemeral streams within semiarid regions of the western United States. The standard error for the exponent is about 0.3 with respect to individual streams. They indicate additionally that the coefficient a_W has a value of about 6 s^c/ft^{3c-1}, when the discharge is expressed in cubic feet per second. The standard error is perhaps 4 s^c/ft^{3c-1} or larger. However, the parameter a_W is imbedded along with the infiltration rate in the parameter *b* in Equations C.32 and C.33, and parameter *b* accordingly is locally specific to the channel-bed permeability.

The valley-floor channels within the Antelope Valley watershed can be characterized adequately by assuming the exponent *c* equals 0.5. However, streamflow data for Big Rock Creek was used to estimate a value for the coefficient *b*. Three streamgaging stations are located on Big Rock Creek that can be used to estimate the coefficient. These are Big Rock Creek near Valyermo (which is located at the mountain front), Big Rock Creek above Pallett Creek (which is located about 18,000 ft downstream from the mountain front), and Big Rock Creek at Highway 138 (which is located about 53,000 ft downstream from the mountain front). The location of these stations is shown on Figure C.36.

While low flows are significantly depleted along the channel reach from the mountain front to above Pallett Creek, both low and high flows are depleted downstream from Pallett Creek. The streamflow data for Big Rock Creek near Valyermo and Big Rock Creek above Pallett Creek indicate streamflow loss between those sites tend to be minimal for intermediate and high streamflows. Figure C.37 shows a scatter diagram for streamflows at the two sites, where the horizontal axis represents the streamflow for the upstream site. For intermediate and high upstream flows, the downstream flows tend to be not much different than the upstream flows. The streamflow data for Big Rock Creek near Valyermo and Big Rock Creek at Highway 138 indicate significant streamflow loss between those sites, which necessarily must be occurring between Pallett Creek and Highway 138. Figure C.38 shows a scatter diagram for streamflow at the two sites, where again the horizontal axis represents the streamflow for Big Rock Creek near Valyermo. For nearly all streamflows, the downstream flows are much less than the upstream flows. While the downstream flows reflect in part inflow from Pallett Creek and other tributaries, they significantly reflect channel losses downstream from Pallett Creek.

The channel-loss model was calibrated to the difference in streamflow between mountain front and Highway 138. The streamflow data for Big Rock Creek above Pallett Creek was in the calibration because the record period is very short. However, the data for Big Rock Creek above Pallett Creek was sufficient to establish that the effective channel

30

length from the mountain front to Highway 138 is the channel length from Pallett Creek to Highway 138, which is 35,000 ft. The parameters b and c were estimated such that the simulated daily streamflows at Highway 138 fit the measured streamflows at that location. Daily streamflow for Big Rock Creek near Valyermo and Pallett Creek were used as the inputs to the model. The resulting parameter values are 0.00025 s^{c-1}/ft^{3c-2} for b and 0.5 for c. Assuming the coefficient a_W in Equation C.30 equals 6 s^c/ft^{3c-1}(Leopold and others, 1964), and assuming the channel evaporation losses are small (Goodrich and others, 2004), the calibrated value for the parameter b implies a channel infiltration rate of 3.6 ft/d.

The channel reach used in the calibration is located near the apex of the Big Rock Creek alluvial fan. The channel bed is composed of cobbles, gravel, and coarse sand. Furthermore, the unsaturated zone below the channel bed is characterized by similar materials. The infiltration rate derived from the calibration is consistent with such materials. However, the infiltration may not be applicable further down the alluvial fan, where the channel bed and underlying unsaturated zone is composed of less coarse materials. Nevertheless, the infiltration rate of 3.6 ft/d was applied to all the channel reaches within the Antelope Valley watershed.

The infiltration rate derived from the calibration is generally larger than rates associated with other, but not all, studies within semiarid areas. For example, Niswonger and others (2004) collected streamflow-recharge data on Trout Creek within the Humboldt River basin, Nevada. When the streamflow recharge relation described by Equation C.32 is applied to the data, a channel-bed infiltration of 0.2 ft/d is derived. Burkham (1970) collected streamflow-recharge data on streams within the Tucson area, Arizona. Those data indicate infiltration rates range from 0.02 to 0.2 ft/d among individual streams. Lee (1912) collected streamflow-recharge data within the Owens Valley, California. Those data indicate infiltration rates range from 0.9 to 3 ft/d among individual streams. Ronan and others (1998) documented infiltration rates for an ephemeral stream in western Nevada. Based on measurement at small time scales, they concluded the infiltration rates ranged typically from 2 to 12 ft/d.

C.3.3.4   Streamflow Discharges to Playas.

During wet years, streamflow reaches the playas within the Antelope Valley watershed, and that streamflow, correspondingly, does not produce significant groundwater recharge. The Rosamond Lake, Rogers Lake, and other playas occur within the watershed. Most of the watershed is tributary to the Rosamond Lake playa, which can spill onto the Rogers Lake playa. Streamflow discharges onto playas are dependent on the runoff and channel losses. During dry years, the infiltration capacity of the stream channels typically exceeds the runoff, and all the runoff infiltrates before reaching a playa. During sufficiently wet years, the runoff exceeds the infiltration capacity, and streamflow reaches a playa. The playa floodwater subsequently evaporates from the lake surface without producing significant groundwater recharge.

Big Rock Creek is a significant contributor to episodic playa flooding, and it was used as an analog of flooding from other streams within the Antelope Valley watershed. Big Rock Creek was used because useful measurements are available. The streamgaging site Big Rock Creek near Valyermo is located near the mountain front, and it has a 61-year record for the period 1949-2009. However, only the 57-year period 1949-2005 was used for this analysis. Based on the daily streamflow for that period, the channel-loss relation described by Equation C.32 was used to simulate discharge from Big Rock Creek onto the Rosamond Lake playa. The annual simulation results are listed in Table C.28 for water years 1949-2005. The table lists the annual streamflows for Big Rock Creek near Valyermo, and it lists the corresponding streamflow discharge onto the Rosamond Lake playa. Streamflows discharge onto the playa for 38 years during the 57-year simulation period, and the average annual discharge is 9,200 acre-ft/yr.

C.3.3.5 Groundwater Model

A groundwater model was used to evaluate the dynamics of groundwater flow within the mountain-block area of the Big Rock Creek watershed. The purpose was to identify the partitioning of groundwater outflow between mountain-front streamflow and underflow through the bedrock. The Big Rock Creek streamflow at the mountain front exhibits perennial baseflow, which is sustained by groundwater inflows to the channel within the mountain-block area. The model was used to assess what proportion of the groundwater outflow from the watershed is manifested as mountain-front streamflow.

C.3.3.5.1 Model Development

The Big Rock Creek watershed is underlain by fractured granitic rocks. The transmissivity of the rocks is represented by the fractures. However, specific-capacity data compiled from well completion reports and converted to transmissivity values and then to hydraulic conductivity values (Peter Leffler, 2007, written communication) indicate that transmissivity-producing fracturing has a limited extent below the land surface. Figure C.39 shows the relation between hydraulic conductivity and depth for bedrock wells within the San Gabriel Mountains. Shown also on the figure is an exponential relation representing the decay of conductivity with depth in the form

$$K = K_0 e^{-\lambda z} \quad (C.35)$$

where
K is the hydraulic conductivity at depth,
K_0 is the hydraulic conductivity at zero depth,
z is the depth below the land surface, and
λ is the decay constant.

The parameters values for the relation are 0.31 ft/d for K_0 and -0.0066 for λ. The decay constant for the relation represents a reduction in conductivity by one-half for each 100 ft. At a depth of 1,000 ft, the ratio K/K_0 is 0.001.

This exponential depth dependency most likely results from a system of horizontal and vertical fracturing within which the horizontal fractures provide much of the shallow transmissivity and the vertical fractures provide much of the deep transmissivity. This would occur if the horizontal fracturing is characterized by much longer length scales than the vertical fracturing, which is likely the case. The corresponding hydrogeologic conceptual model is that of a fracture-rock groundwater system characterized by a transmissive layer parallel to the land surface within the watershed. The layer is assumed to a depth of 1,000 ft below the land surface, and the hydraulic conductivity is assumed to decay exponentially with depth.

The model was constructed using the computer program FEMFLOW3D (Durbin and Berenbrock, 1985; Durbin and Bond, 1998; and Durbin, 2007). The program version used is that described by Durbin (2007). Figure C.40 shows the geographic domain of the groundwater system. As indicated on the figure, the domain includes regions where the granitic rocks crop out and regions where they are overlain by alluvial deposits. However, the model represents only the granitic rocks, even where they are overlain by alluvium. Figure C.41 shows a plan view of the finite element mesh, and Figure C.42 shows an oblique view. As shown on the oblique view, the mesh consists of five element layers. Each layer has a constant thickness over the model domain, but the respective layers range in thickness from 100 to 250 ft. The cumulative thickness everywhere is 1,000 ft. The mesh contains about 23,000 nodes and 37,000 elements.

The boundary conditions on the three-dimensional model domain include no-flow surfaces, a specified-head surface, specified-head lines, and a specified-flux surface. The bottom surface and lateral surfaces are no-flow boundaries. The top surface is a specified-head surface where it is overlain by alluvium, and the specified heads are the groundwater levels within the alluvium as represented by Leighton and Phillips (2003). The top surface is a specified-flux boundary where it represents the outcrop of granitic rocks, and the specified fluxes represent precipitation recharge. The stream channels within the watershed are specified-heads, and the specified heads along a channel are the channel elevation.

The precipitation recharge has both geographic and temporal components. The recharge has a geographic distribution that is proportional to the geographic distribution of average annual precipitation. The recharge has a temporal distribution that is proportional to the average distribution of monthly precipitation for the precipitation stations having a continuous record for the 57-year period 1949-2005. Correspondingly, each year in a simulation has the same monthly distribution of recharge as listed in Table C.29. The average annual precipitation represents an annual precipitation volume on the model domain of about 42,000 acre-ft, and the recharge was assumed to equal 20 percent of the precipitation. The recharge percentage used in the model may be higher than the actual value, but the assumption is intended to represent the upper end of the continuum of possible mountain-block recharge.

The boundary condition for the streams is uni-directional, which means that only outward fluxes can occur. If the groundwater head is higher than the stream channel, groundwater discharges into the channel. However, if the groundwater head is lower than the stream channel, streamflow does not recharge into the groundwater system. This condition is sometimes is referred to as a "drain" boundary. The model does not represent rainfall or snowmelt runoff, and the boundary condition simulates the groundwater gains to stream channels.

The aquifer parameters assigned to the model include hydraulic conductivity, specific storage, and specific yield. The groundwater system was considered to be isotropic and laterally homogeneous with respect to hydraulic conductivity. However, the system was considered to be vertically heterogeneous based on the conductivity-depth relation shown on Figure C.39. The specific storage was assumed to equal 10^{-6} ft^{-1} based tabulations in Domenico (1972) and Streltsova (1977), and the specific yield was assumed to equal 0.03 based on tabulations in Morris and Johnson (1967) and Hamill and Bell (1986).

C.3.3.5.2   Model Simulations

Five-year simulations were made with the model using one-month time steps. Based on a steady-state initial condition with respect to the average precipitation recharge, transient state conditions were simulated for the temporal distribution of recharge. However, only the last year of simulation was examined with respect to the partitioning of groundwater outflow to streamflow and underflow. The initial four years was simulated to transition from the steady-state condition to the identical periodicity of a long-term transient-state condition. The last time step characterizes that periodicity.

Figure C.43 shows the simulation results in terms of annual hydrographs of groundwater outflow for the Big Rock Creek watershed. The figure shows hydrographs of groundwater outflow to the stream and the total groundwater outflow. The streamflow equals 77 percent of the total groundwater outflow, which means that the underflow component of the groundwater outflow equals 30 percent of the baseflow component.

C.4.0   Conclusions

Groundwater recharge was estimated using three different approaches. These were the water-balance, chloride, and yield-modeling approaches. The water-balance approach involved estimating the precipitation, evapotranspiration, and playa flooding within the Antelope Valley watershed. The resulting estimated average annual recharge is 55,000 acre-ft. The chloride approach involved estimating the precipitation chloride, groundwater chloride, and average annual precipitation volume. The resulting estimated average annual recharge is 58,000 acre-ft. The yield-modeling approach involved developing precipitation-runoff and precipitation-groundwater relations. The resulting estimated average annual recharge is 56,400 acre-ft. The three methodologies yielded relatively consistent estimates of recharge, but the yield modeling approach probably is the most reliable. Correspondingly, Table C.28 should be used to characterize the natural groundwater recharge within the Antelope Valley watershed.

These three recharge estimates compare well with estimates developed by the U.S. Geological Survey. Durbin (1978) developed a groundwater model for the Antelope Valley basin. Recharge was estimated for input to the model using a yield-modeling approach similar to that described above. The resulting recharge estimate was 40,700 acre-ft/yr. Leighton and Phillips (2003) developed a second groundwater model. While they started with the Durbin (1978) recharge estimate, the final recharge used in the model was 30,300 acre-ft/yr.

C.5 References Cited

Avon, L., and Durbin, T. J., 1992, Evaluation of the Maxey-Eakin method for estimating recharge to ground-water basins in Nevada: Journal American Water Resources Association, vol. 30, no. 1, p. 99-111.

Barry, R. G., 1981, Mountain weather and climate: Methuen, London.

Baugh, W. M., and Groeneveld, D. P., 2006, Broadband vegetation index performance evaluated for a low-cover environment: International Journal Remote Sensing, vol. 27, pp. 4715-4730.

Benson, M. A., 1962a, Plotting positions and economics for engineering planning: Journal Hydraulics Division, vol. 88, pp.57-71.

Benson, M. A., 1962b, Evolution of methods for estimating occurrence of floods: U. S. Geological Survey Water-Supply Paper 1580A.

Burkham, D.E., 1970, Depletion of streamflow by infiltration in the main channels of the Tucson Basin, southeastern Arizona: U.S. Geological Survey Water-Supply Paper 1939-B, 36 p.

California Department of Water Resources, 2003, California's groundwater: Bulletin 118, http://www.groundwater.water.ca.gov/ bulletin118/update2003/index.cfm.

California Department of Water Resources, 2007, California Irrigation Management Information System data: http://www.cimis.water.ca.gov/cimis/data.jsp.

California Spatial Information Library, 2007, Calview Landsat 7 images: http://archive.casil.ucdavis.edu/casil/remote_sensing/landsat/landsat7/calview/.

Chong, D. L. S., Mougin, E., and Gastellu-Etchegorry, J. P., 1993, Relating the global vegetation index to net primary productivity and actual evaporation over Africa: International Journal Remote Sensing, vol. 14, pp. 1517-1546.

Claassen, H. C., Reddy, M. M., and Halm, D. R., 1986, Use of chloride in determining hydrologic-basin water budgets—A 3-year case study in the San Juan Mountains, Colorado, USA: Journal Hydrology, no. 85, pp. 49-71.

Daly, C., Nielson, R. P., and Phillips, D. L., 1994, A statistical-topographic model for mapping climatological precipitation over mountainous terrain: Journal Applied Meteorology, vol. 33, pp. 140-158.

Dettinger, M. D., 1989, Reconnaissance estimates of natural recharge to desert basins in Nevada using chloride-balance calculations: Journal Hydrology, vol. 7, pp. 178-197.

Dettinger, M. D., Redmond, K., and Cayan, D., 2004, Winter orographic precipitation ratios in the Sierra Nevada—Large-scale atmospheric circulations and hydrologic consequences: Journal Hydrometeorology, vol. 5, pp. 1102-1116.

Donovan, D. J., and Katzer, T., 2000, Hydrologic implications of greater ground-water recharge to Las Vegas Valley, Nevada: Journal American Water Resources Association, vol. 36, no. 5, pp. 1133-1148.

Domenico, P. A., 1972, Concepts and models in groundwater hydrology: McGraw-Hill, New York.

Doorenbos, J., and Pruitt, W. O., 1977, Guidelines for predicting crop water requirements: Food and Agricultural Organization Irrigation and Drainage Paper 24.

Durbin, T.J., 1978, Calibration of a mathematical model of the Antelope Valley groundwater basin, California: U.S. Geological Survey Water-Supply Paper 2046, 51 p.

Durbin, T. J., and Berenbrock, C., 1985, Three-dimensional simulation of free-surface aquifers by the finite-element method: U. S. Geological Survey Water-Supply Paper 2270, pp. 51-67.

Durbin, T. J., Bond, L. D., 1998, FEMFLOW3D—A finite-element program for the simulation of three-dimensional aquifer, Version 1.0: U. S. Geological Survey Open-File Report 97-810.

Durbin, T. J., 2007, FEMFLOW3D—A finite-element program for simulation of three-dimensional aquifers, Version 3.0: Timothy J. Durbin, Inc.

Eagleson, P. S., 1982, Ecological optimality in water-limited natural soil-vegetation systems. 1. Theory and hypothesis: Water Resources Research, vol. 18, no. 2, pp. 325-340.

Eagleson, P. S., 2002, Echohydrology—Darwinian expressions of vegetation form and function: Cambridge University Press, Cambridge, England.

ESRI, 2001, ArcGIS 9—Using ArcGIS spatial analyst: ESRI, Redlands, Calif.

French, R. H., Miller, J. J., and Dettling, C. R., 2005, Estimating playa lake flooding—Edwards Air Force Base, California USA: Journal Hydrology, no. 306, pp. 146-160.

Goodrich, D. C., Williams, D. G., Unkrich, C. L., Hogan, J. F., Scott, R. L., Hultine, K. R., Pool, D., Coes, A. L., and Miller, S., 2004, Comparison of methods to estimate ephemeral channel recharge—Walnut Gulch, San Pedro River basin, Arizona in Hogan, J. F., Phillips, F. M., and Scanlon, B. R., Groundwater recharge in a desert environment—The southwest United States: American Geophysical Union Water Science and Application 9, pp. 77-100.

Hamill, L., and Bell, F. G., 1986, Groundwater resource development: Butterworths, London.

Hedman, E. R., 1970, Mean annual runoff as related to channel geometry of selected streams in California: U. S. Geological Survey Water-Supply Paper 1999-E.

Hedman, E. R.; Moore, D. O.; Livingston, R. K., 1972, Selected streamflow characteristics as related to channel geometry of perennial streams in Colorado: U. S. Geological Survey Open-File Report 72-160.

Hedman, E. R., and Osterkamp, W. R., 1982, Streamflow characteristics related to channel geometry of streams in western United States: U. S. Geological Survey Water-Supply Paper 2193.

Huete, A. R., and Liu, H. Q., 1994, An error and sensitivity analysis of the atmospheric and soil-correcting variants of *NDVI* for the MODIS-EOS: Transactions Geoscience and Remote Sensing, vol. 32, pp. 897-905.

Irving, W. M., 1982, Chloride ion concentrations as an aid to estimating recharge to the Woburn sands: Quarterly Journal Engineering Geology, no. 15, pp. 47-54.

Izbicki, J. A., Radyk, J., and Michel, R. L., 2000, Water movement through a thick unsaturated zone underlying an intermittent stream in the western Mojave Desert, southern California USA: Journal Hydrology, no. 238, pp. 194-217.

Johnston, C. D., 1987, Distribution of environmental chloride in relation to subsurface hydrology: Journal Hydrology, no. 94, pp. 67-88.

Kerr, Y. H., Imbernon, J., Dedieu, G., Hautecoeur, O., Lagouarade, J. P., and Seguin, B., 1989, HOAA AVHRR and its uses for rainfall and evapotranspiration monitoring: International Journal Remote Sensing, vol. 10, 847-854.

Kustas, W. P., Perry, E. M., Doraiswamy, P. C., and Moran, M. S., 1994, Using satellite remote sensing to extrapolate evapotranspiration estimates in time and space over a semiarid rangeland basin: Remote Sensing of Environment, vol. 49, pp. 275-286.

Lee, C. H., 1912, An intensive study of the water resources of a part of Owens Valley, California: U.S. Geological Survey Water-Supply Paper 294, 135 p.

Leighton, D. A., and Phillips, S. P., 2003, Simulation of ground-water flow and land subsidence in the Antelope Valley ground water basin, California: U. S. Geological Survey Water-Resources Investigations Report 03-4016.

Leopold, L. B., and Maddock, T., 1953, The hydraulic geometry of stream channels and some physiographic implications: U. S. Geological Survey Professional Paper 252.

Leopold, L. B., Wolman, M. G., and Miller, J. P., 1964, Fluvial process in geomorphology: W. H. Freeman and Company, San Francisco.

Linsley, R. K., Kohler, M. A., and Paulhus, J. L. H., 1982, Hydrology for engineers, Third edition: McGraw-Hill Book Company, New York.

Liu, H. Q., and Huete, A. R., 1995, A feedback based modification on the *NDVI* to minimize canopy background and atmospheric noise: Transactions Geoscience and Remote Sensing, vol. 33, pp. 457-465.

Mandel, S., and Shiftan, Z. L., 1981, Groundwater resources—Investigation and development: Academic Press, New York.

Maxey, G. B., and Eakin, T. E., 1949, Ground water in the White River Valley, White Pine, Nye, and Lincoln counties, Nevada: Nevada State Engineer Bulletin 8.

Morris, D. A., and Johnsom, A. I., 1967, Summary of hydrologic and physical properties of rock and soil materials, as analyzed by the hydrologic laboratory of the U. S. Geological Survey, 1948-1960: U. S. Geological Survey Water Supply Paper 1839D.

Niswonger, R. G., Prudic, D. E., Pohll, G., and Constantz, J., 2004, Incorporating seepage losses into the unsteady streamflow equations for simulating intermittent flow along mountain front streams: Water Resources Research, vol. 41, W06006, 16 p.

Noy-Meir, I., 1973, Desert ecosystems—Environment and producers: Annual Review of Ecology and Systematics, vol. 4, pp. 25-44.

Oregon Climatic Center, 2007, PRISM data index: http://www.ocs.orst.edu/index.html.

Osterkamp, W. R., and Hedman, E. R., 1982, Perennial-streamflow characteristics related to channel geometry and sediment in Missouri River basin: U. S. Geological Survey Professional Paper 1242.

Osterkamp, W. R., Hedman, E. R., and Wiseman, A. G., 1982, Geometry, basin-characteristics, discharge, and particle-size data from gaged stream-channel sites, Western United States: U. S. Geological Survey Open-File Report 82-93.

Pandey, G. D., Cayan, D., and Georgakakos, K., 1999, Precipitation structure in the Sierra Nevada of California: Journal Geophysical Research, vol. 104, pp. 12 019-12 030.

Pierrehumbert, R., 1984, Linear results on the barrier effects of mesoscale mountains: Journal Atmospheric Sciences, vol. 41, pp. 1356-1367.

Rodriguez-Iturbe, I., and Porporato, A., 2004, Echohydrology of water-controlled ecosystems: Cambridge University Press, Cambridge, England.

Ronan, A. D., Prudic, D. E., Thodal, C. E., and Constantz, J., 1998, Field study of diurnal temperature effects of infiltration and variably saturated flow beneath an ephemeral stream: Water Resources Research, vol. 34, pp. 2137-2153.

Rouse, J. W., Haas, R. H., Schell, J. A., and Deering, D. W., 1974, Monitoring vegetation systems in the Great Plains with ERTS: Proceedings Third ERTS Symposium, NASA SP-351, pp. 309-317.

Russell, C. E., and Minor, T., 2002, Reconnaissance estimates of recharge based on an elevation-dependent mass-balance approach: Desert Research Institute Publication No. 45164.

Seevers, P. M., and Ottman, R. W., 1994, Evapotranspiration estimating using normalized difference vegetation index transformation of satellite data: Hydrological Sciences Journal, vol. 39, pp. 333-345.

Streltsova, T. D., 1977, Storage properties in fractured formations, in Dilamarter, R. R., and Csallany, S. C., eds., Hydrologic problems in karst regions: University of Kentucky, pp. 188-192.

Szilagyi, J., 2002, Vegetation indices to aid areal evapotranspiration estimations: Journal Hydrologic Engineering, vol. 7, pp. 368-372.

Szilagyi, J., Parlange, M. B., Rundquist, D. C., and Gosselin, D. C., 1998, *NDVI* relationship to monthly evaporation: Geophysical Research letters, vol. 25, pp. 1753-1756.

Tyler, S. W., McKay, W. A., and Mihevc, T. M., 1992, Assessment of soil moisture movement in nuclear subsidence craters: Journal Hydrology, pp. 159-181.

Tyler, S. W., Chapman, J. B., Conrad, S. H., Hammermiester, D. P., Blout, D. O., Miller, J. J., Sullt, M. J., and Ginanni, J. M., 1996, Soil-water flux in the southern Great Basin—Temporal and spatial variations over the last 120,000 years: Water Resources Research, vol. 32, pp. 1481-1499.

U. S. Geological Survey, 2007a, National elevation dataset: http://seamless.usgs.gov/Website/Seamless/products/1arc.asp.

U. S. Geological Survey, 2007b, National water information system streamflow data: http://waterd   ata.usgs.gov/ca/nwis/sw.

U. S. Geological Survey, 2007c, Earth resources observation and science: http://edcsns17.cr.usgs.gov/EarthExplorer/.

U. S. Geological Survey, 2007d, National water information system water-quality data: http://nwis.waterdata.usgs.gov/ca/nwis/qwdata.

Vacher, H. L., and Ayers, J. F., 1980, Hydrology of small oceanic islands—Utility of an estimate of recharge inferred from the chloride concentration of the freshwater lenses: Journal Hydrology, no. 45, pp. 21-37.

Western Regional Climatic Center, 2009, California climatic data archive: http://www.calclim.dri.edu/index.html.
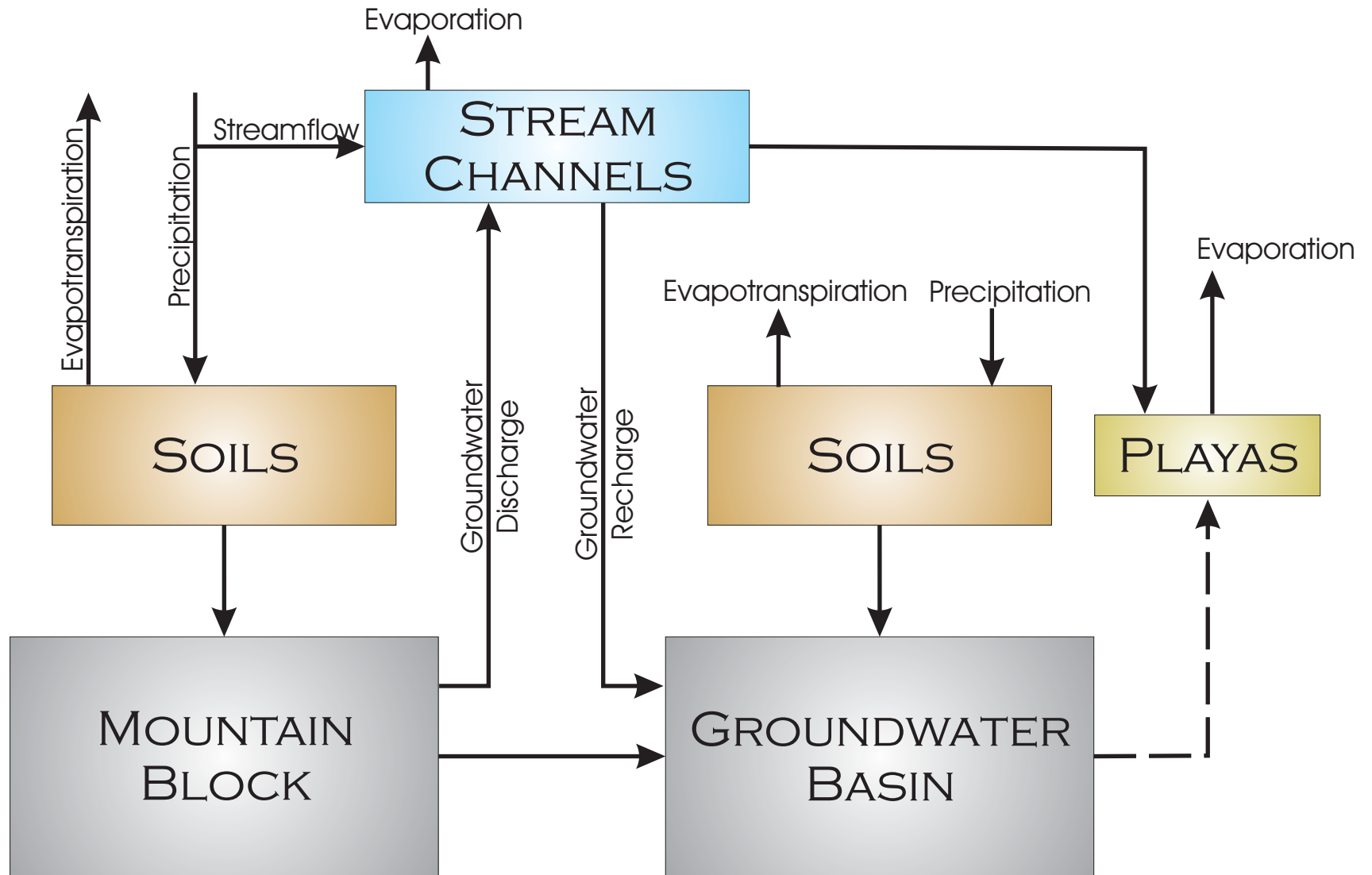
Figure C.1 Occurrence of Natural Recharge from Precipitation
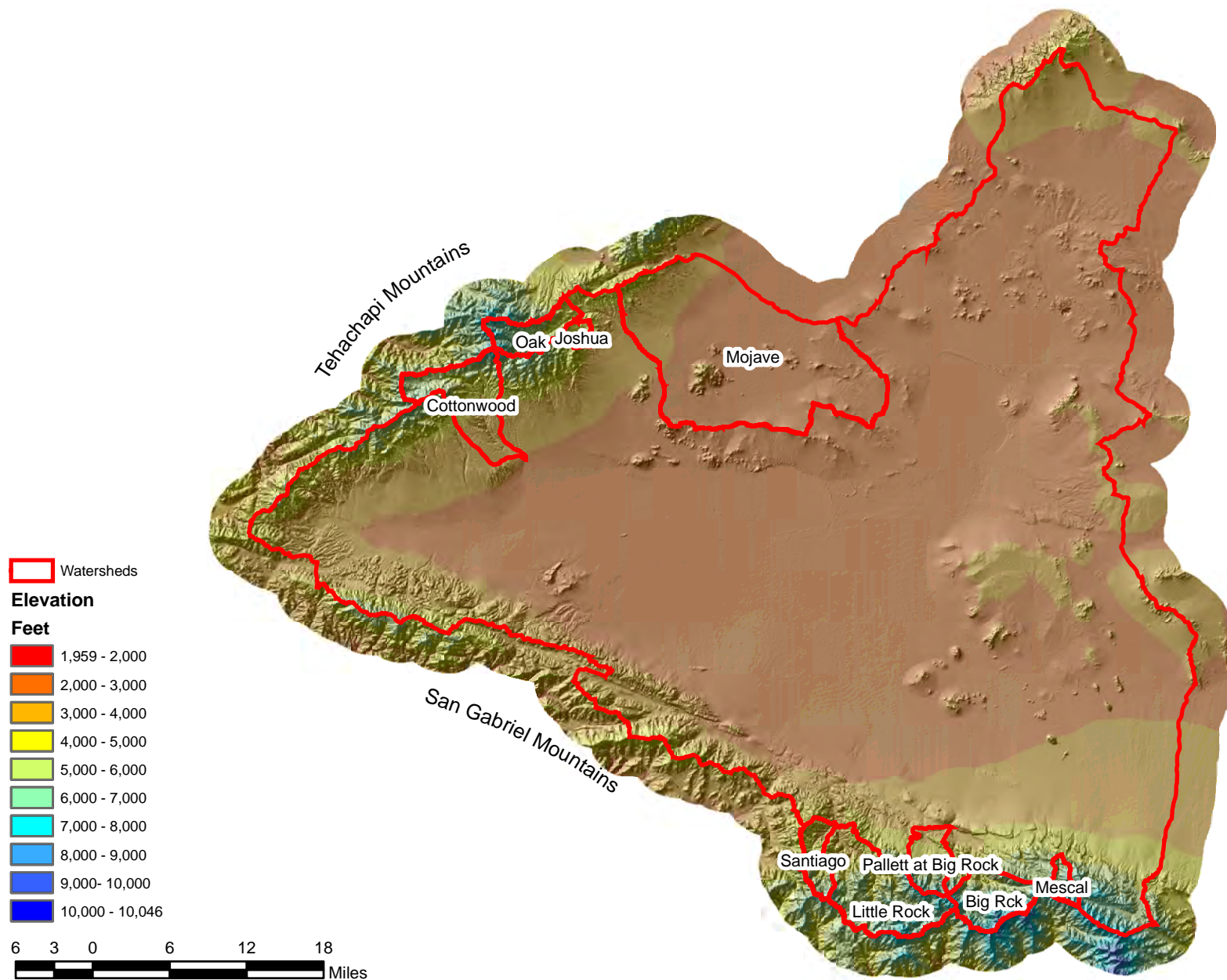
Figure C.2 Topography of the Antelope Valley Watershed
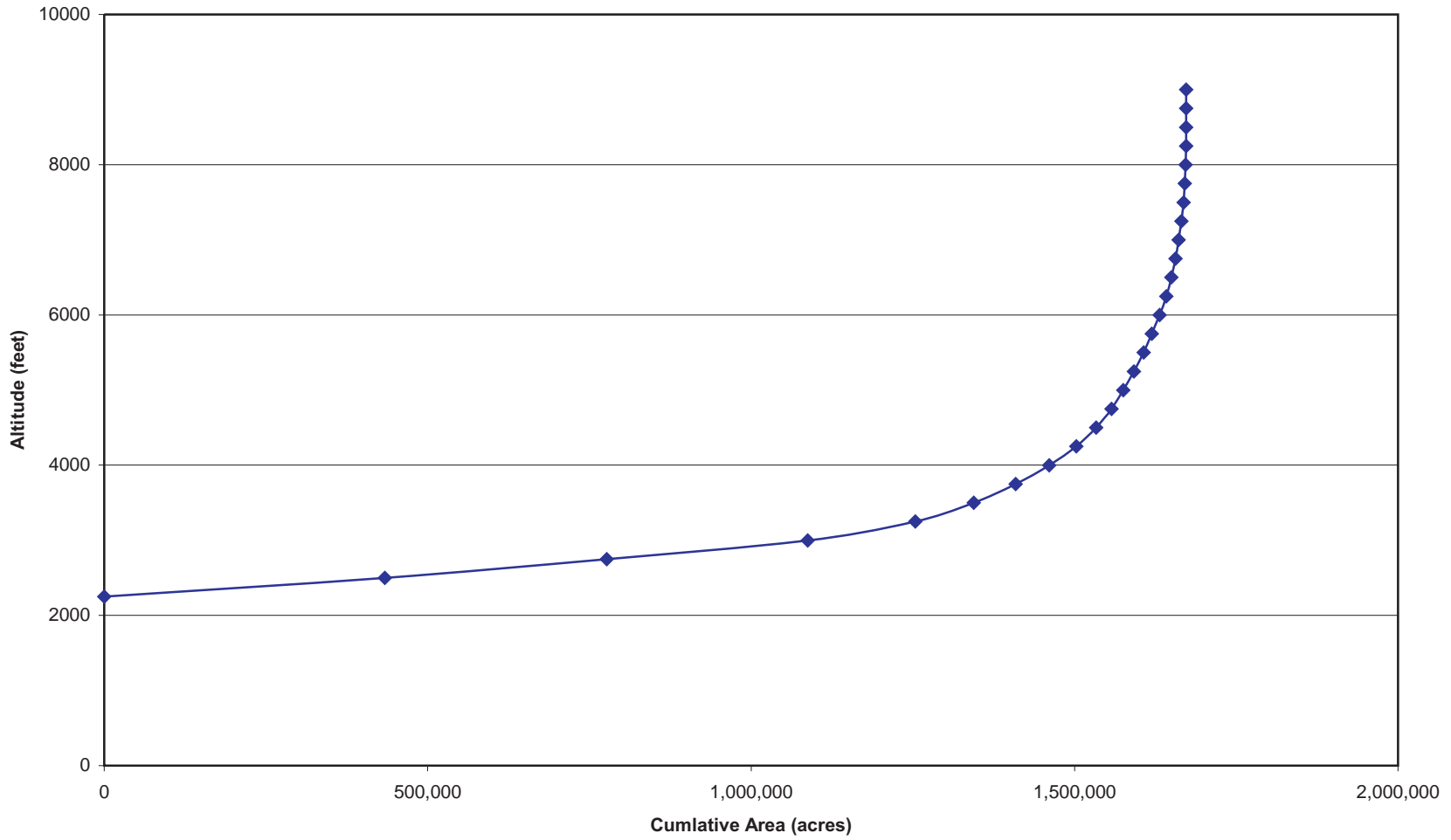
Figure C.3 Cumulative Distribution of Altitude For Antelope Valley

Big Rock Creek Near Valyermo
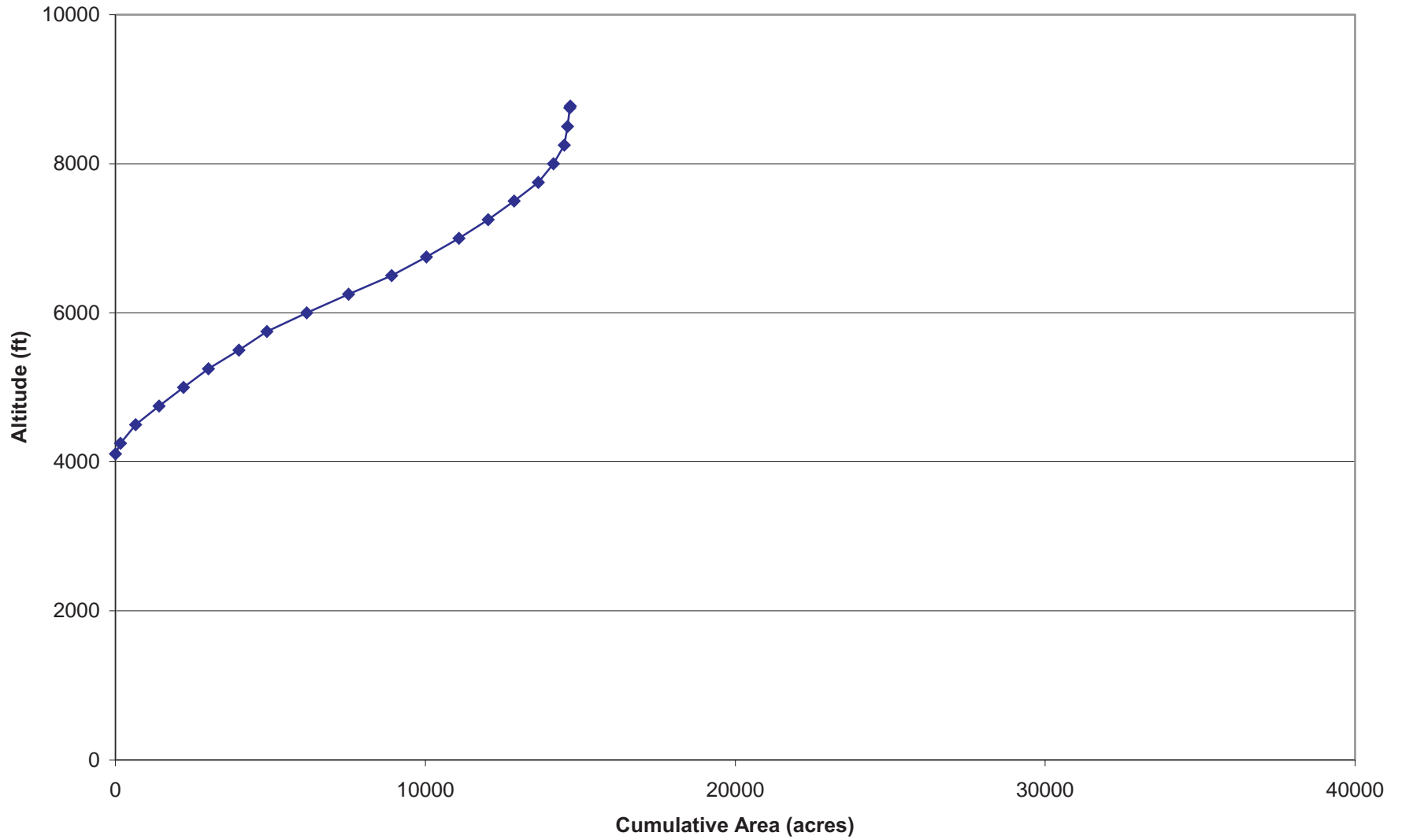
Figure C.4a Cumulative Distribution of Altitude For Big Rock Creek

Little Rock Creek Above Reservoir
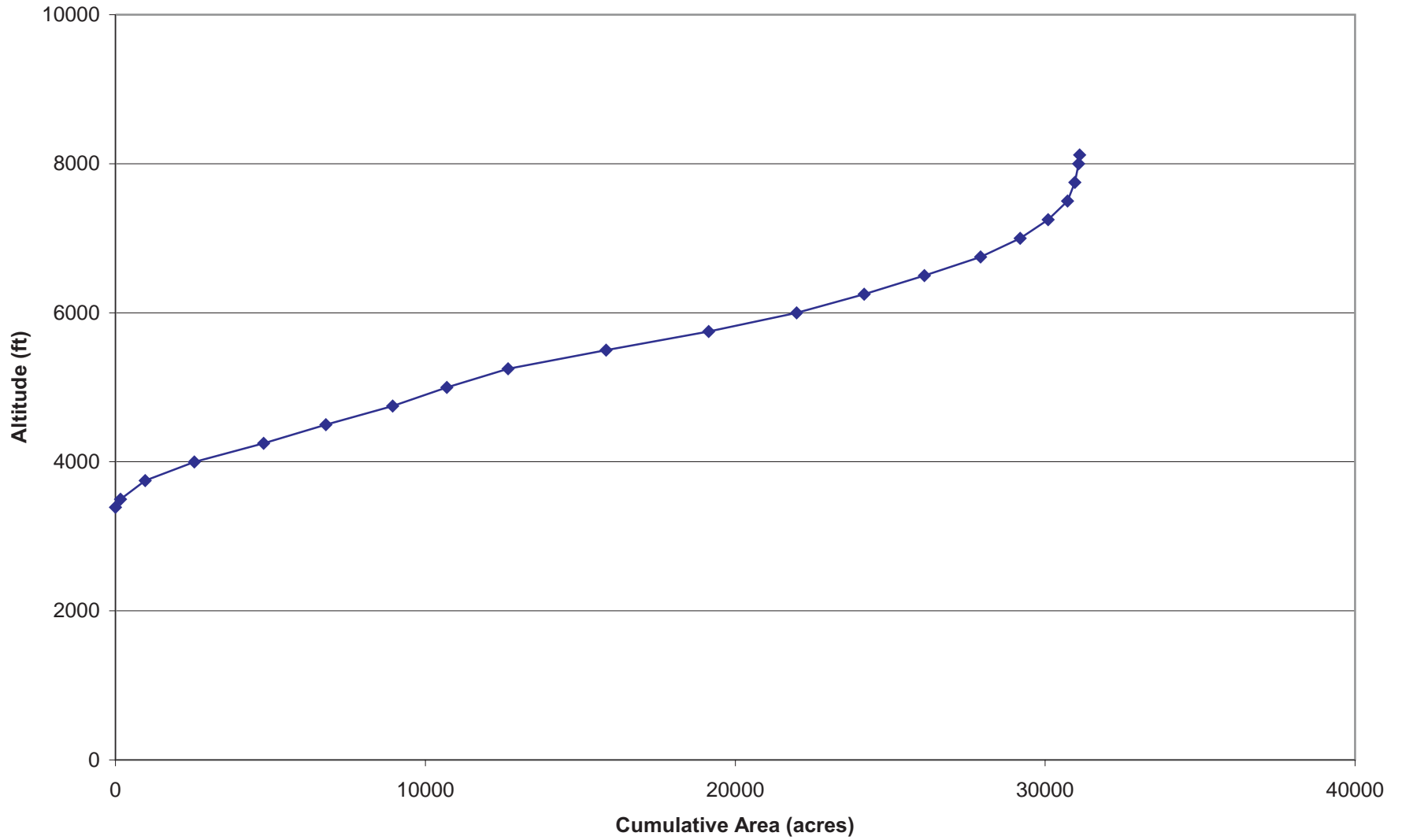
Figure C.4b Cumulative Distribution of Altitude For Little Rock Creek

Mescal Creek
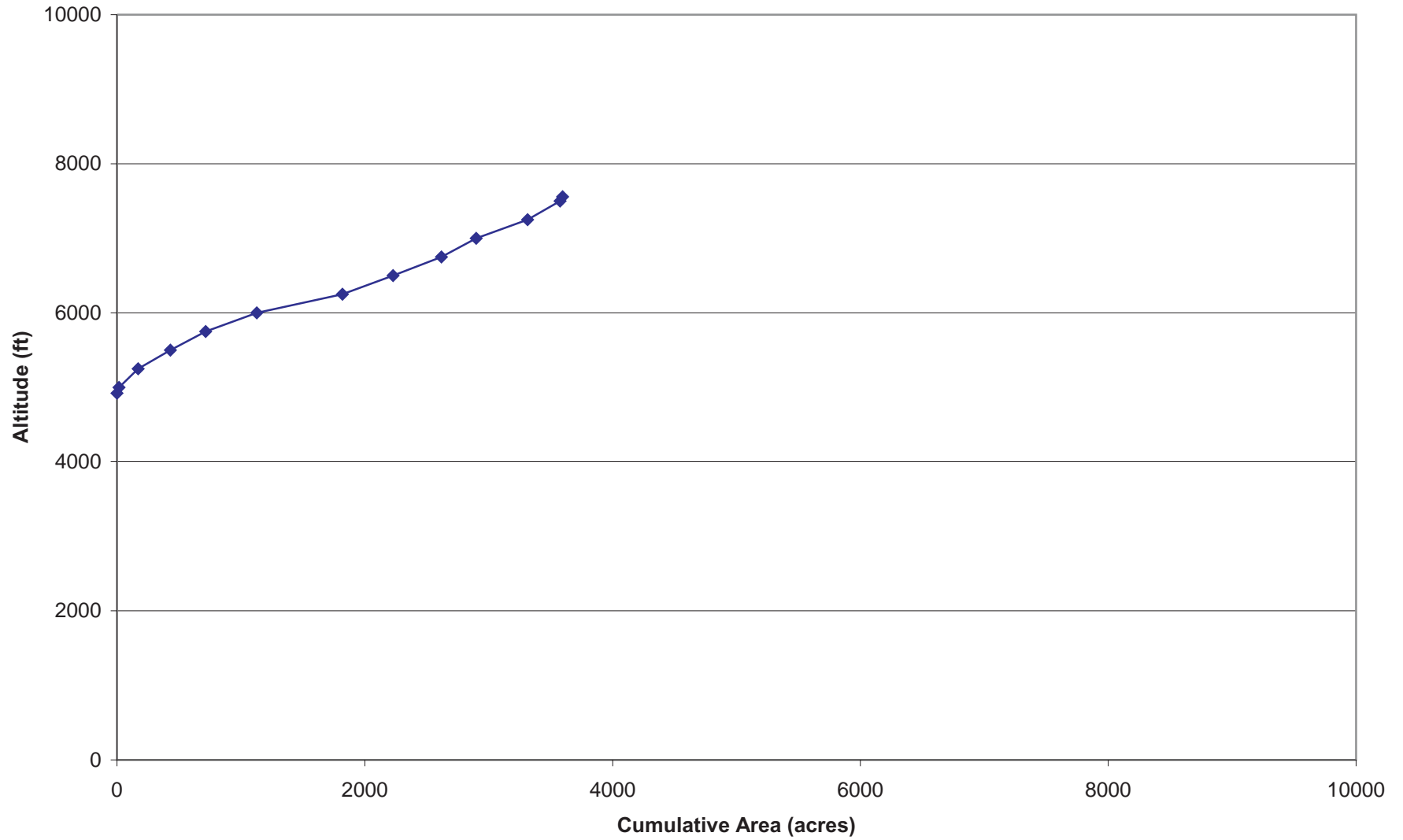
Figure C.4c Cumulative Distribution of Altitude For Mescal Creek

Pallett Creek
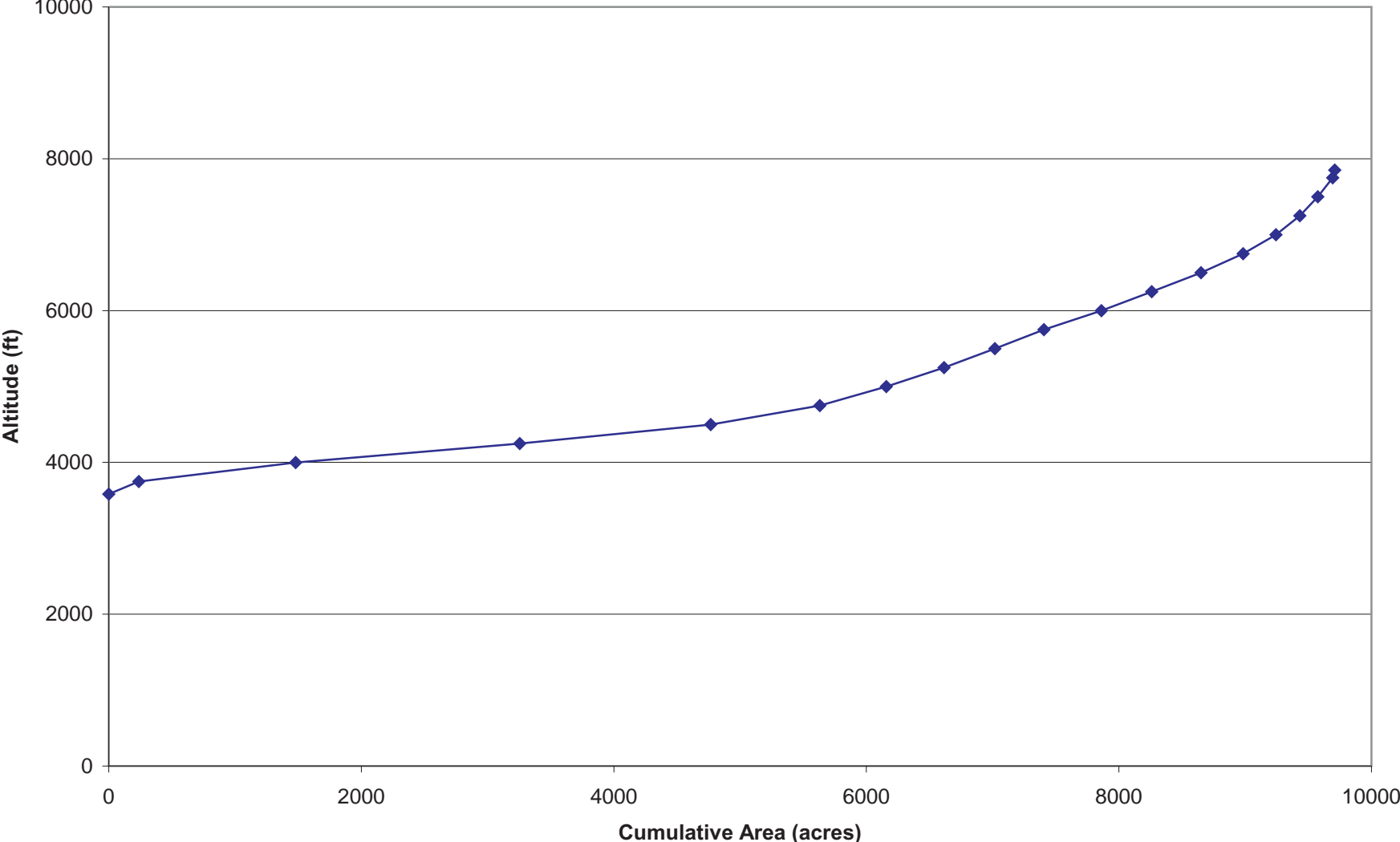
Figure C.4d Cumulative Distribution of Altitude For Pallett Creek
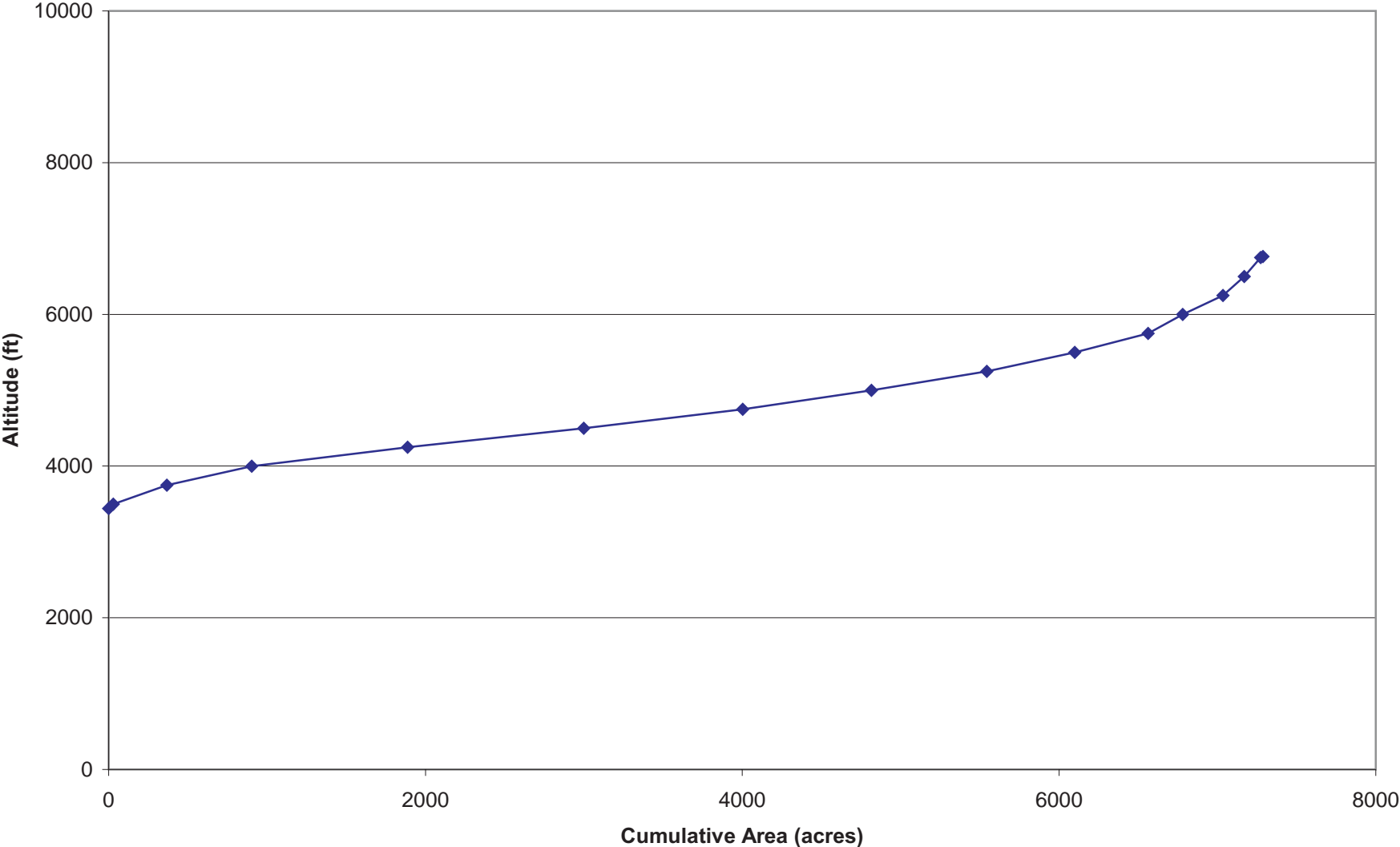
Figure C.4e Cumulative Distribution of Altitude For Santiago Canyon Creek
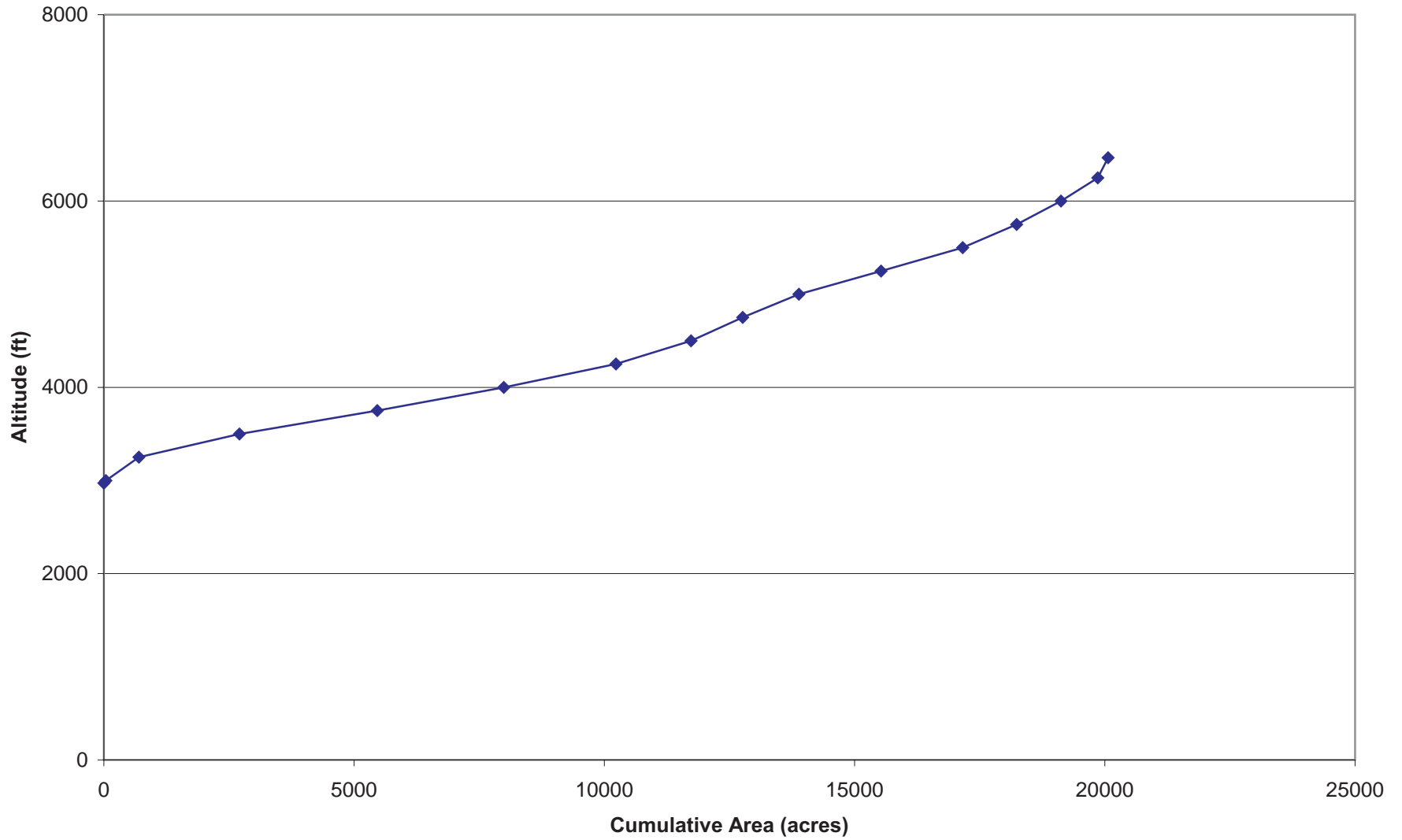
Figure C.5a Cumulative Distribution of Altitude For Cottonwood Creek
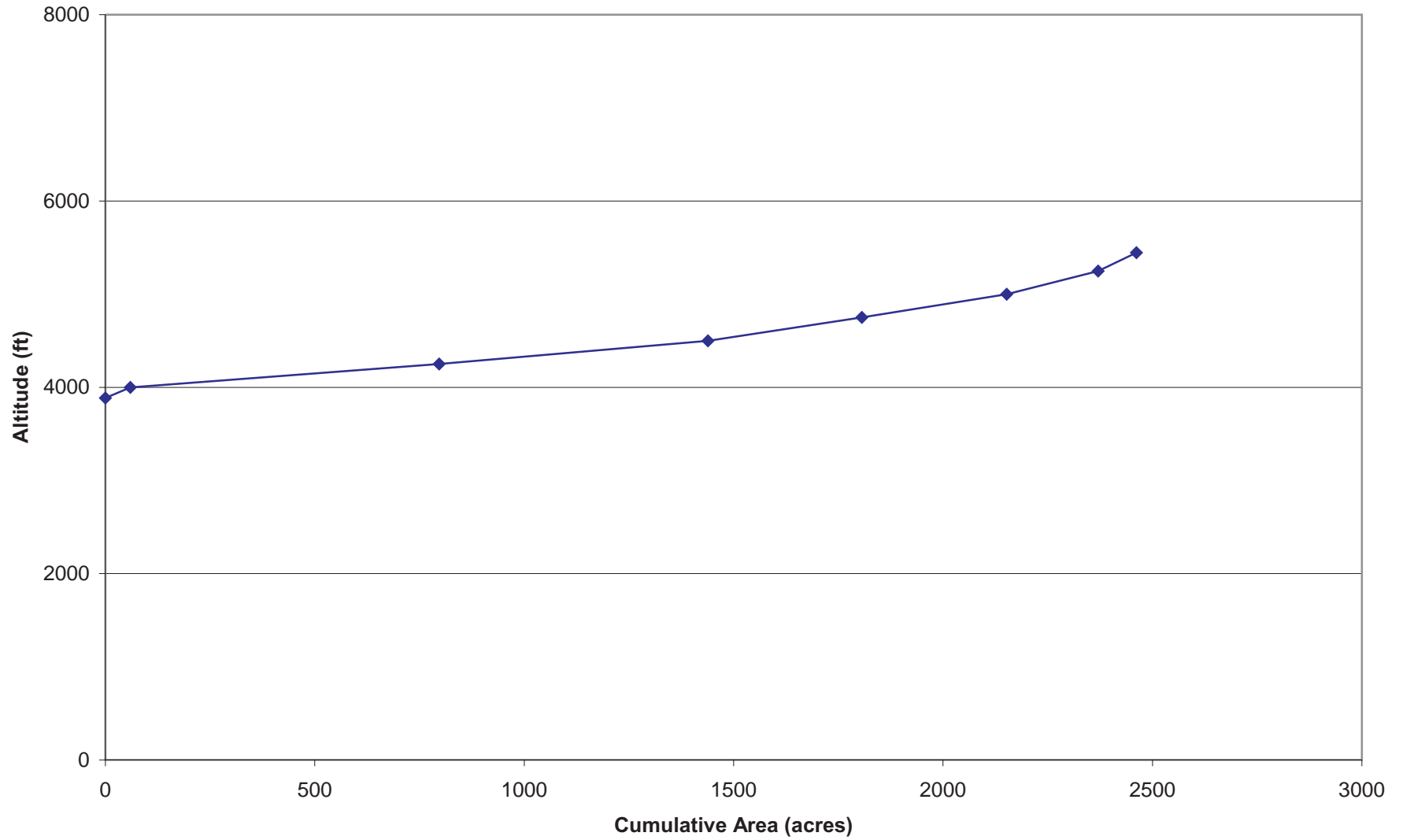
Figure C.5b Cumulative Distribution of Altitude For Joshua Creek

Mojave Creek at Forbes Avenue
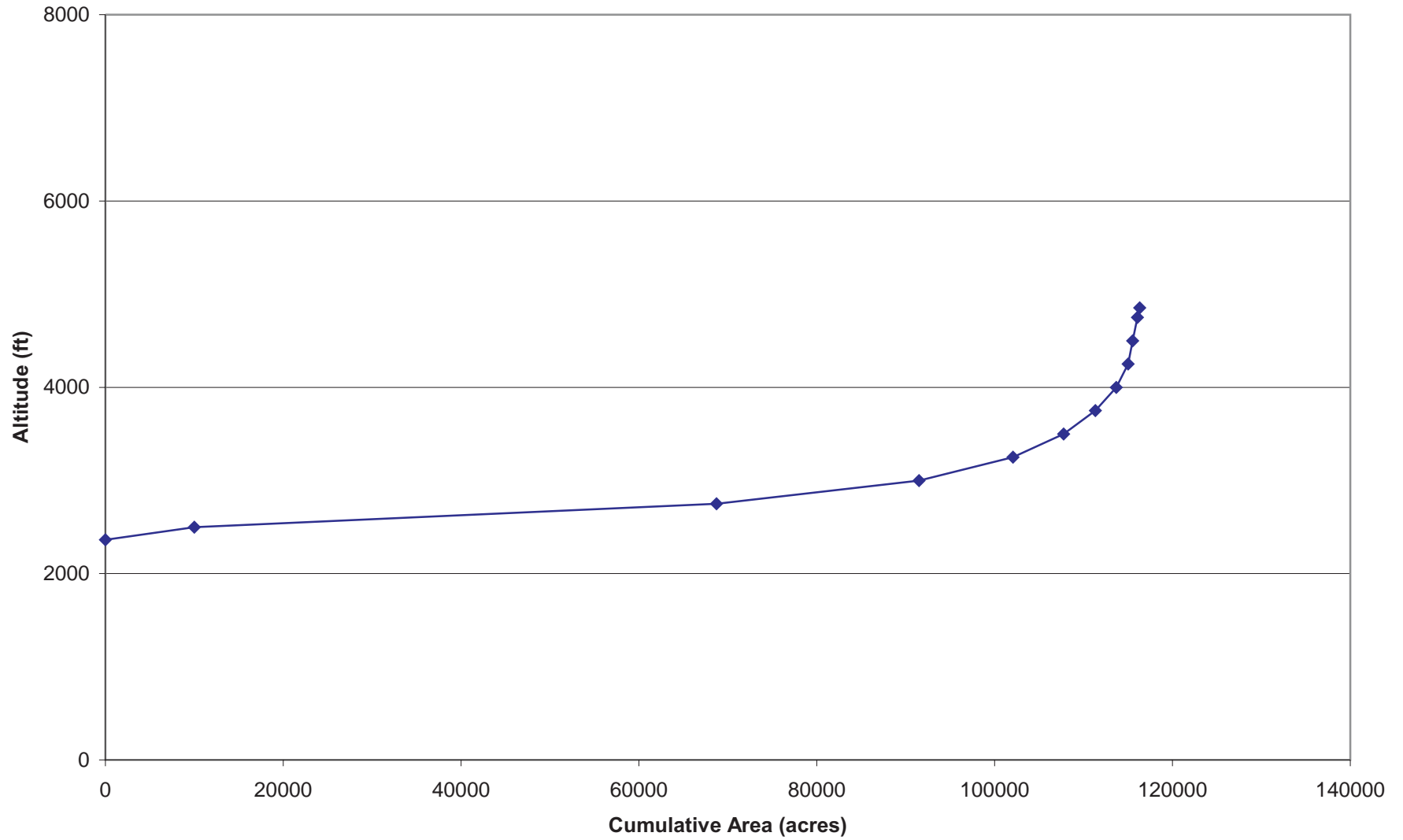
Figure C.5c Cumulative Distribution of Altitude For Mojave Creek
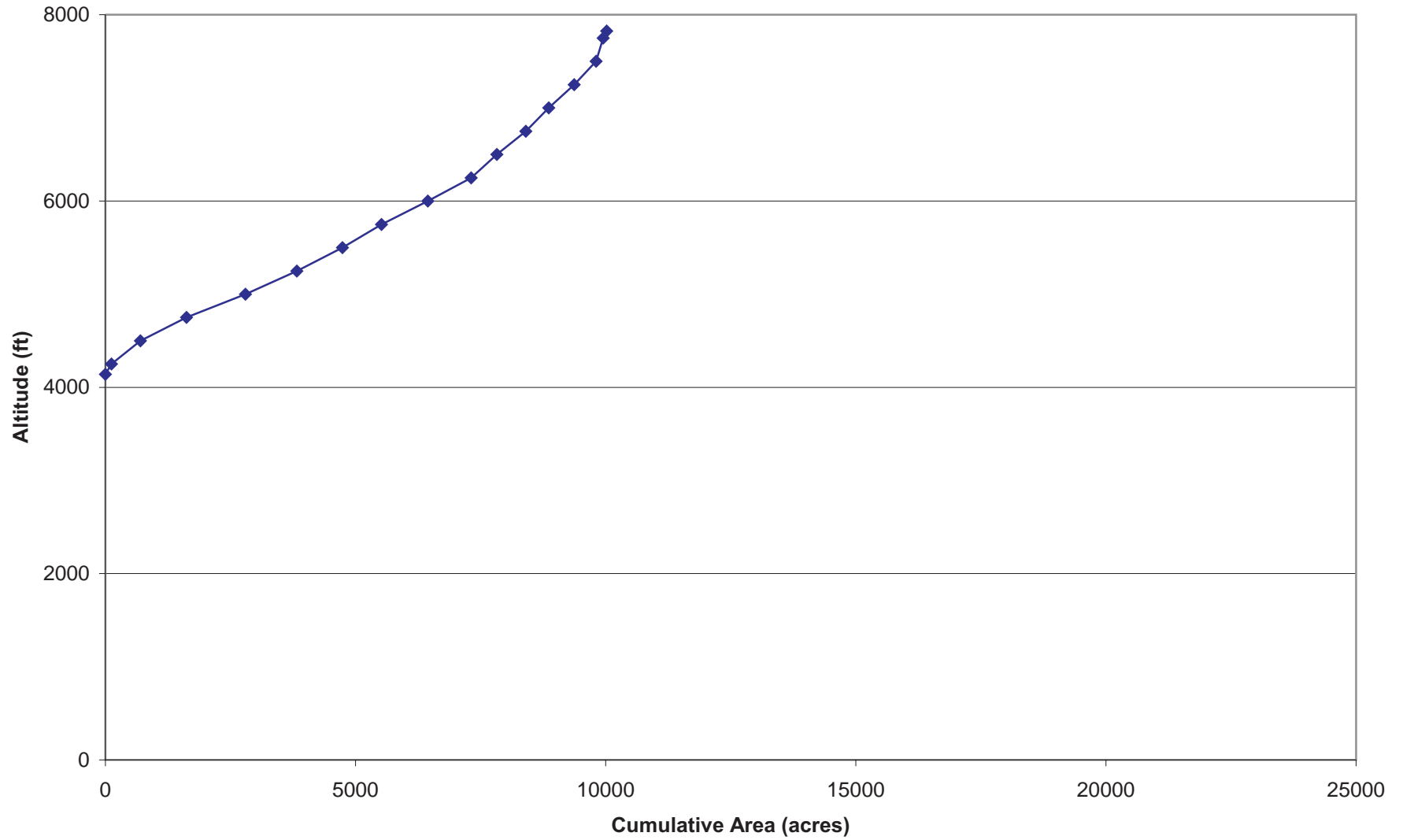
Figure C.5d Cumulative Distribution of Altitude For Oak Creek
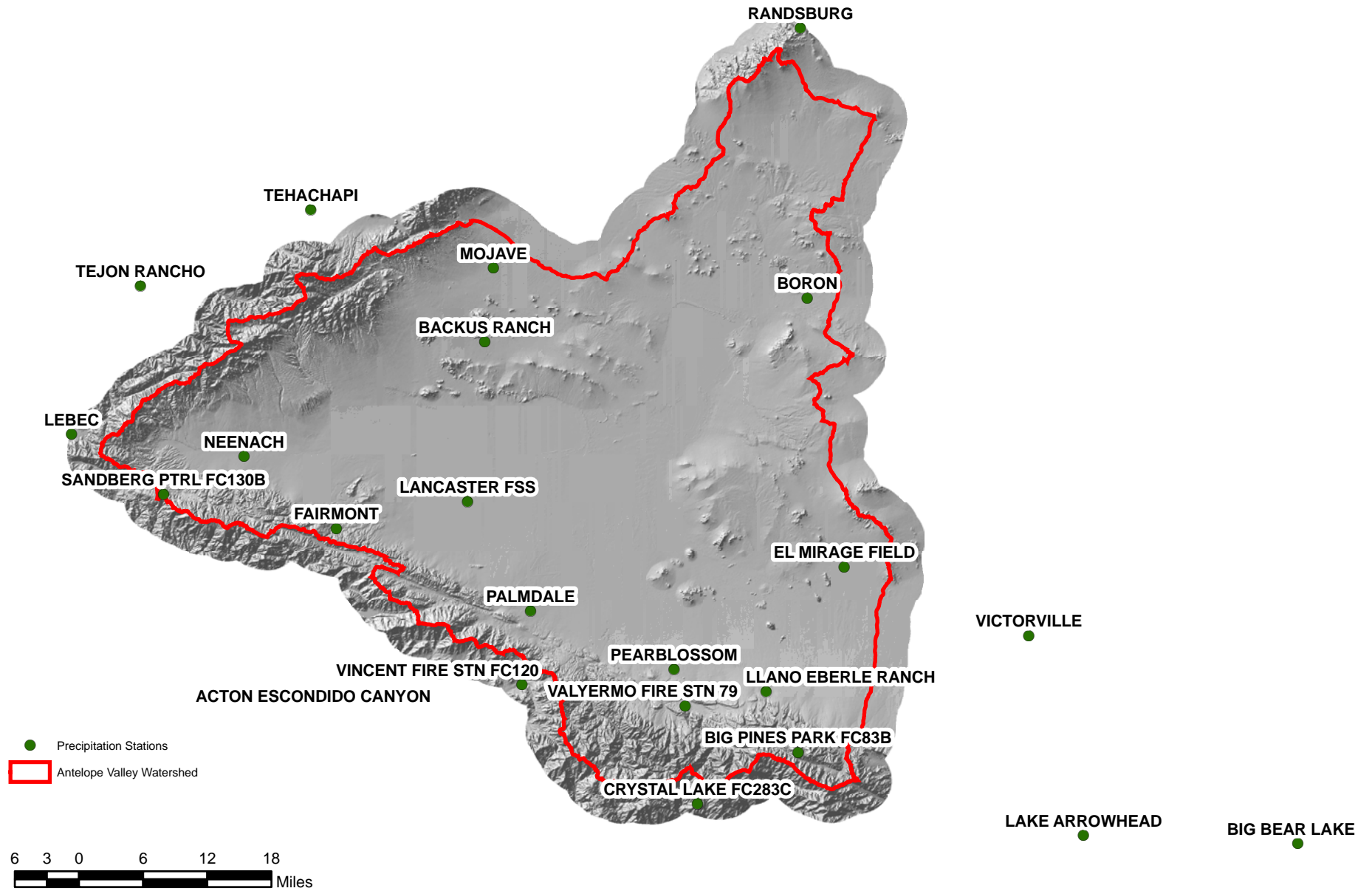
Figure C.6 Precipitation Stations Within and Nearby Antelope Valley

RANDSBURG

TEHACHAPI

MOJAVE

TEJON RANCHO

BORON

BACKUS RANCH

LEBEC

NEENACH

SANDBERG PTRL FC130B

LANCASTER FSS

FAIRMONT

EL MIRAGE FIELD

PALMDALE

VICTORVILLE

PEARBLOSSOM

VINCENT FIRE STN FC120

LLANO EBERLE RANCH

ACTON ESCONDIDO CANYON

VALYERMO FIRE STN 79

BIG PINES PARK FC83B

Precipitation Stations

Antelope Valley Watershed

CRYSTAL LAKE FC283C

LAKE ARROWHEAD

BIG BEAR LAKE

6 3 0   6   12   18

Miles

Acton Escondido

Figure C.7a Double-Mass Plot of Annual Precipitation at Acton Escondido

Backus Ranch
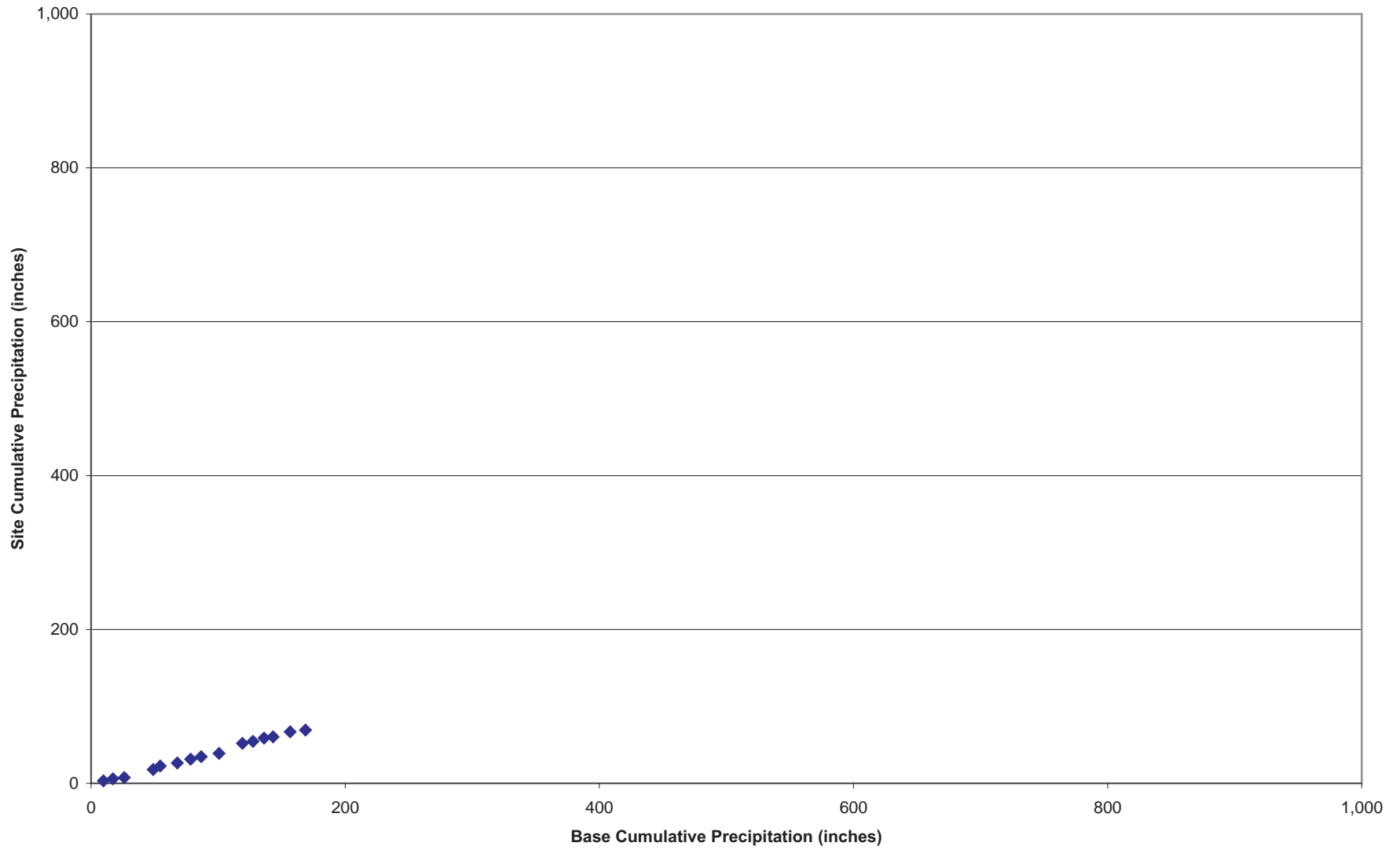
Figure C.7b Double-Mass Plot of Annual Precipitation at Backus Ranch

Big Bear Lake
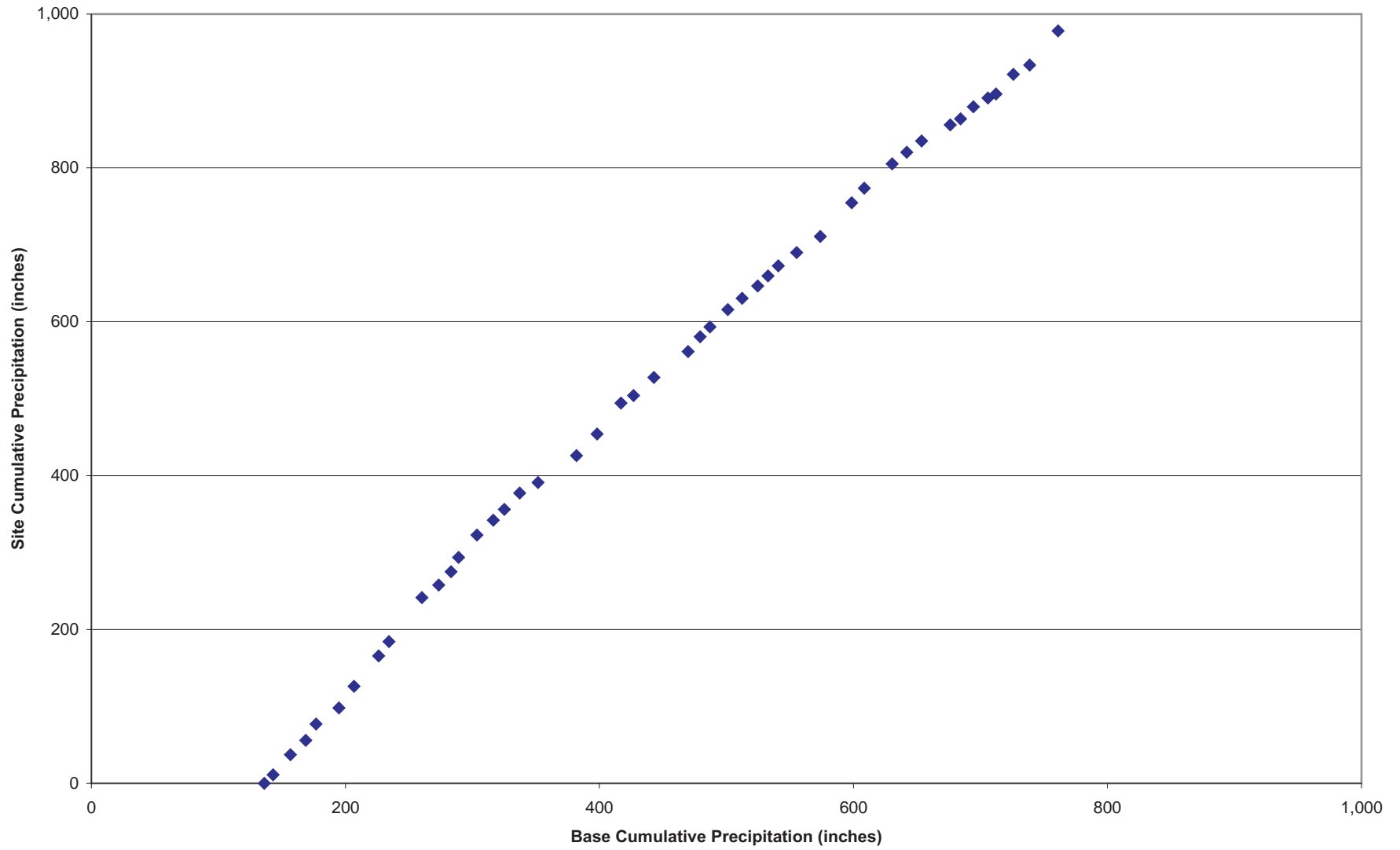
Figure C.7c Double-Mass Plot of Annual Precipitation at Big Bear Lake
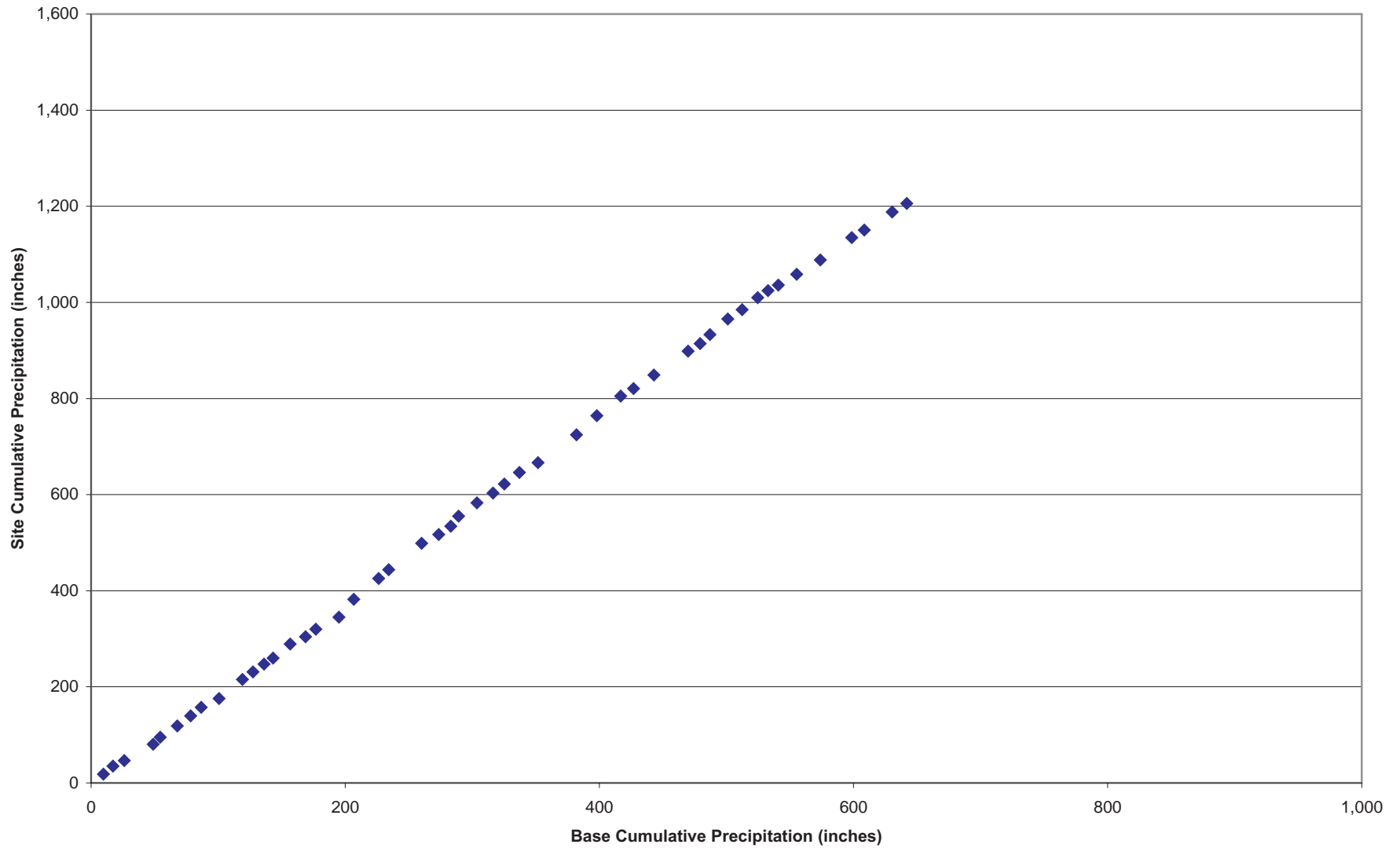
Figure C.7d Double-Mass Plot of Annual Precipitation at Big Pines Park

Boron
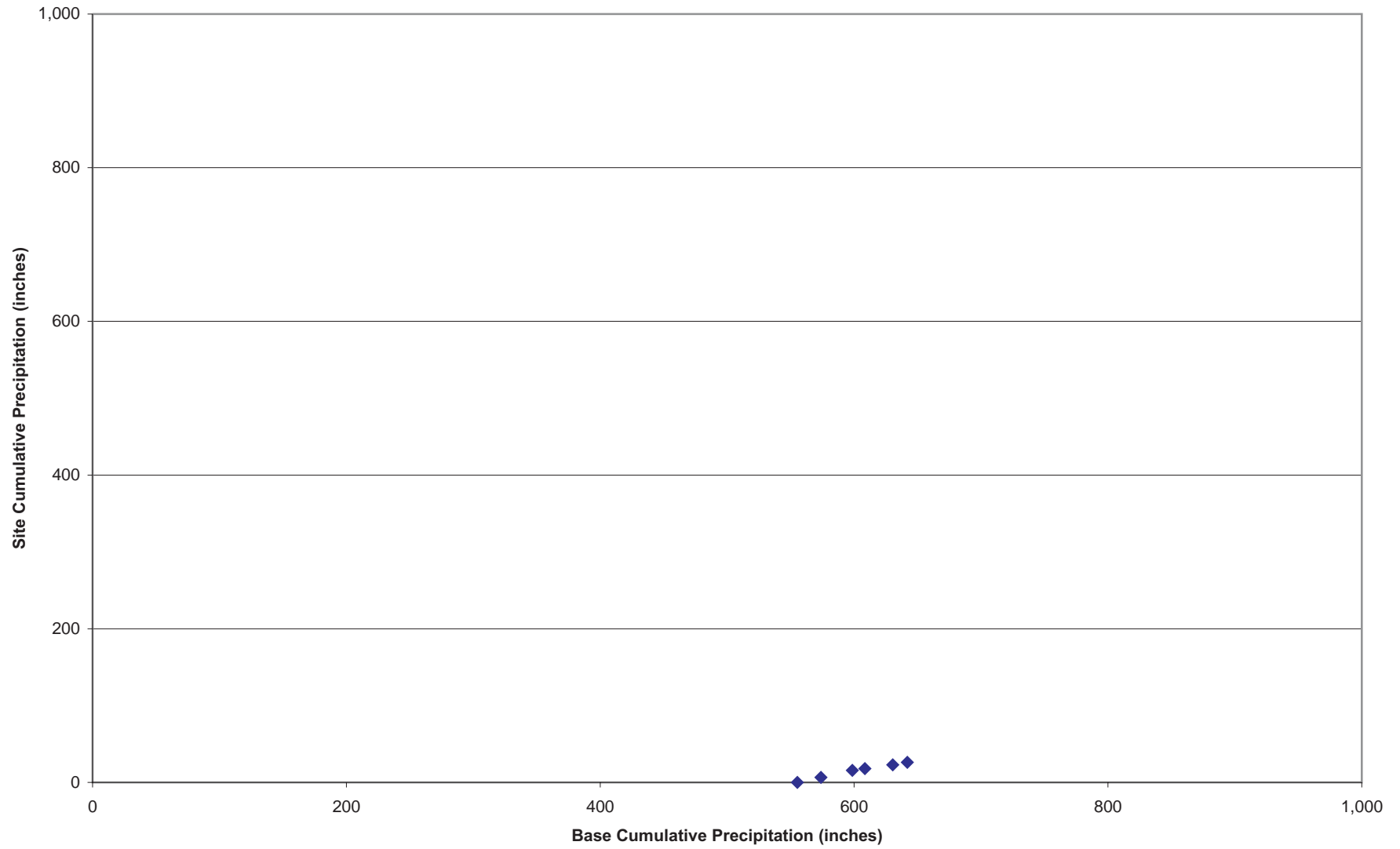
Figure C.7e Double-Mass Plot of Annual Precipitation at Boron

Crystal Lake FC
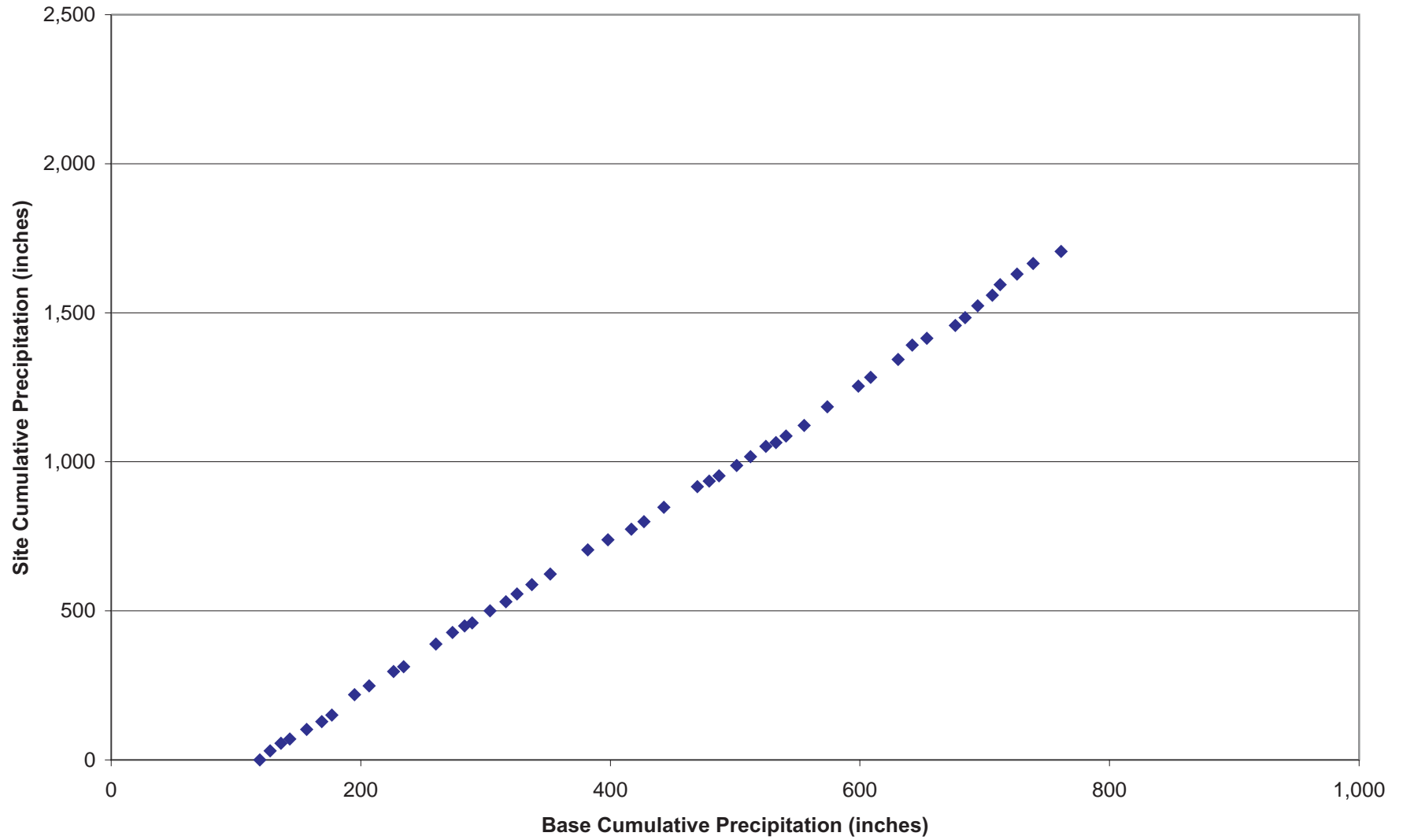
Figure C.7f Double-Mass Plot of Annual Precipitation at Crystal Lake FC

El Mirage Field
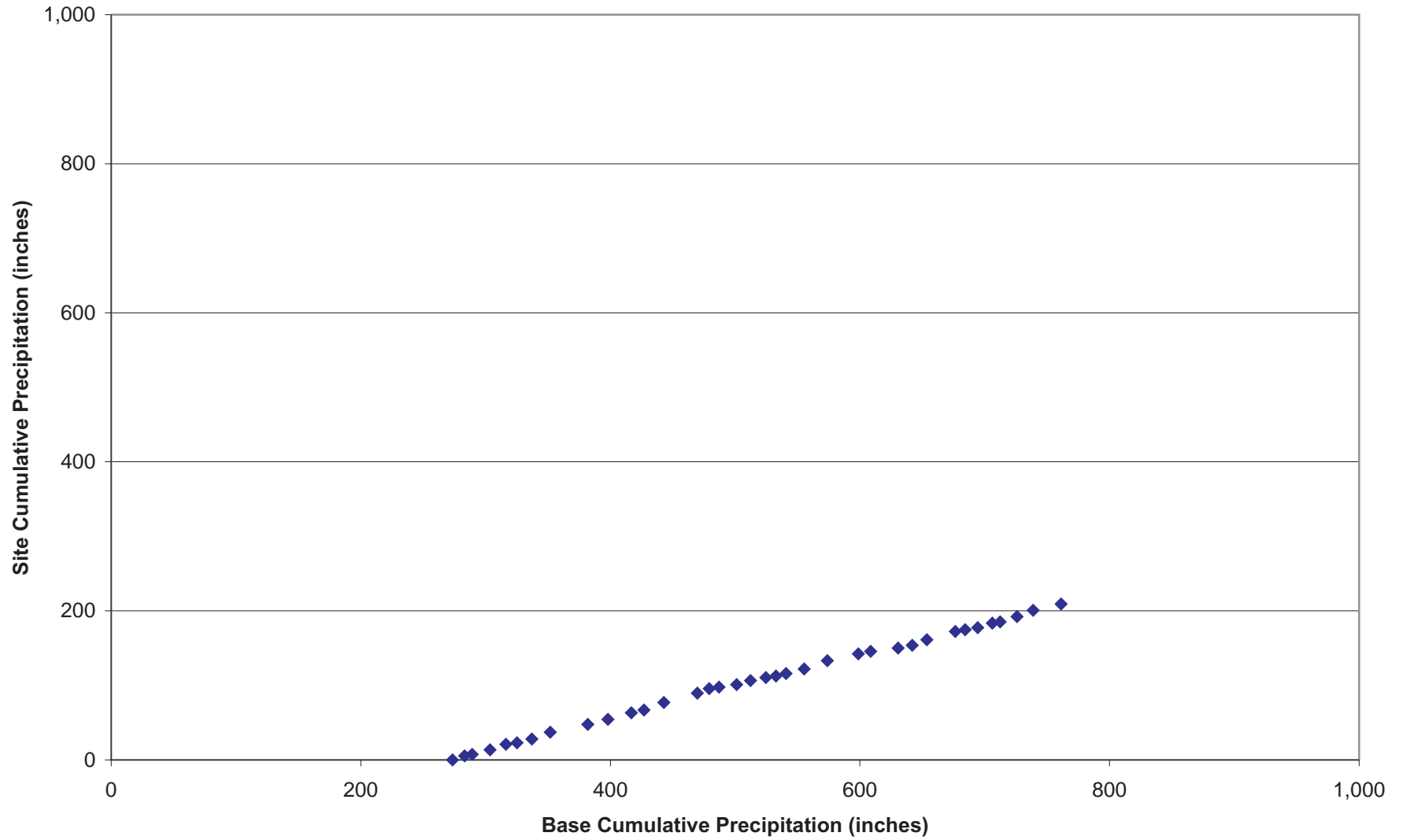
Figure C.7g Double-Mass Plot of Annual Precipitation at El Mirage Field
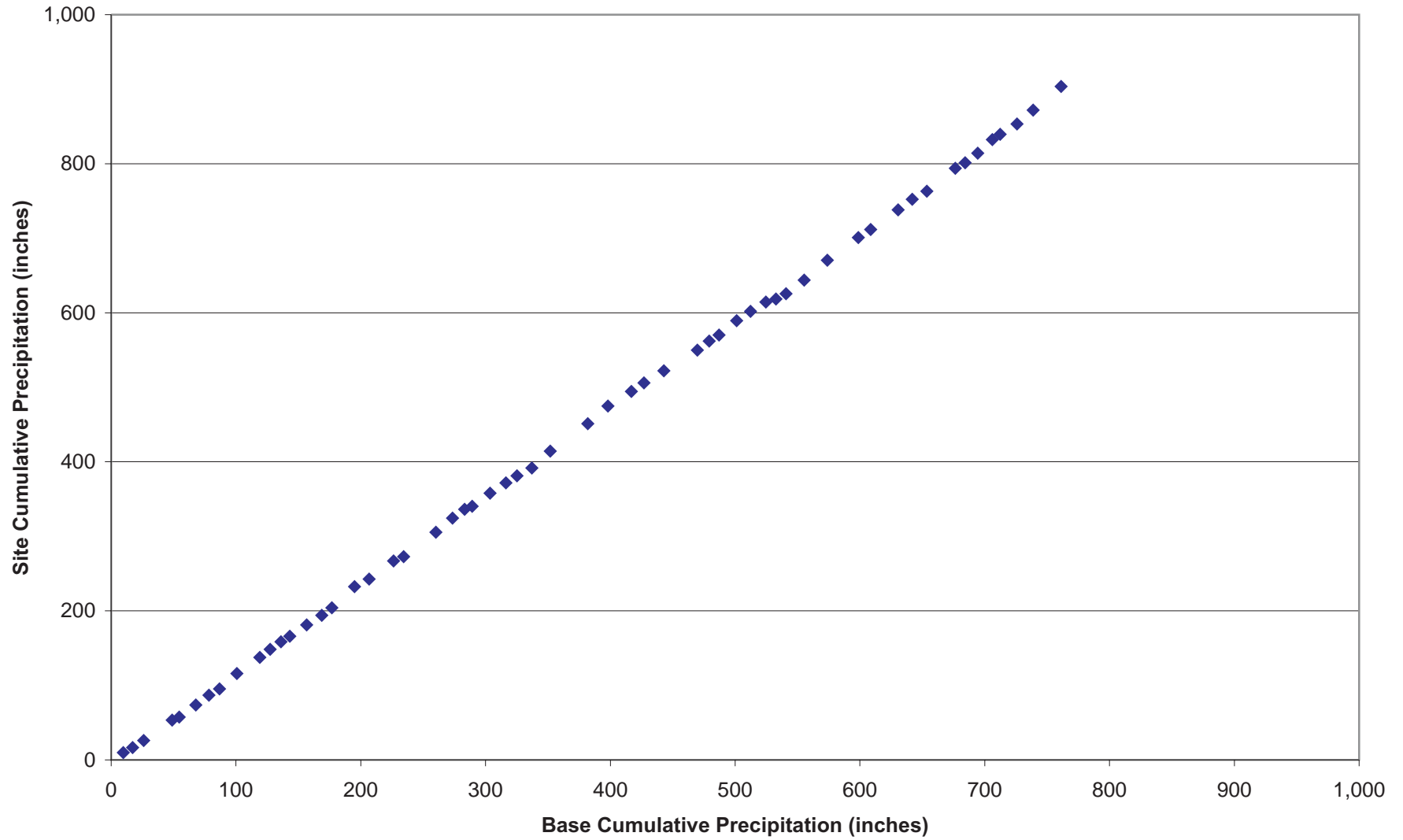
Figure C.7h Double-Mass Plot of Annual Precipitation at Fairmont
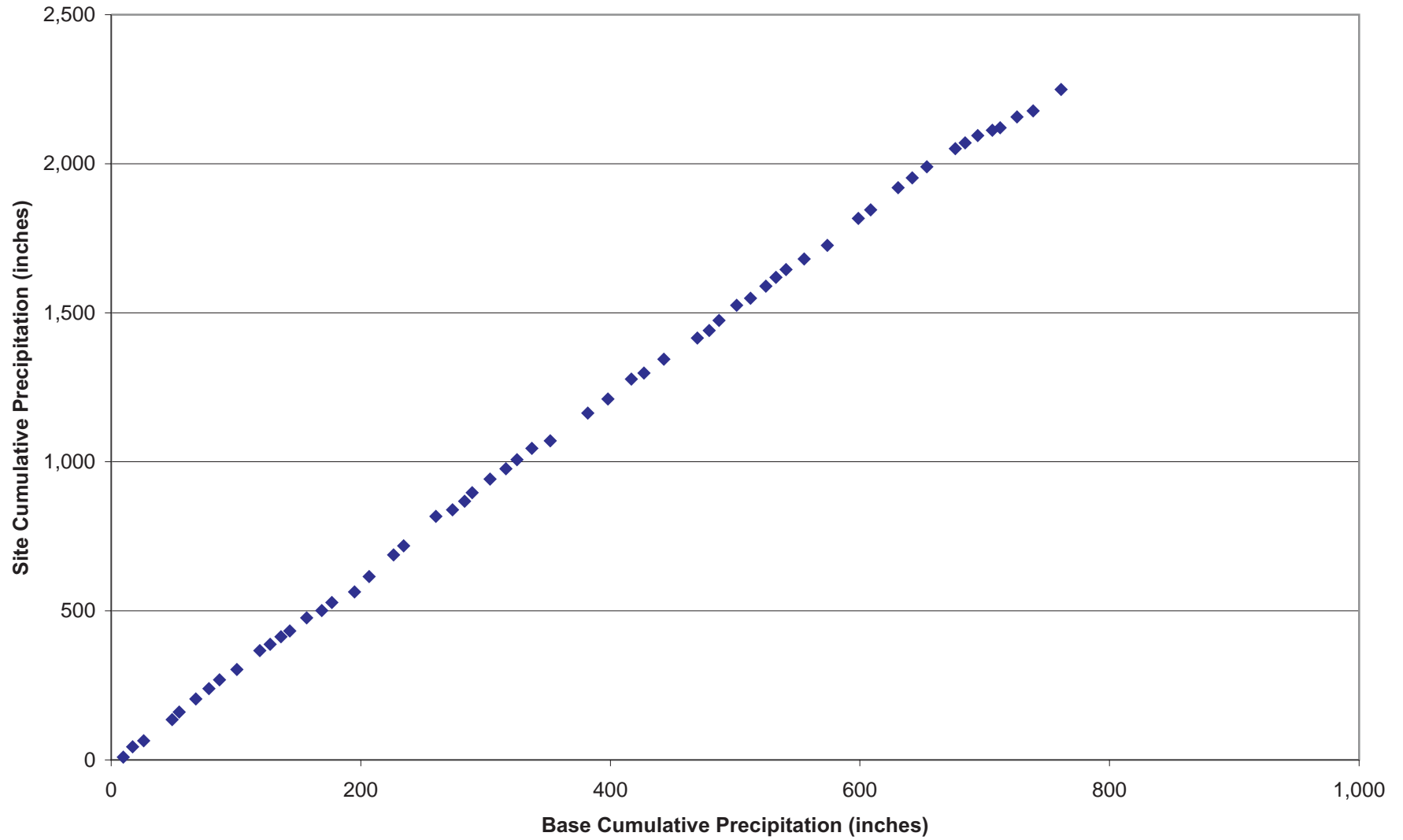
Figure C.7i Double-Mass Plot of Annual Precipitation at Lake Arrowhead

Lancaster FSS
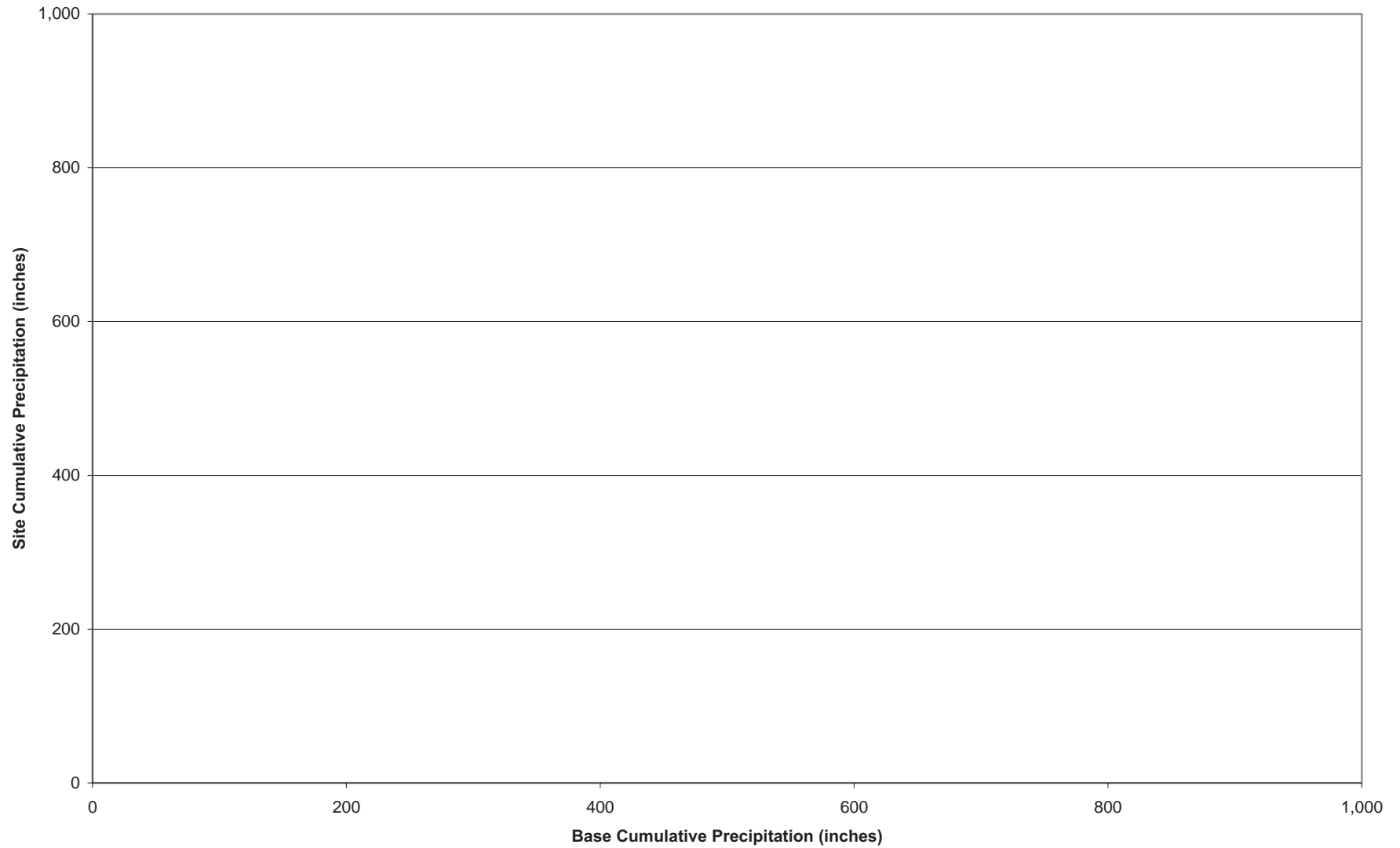
Figure C.7j Double-Mass Plot of Annual Precipitation at Lancaster FSS
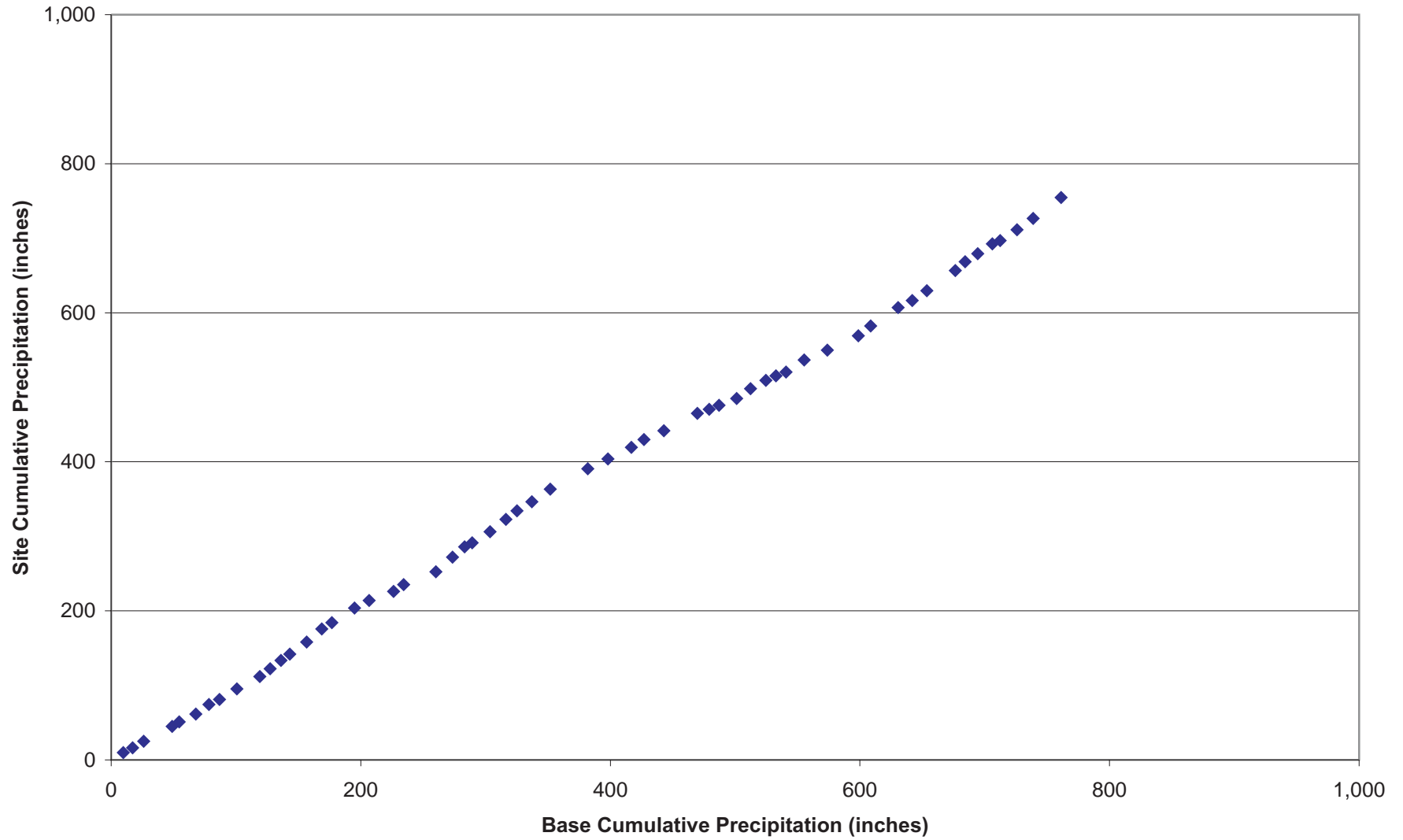
Figure C.7k Double-Mass Plot of Annual Precipitation at Lebec
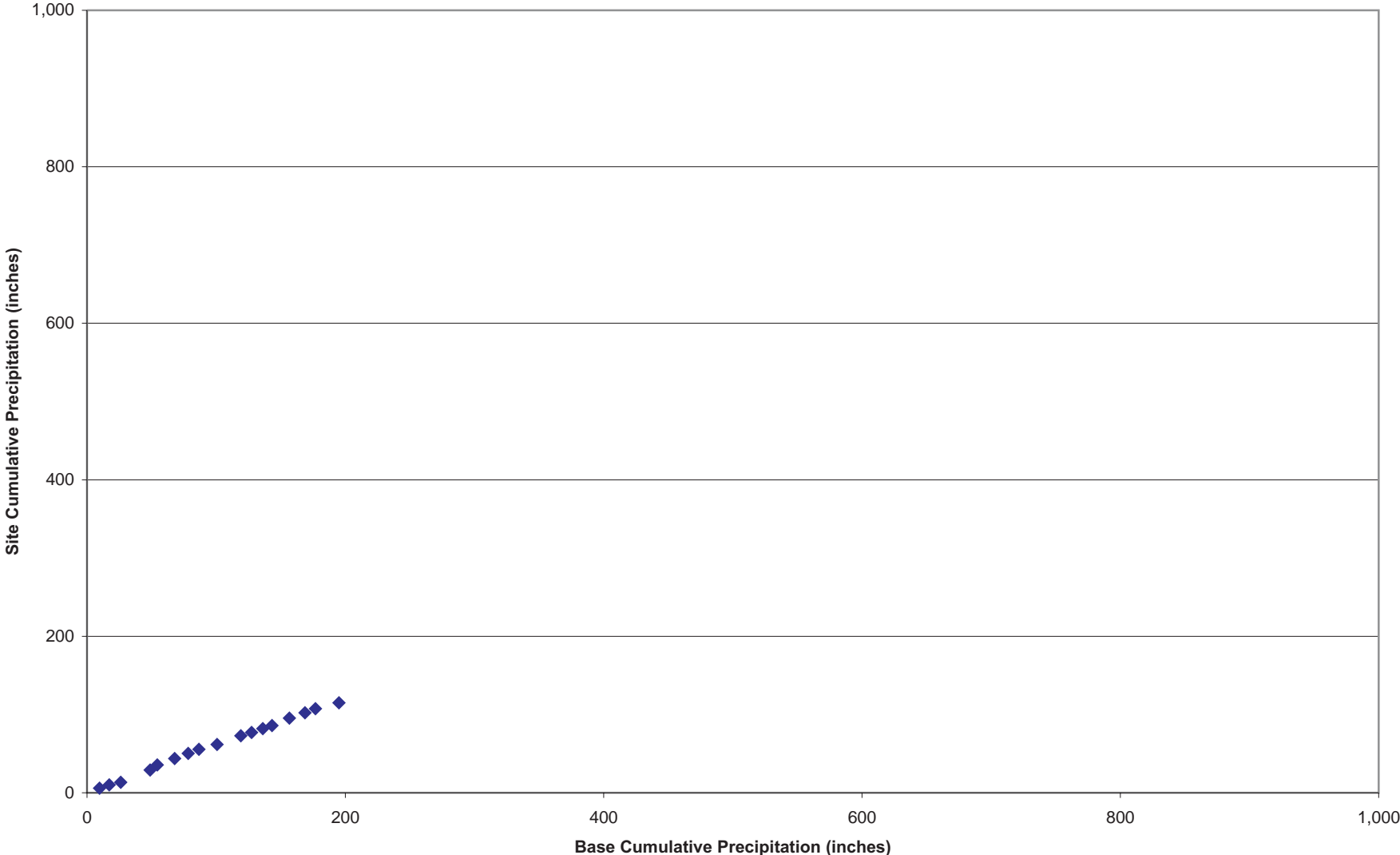
Figure C.7I Double-Mass Plot of Annual Precipitation at Llano Eberle Ranch
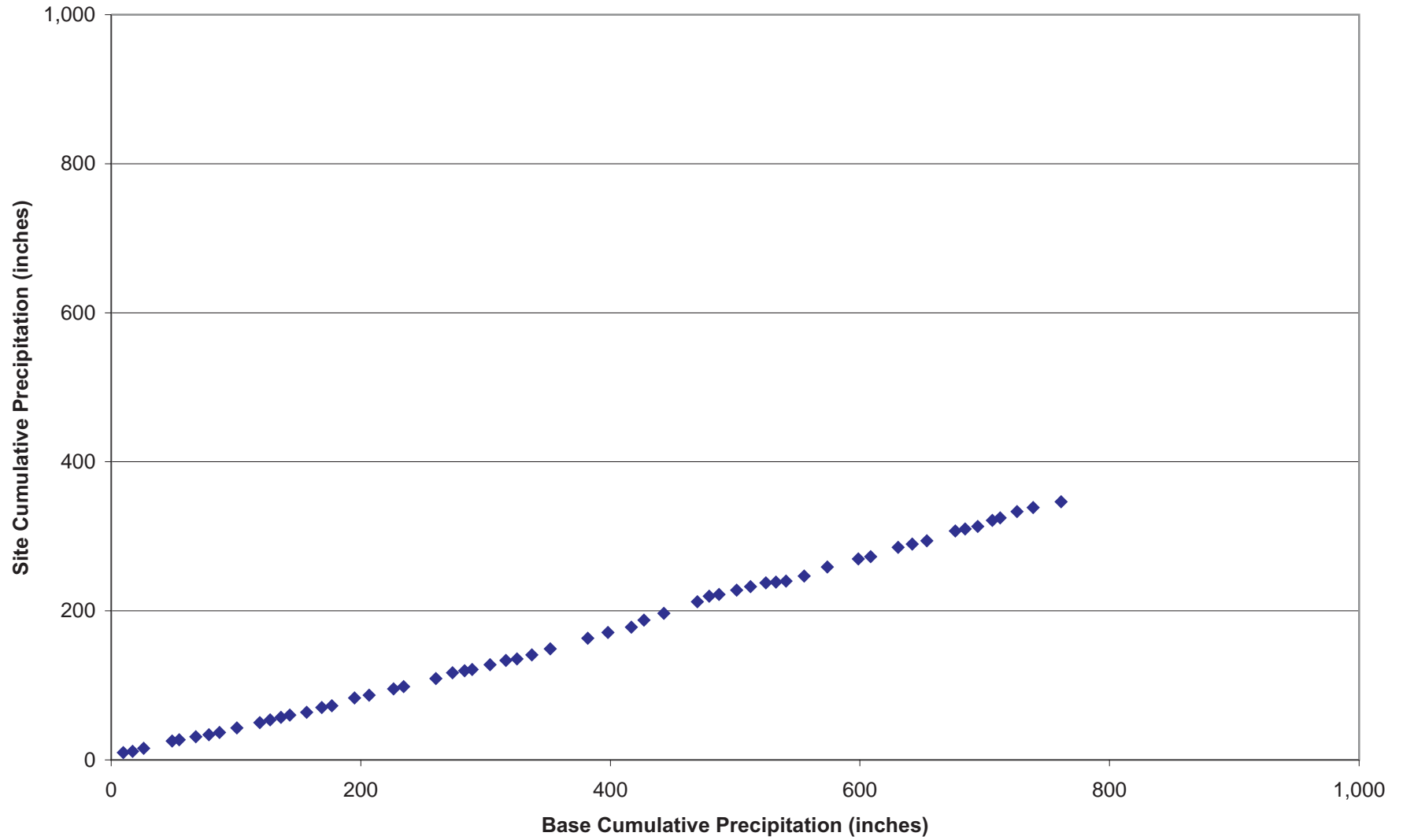
Figure C.7m Double-Mass Plot of Annual Precipitation at Mojave

Neenach
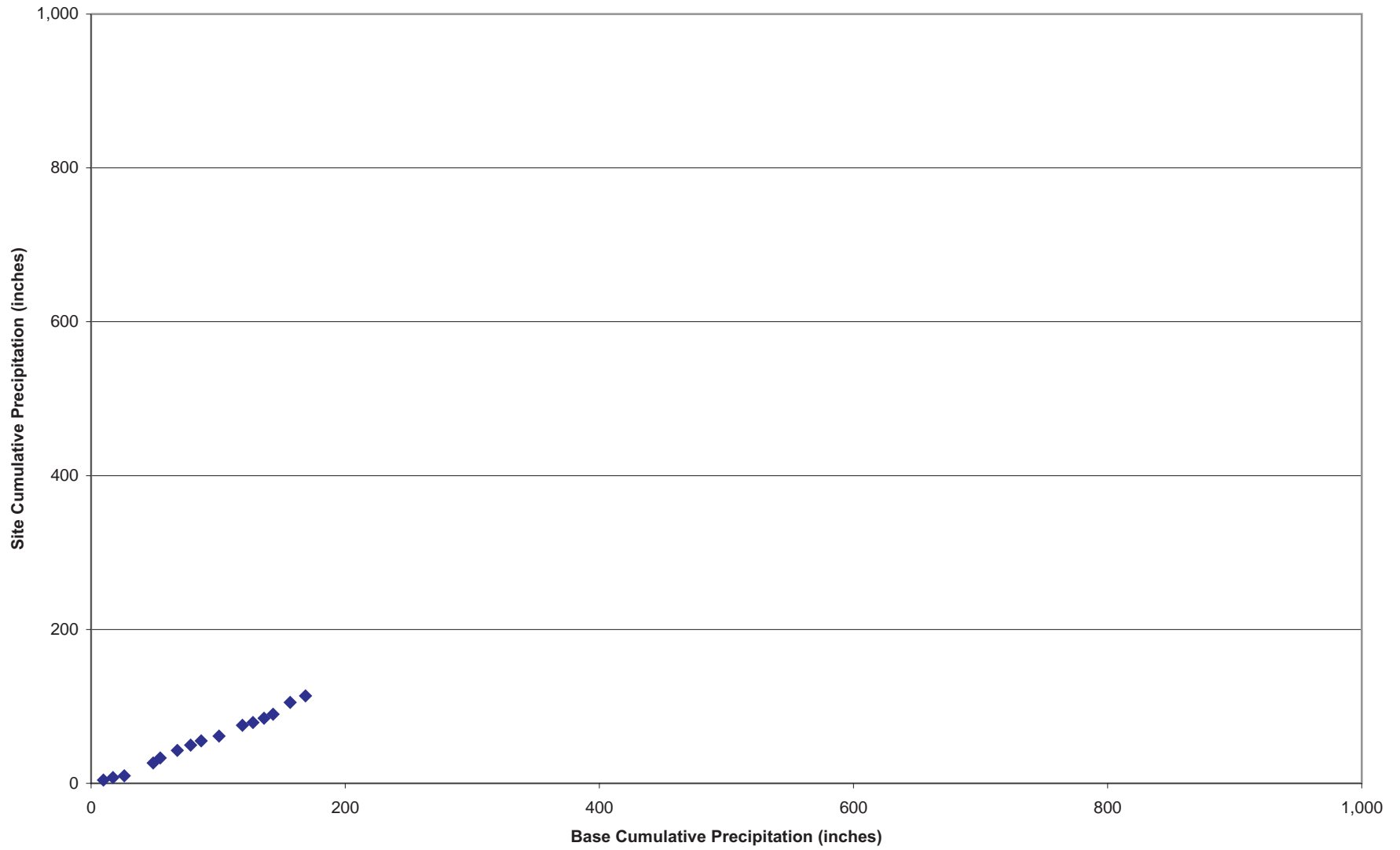
Figure C.7n Double-Mass Plot of Annual Precipitation at Neenach

Palmdale
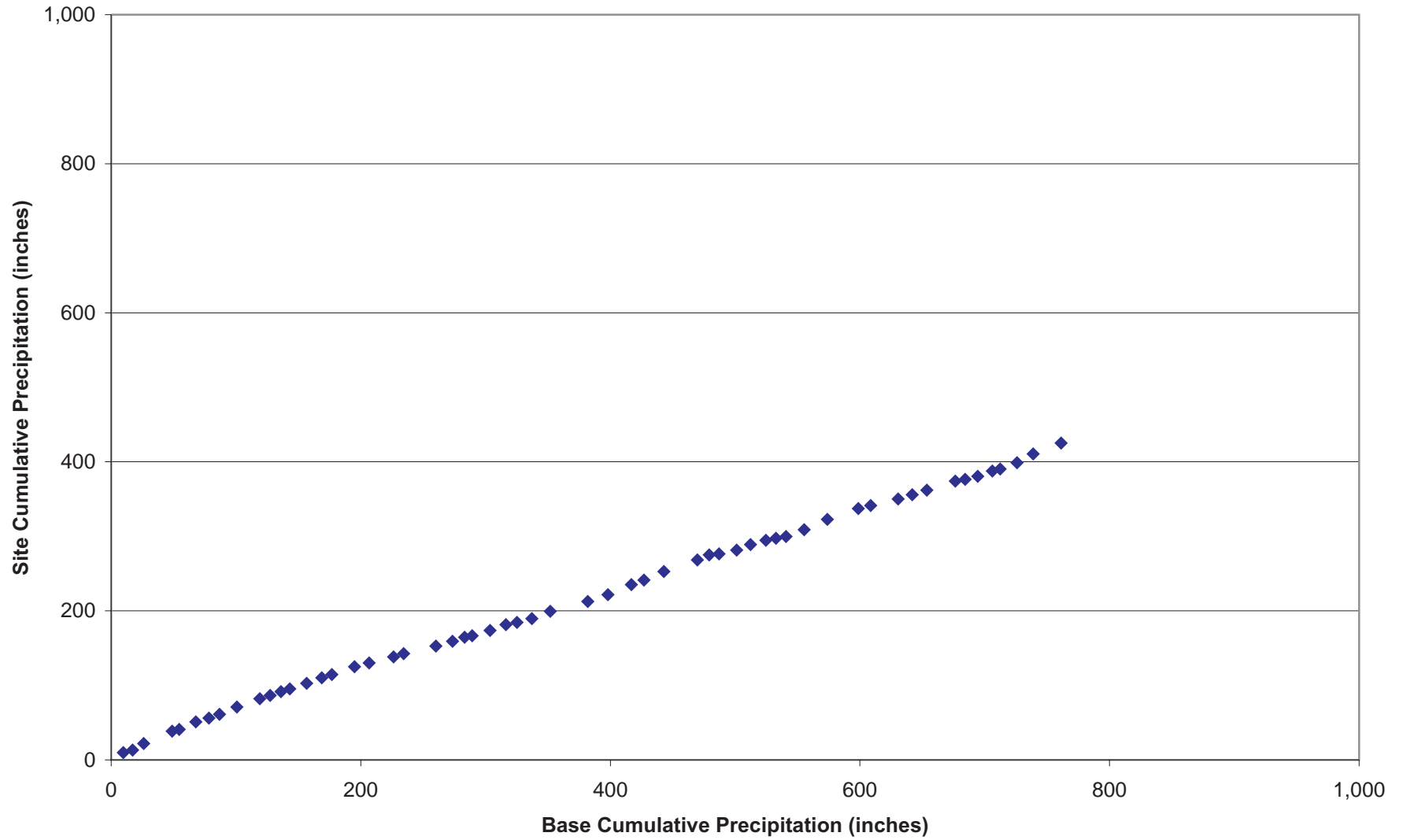
Figure C.7o Double-Mass Plot of Annual Precipitation at Palmdale
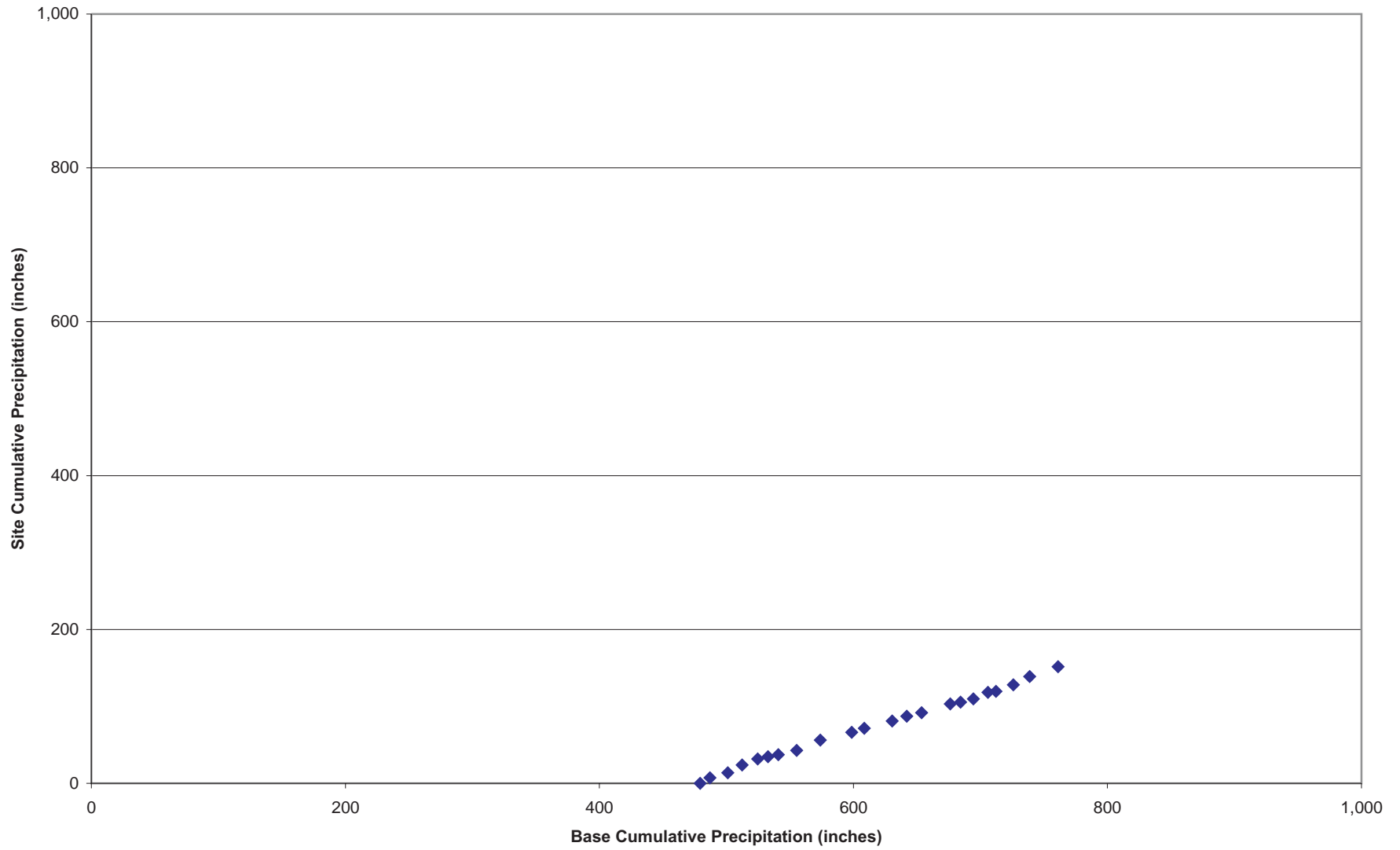
Figure C.7p Double-Mass Plot of Annual Precipitation at Pearblossom

Ransburg
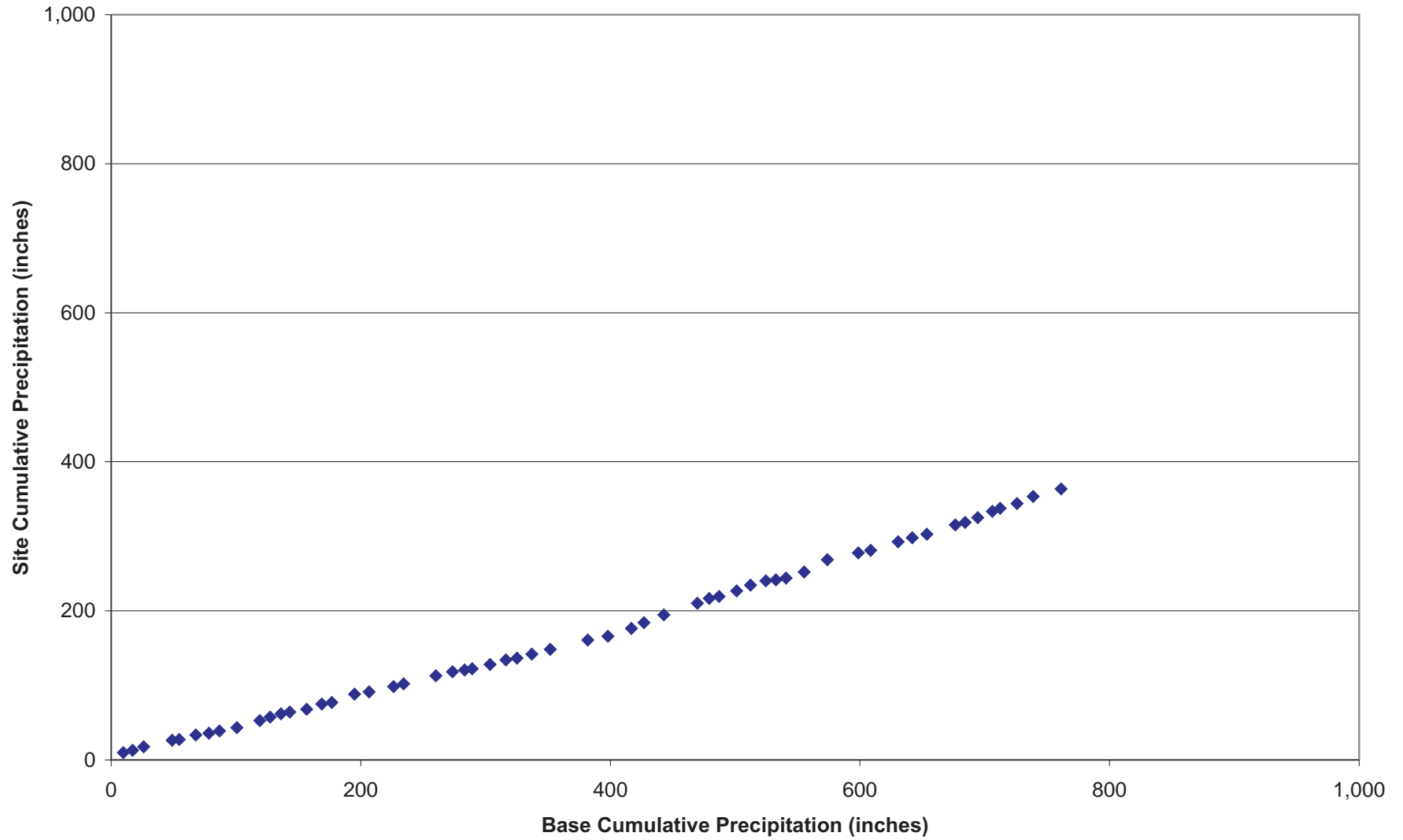
Figure C.7q Double-Mass Plot of Annual Precipitation at Ransburg

Sandberg PTRL
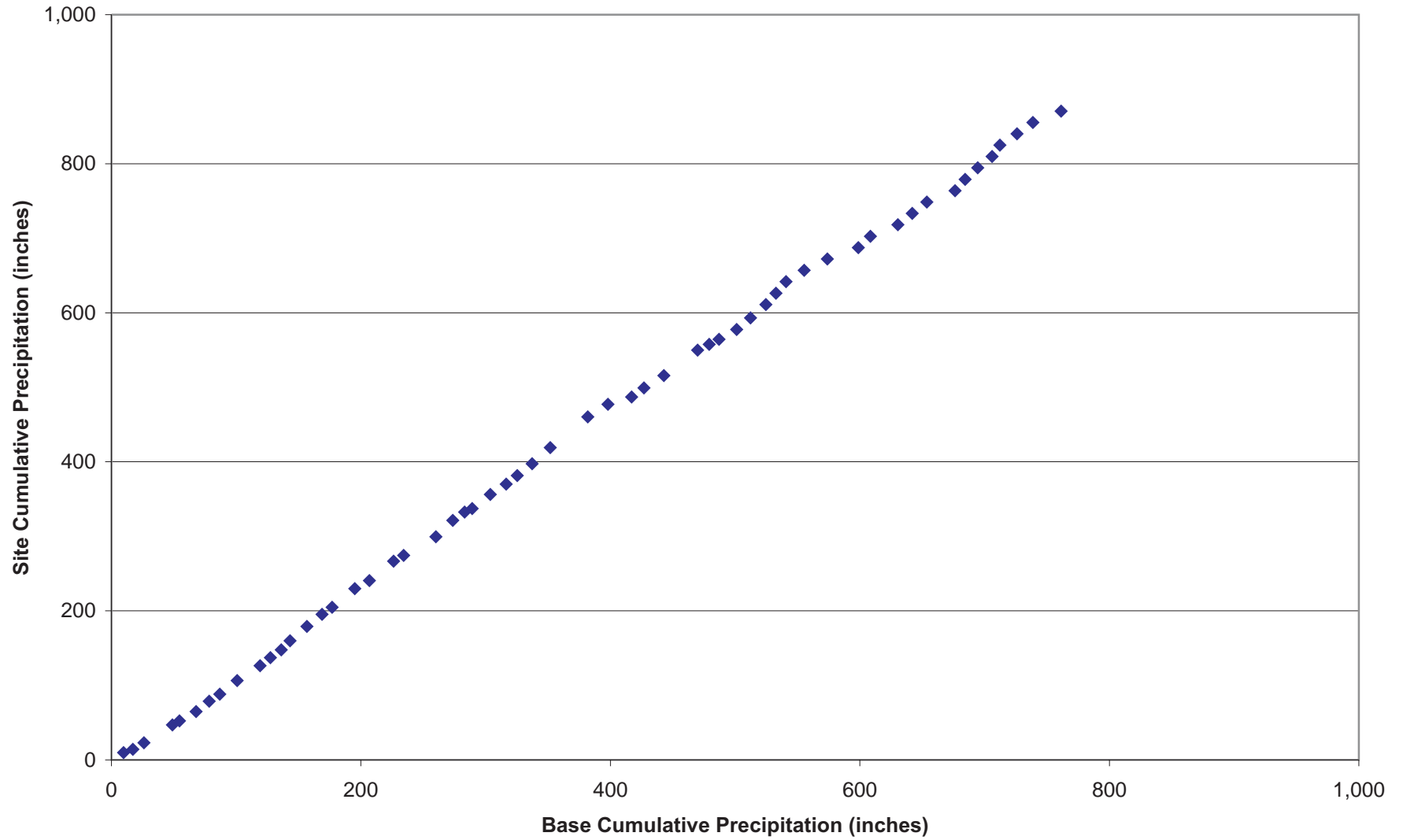
Figure C.7r Double-Mass Plot of Annual Precipitation at Sandberg PTRL
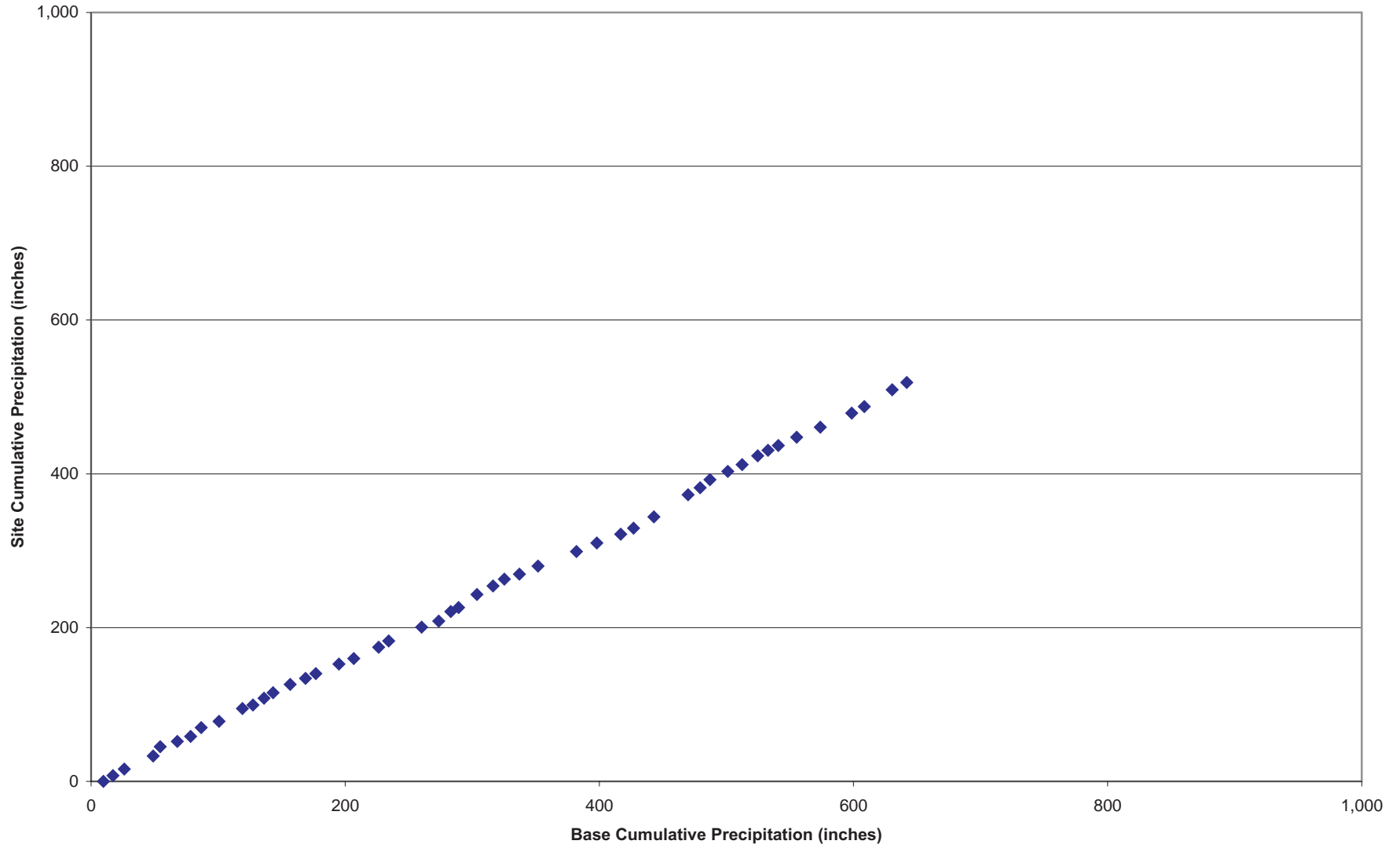
Figure C.7s Double-Mass Plot of Annual Precipitation at Tehachapi

Tejon Rancho
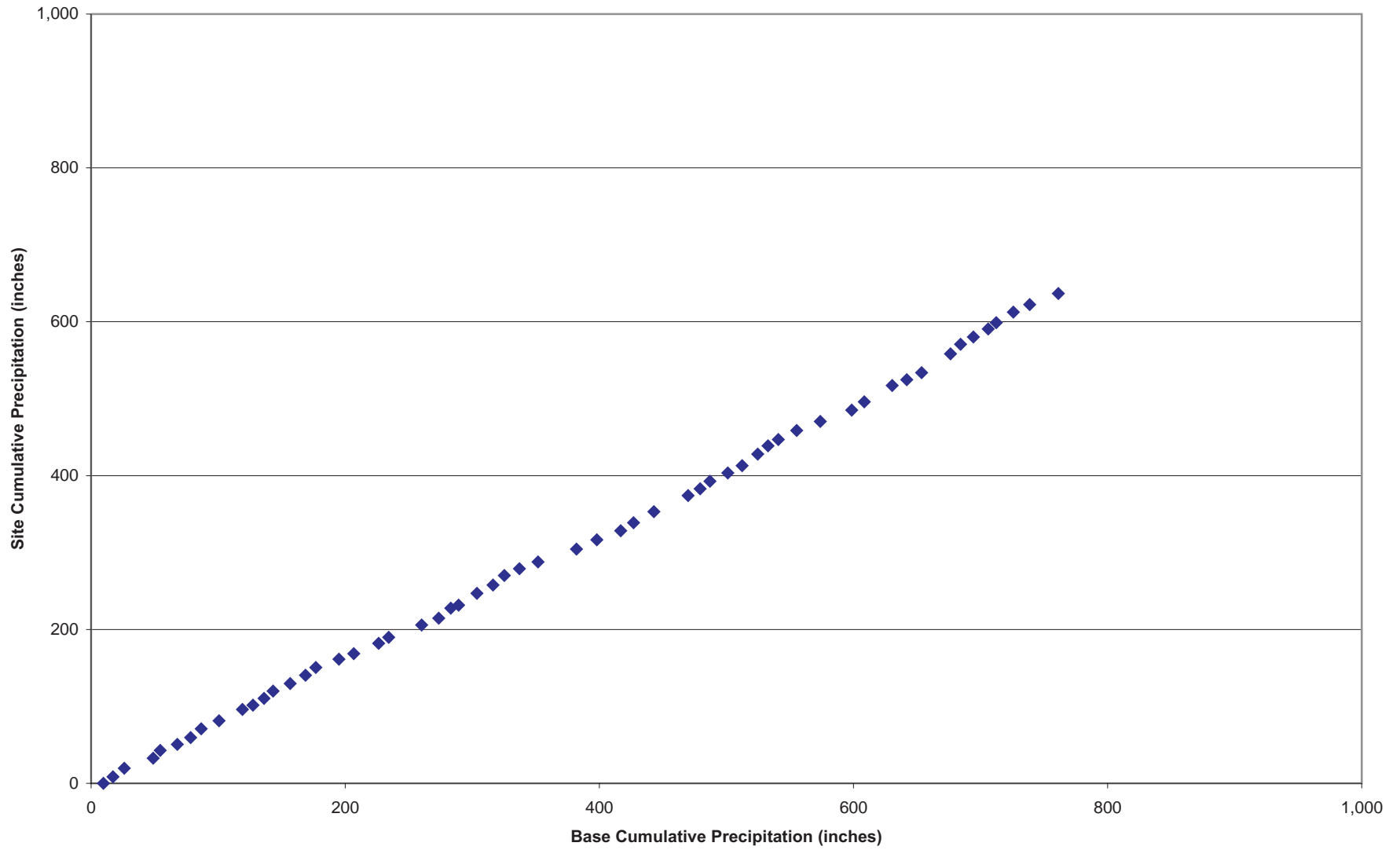
Figure C.7t Double-Mass Plot of Annual Precipitation at Tejon Rancho

Valyermo Fire Station

Site Cumulative Precipitation (inches)

Base Cumulative Precipitation (inches)
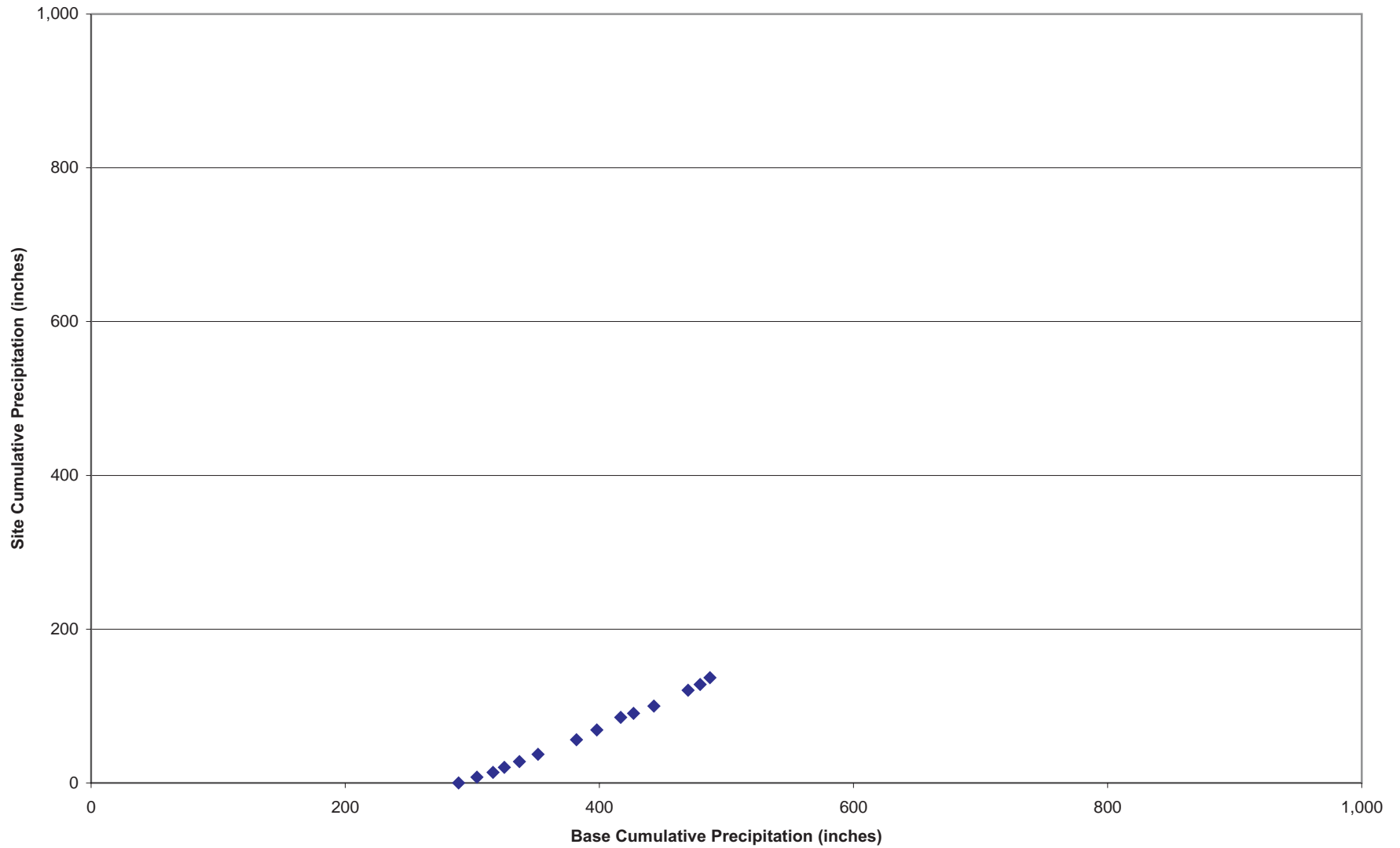
Figure C.7u Double-Mass Plot of Annual Precipitation at Valyermo Fire Station

Victorville

Site Cumulative Precipitation (inches) / Base Cumulative Precipitation (inches)
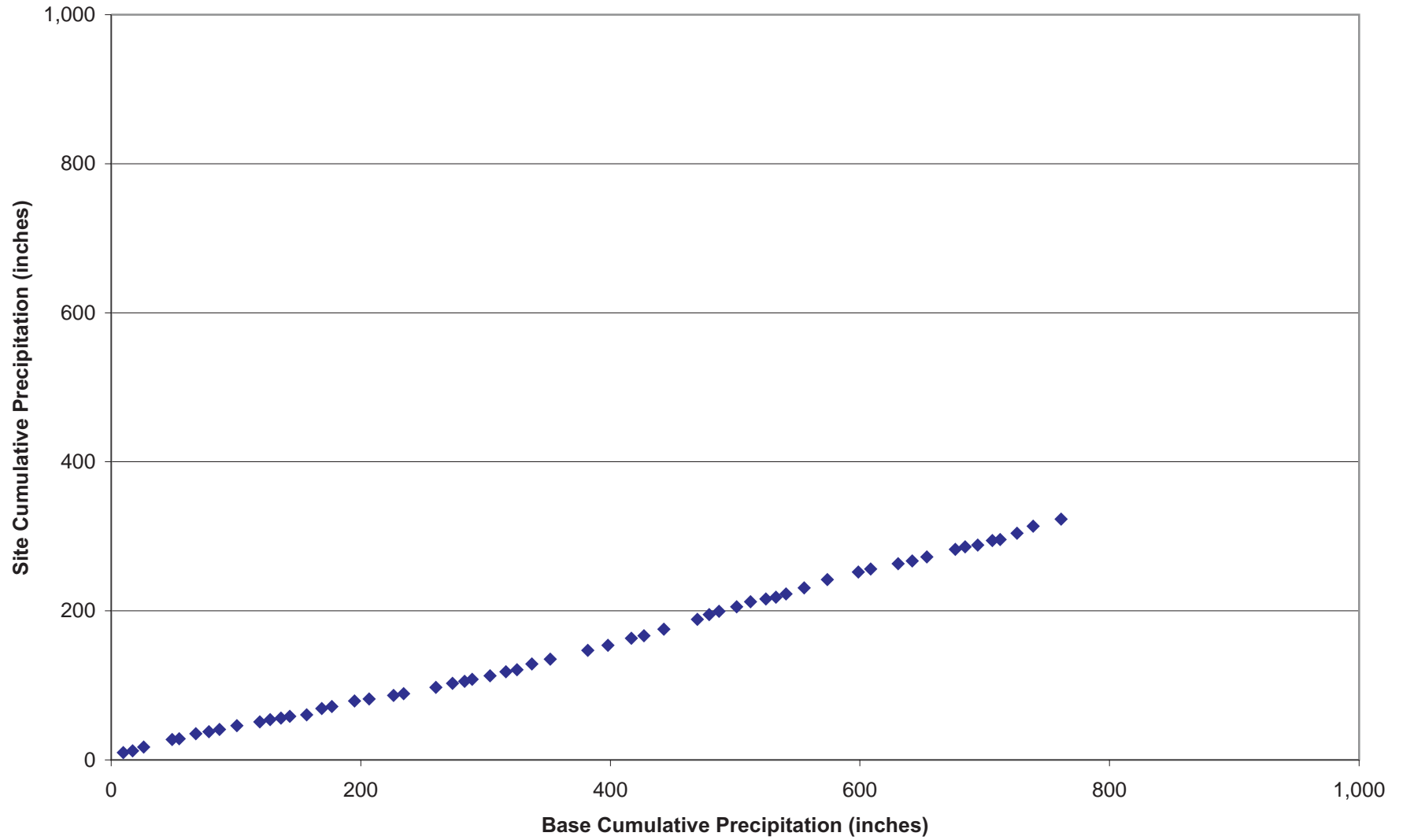
Figure C.7v Double-Mass Plot of Annual Precipitation at Victorville

Vincent Fire Station
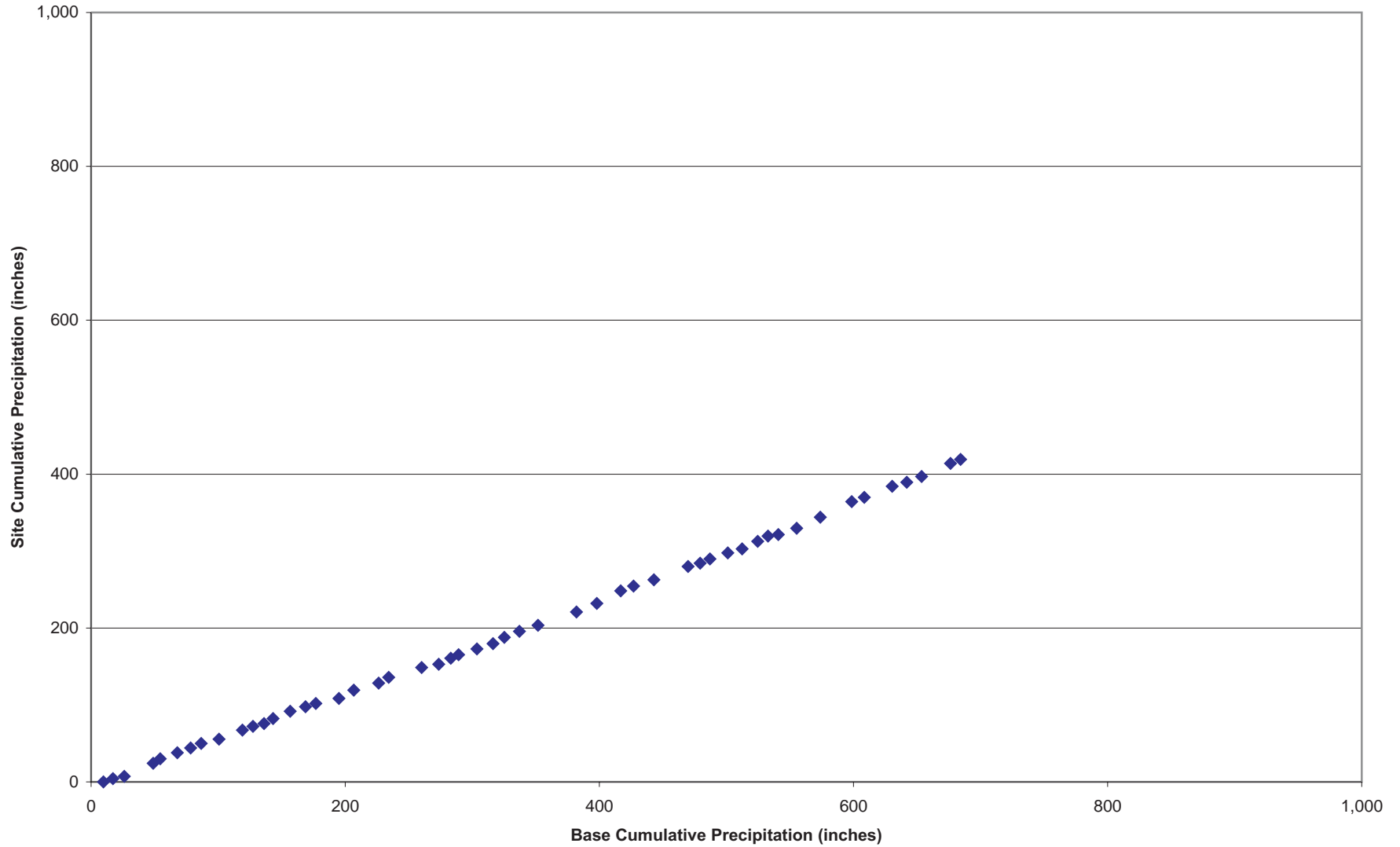
Figure C.7w Double-Mass Plot of Annual Precipitation at Vincent Fire Station
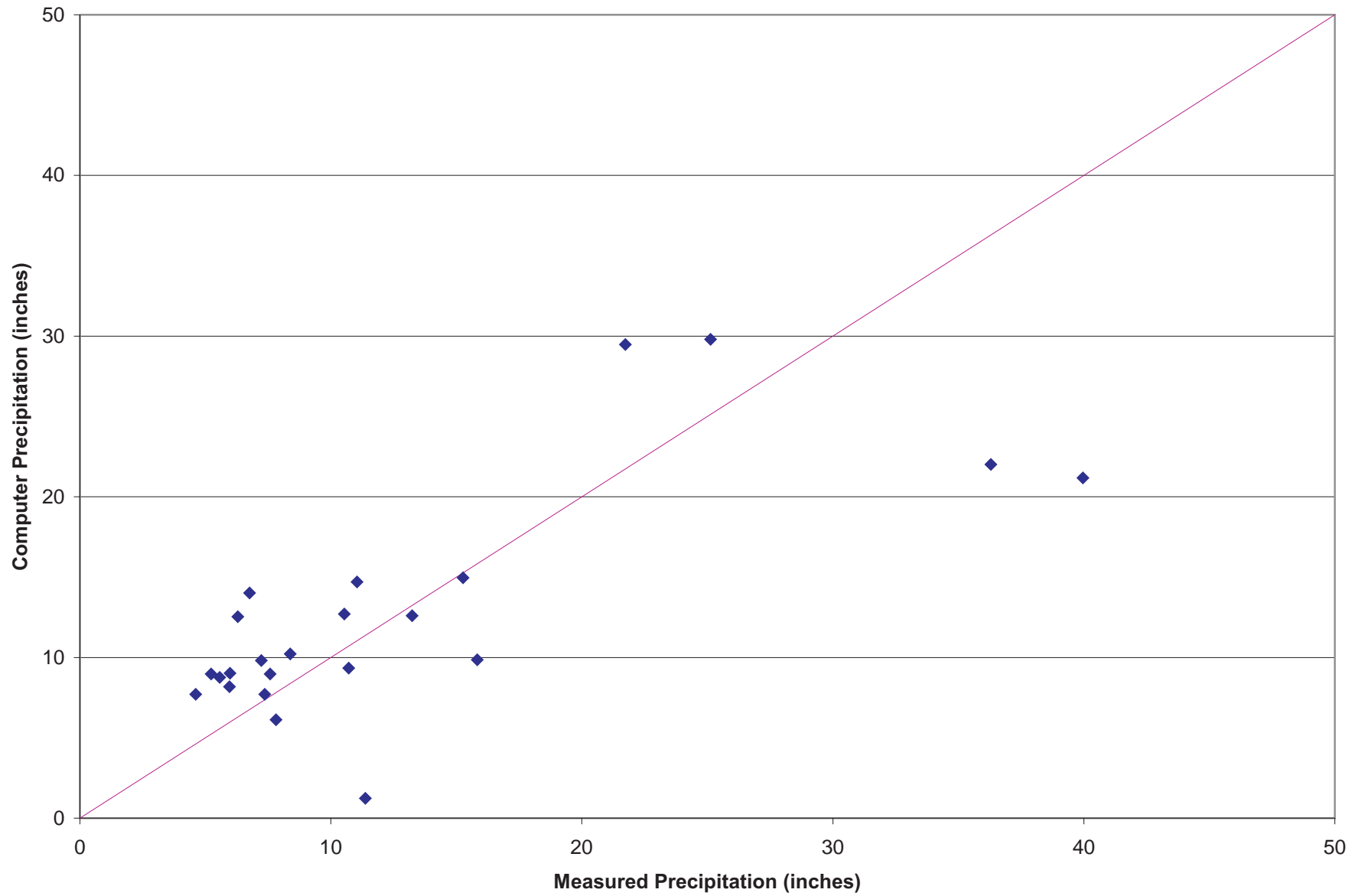
Figure C.8a Comparison of Computed and Measured Average Annual Precipitation Using Invariant Intercept and Slope
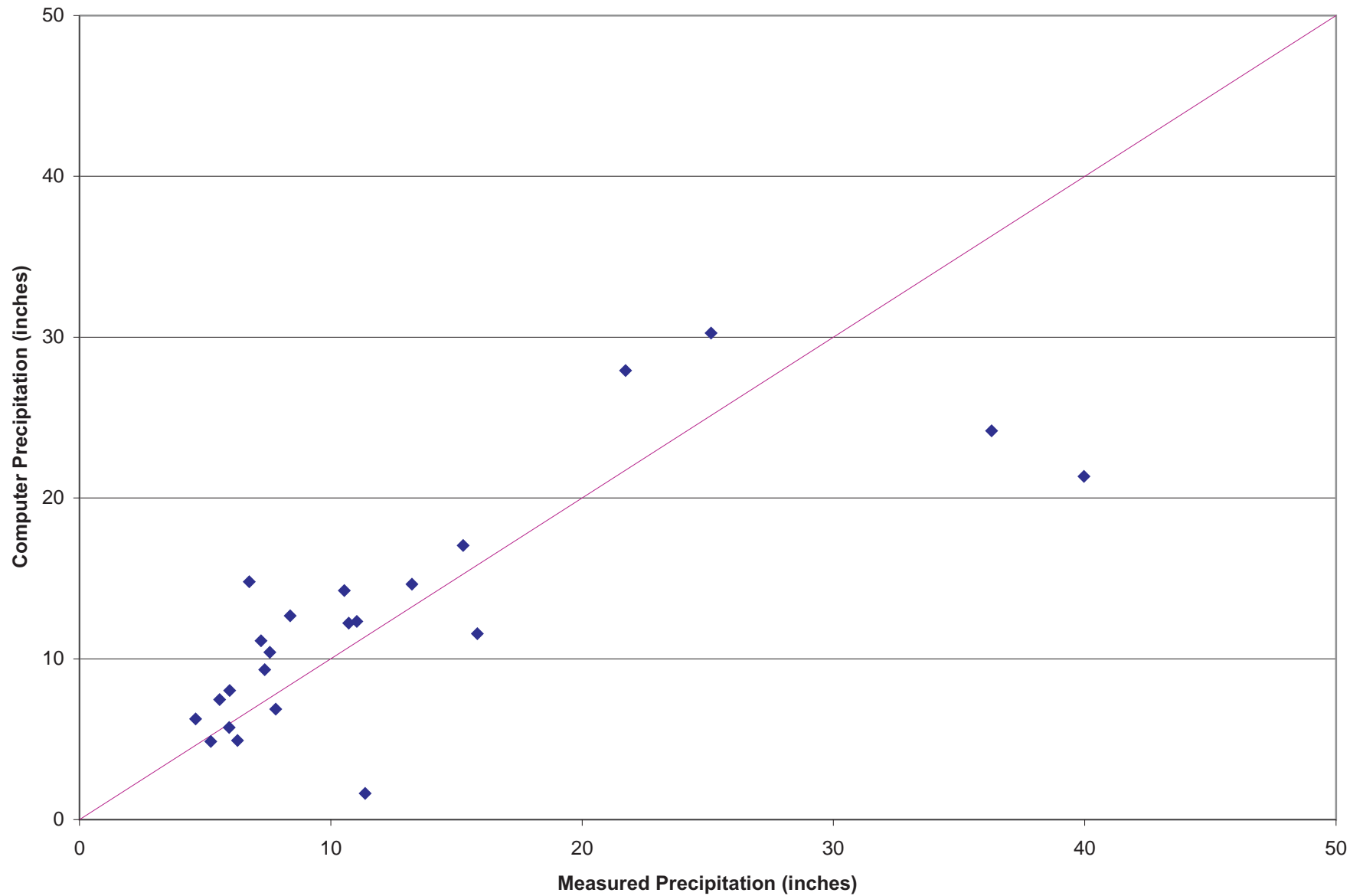
Figure C.8b Comparison of Computed and Measured Average Annual Precipitation Using Linear Intercept and Invariant Slope
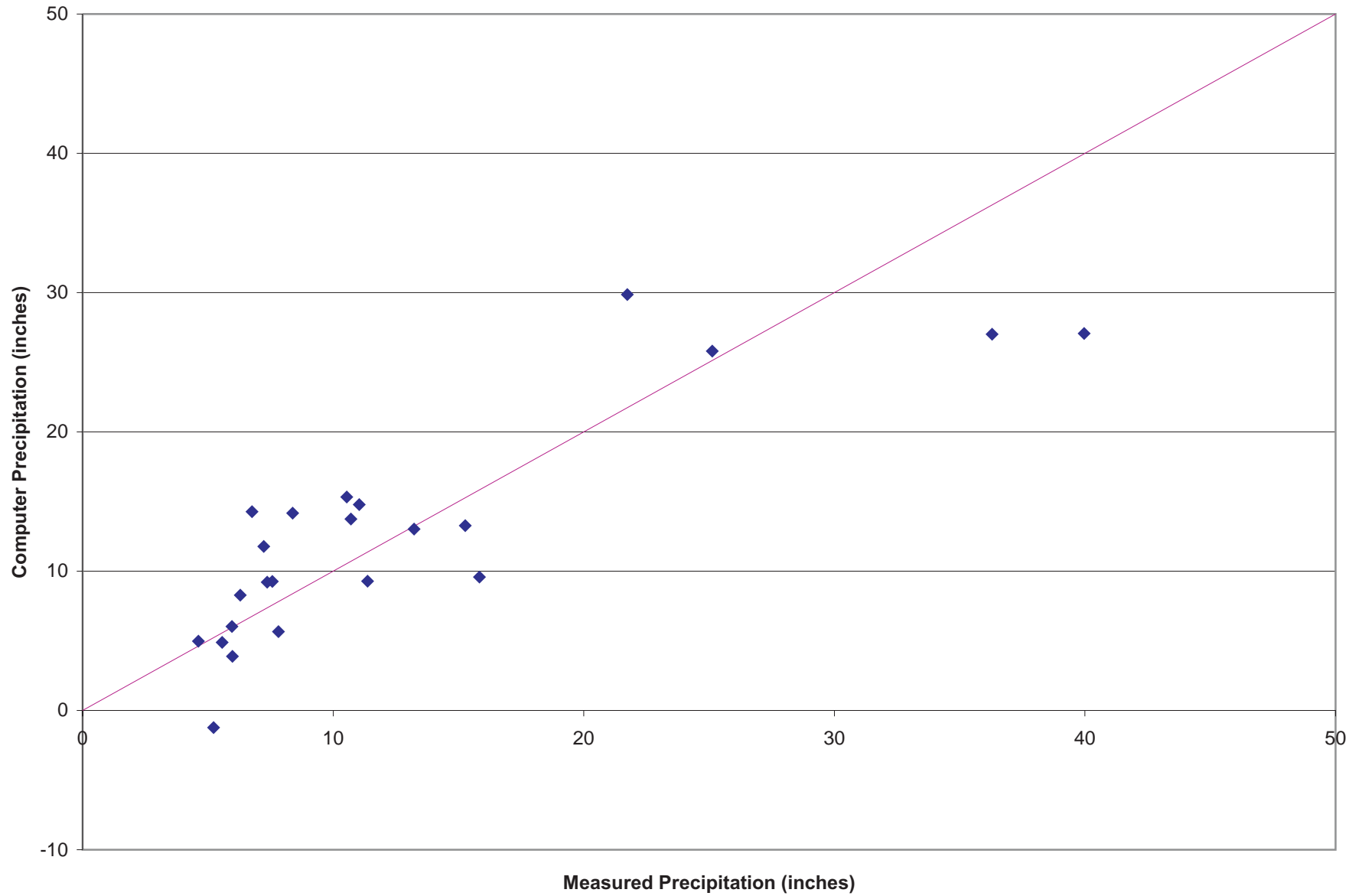
Figure C.8c Comparison of Computed and Measured Average Annual Precipitation Using Quadratic Intercept and Invariant Slope
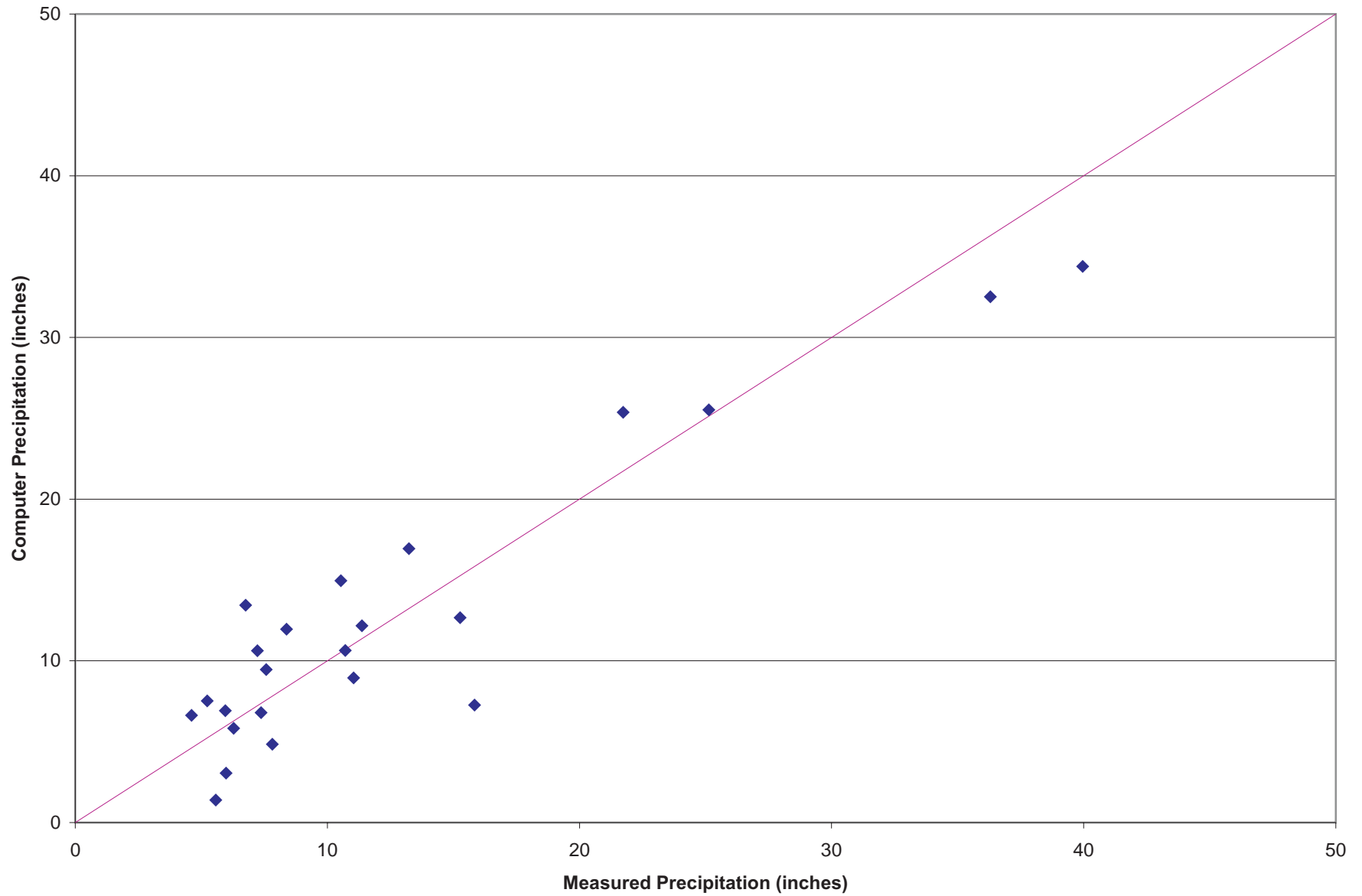
Figure C.8d Comparison of Computed and Measured Average Annual Precipitation Using Cubic Intercept and Invariant Slope
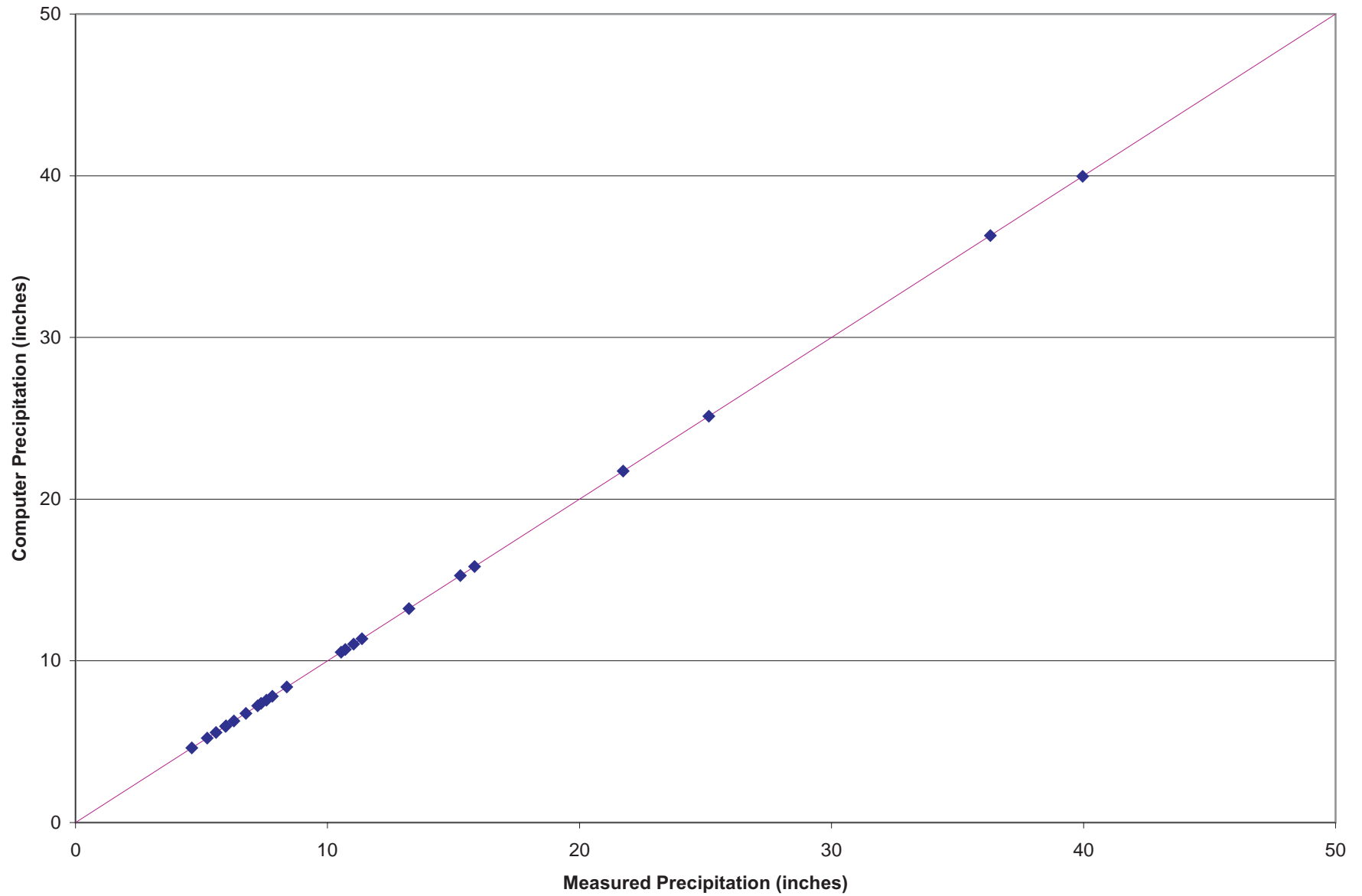
Figure C.8e Comparison of Computed and Measured Average Annual Precipitation Using Contoured Intercept and Invariant Slope
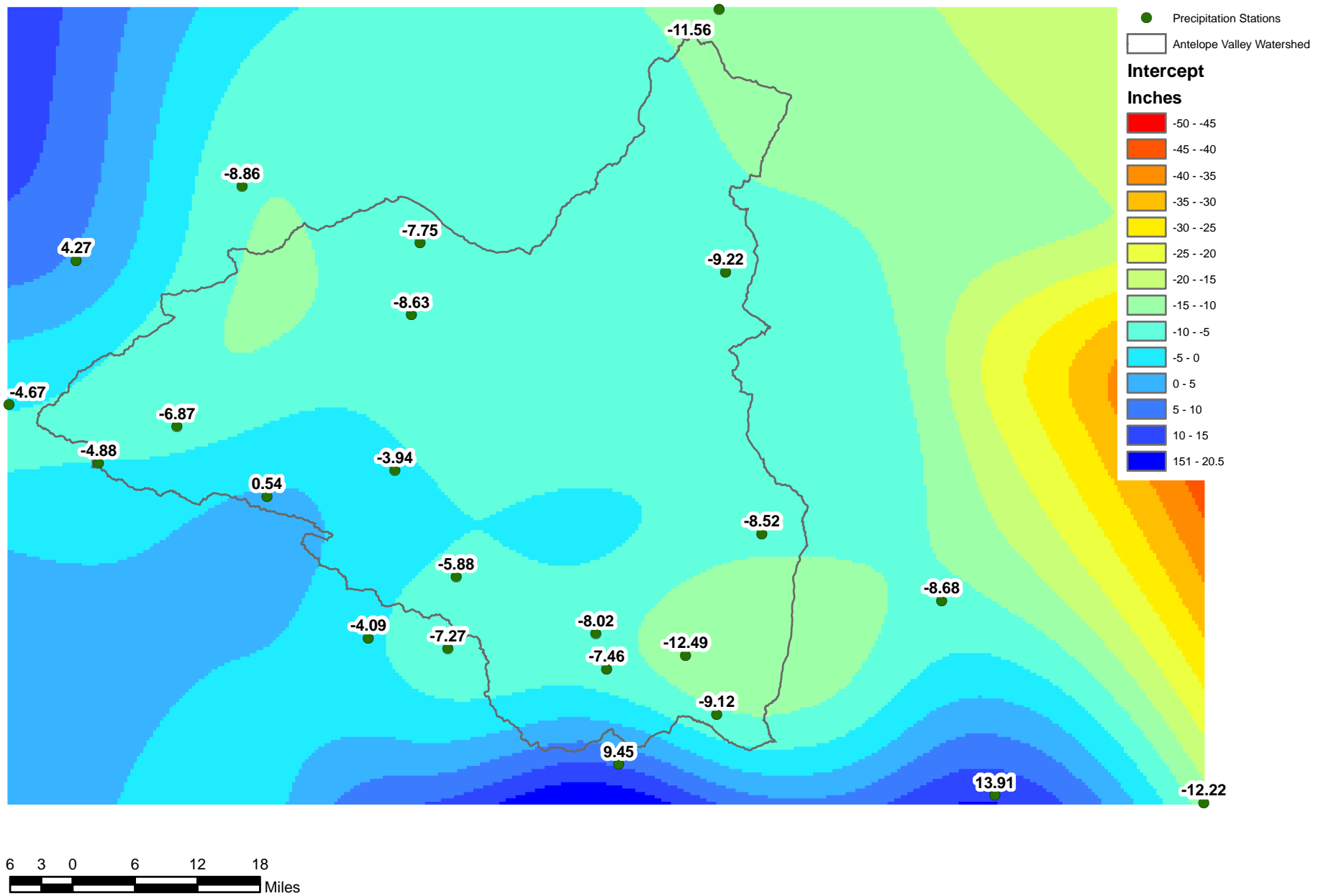
Figure C.9 Contoured Intercept for Precipitation-Altitude Relation
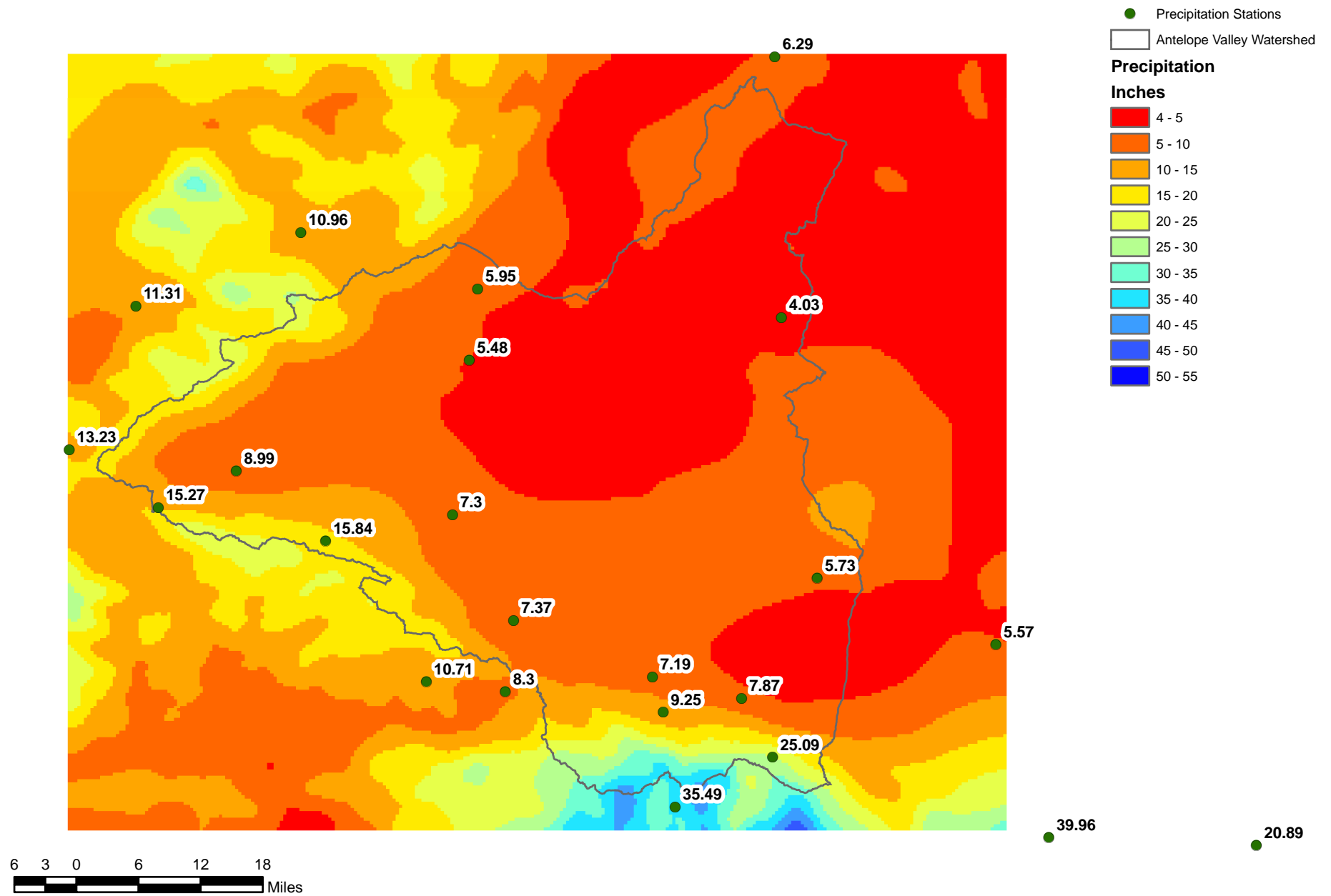
Figure C.10 Geographic Distribution of Average Annual Precipitation Based on Contoured Intercept

Legend:

Subareas

Antelope Valley Watershed

Precipitation

Inches

- 4 - 5
- 5 - 10
- 10 - 15
- 15. - 20
- 20 - 25
- 25 - 30
- 30 - 35
- 35 - 40
- 40 - 45

Map labels:

Northern Buttes

Tehachapi Mountains

Valley Floor

Eastern Buttes

San Gabriel Mountains

Scale: 6 3 0 6 12 18 Miles
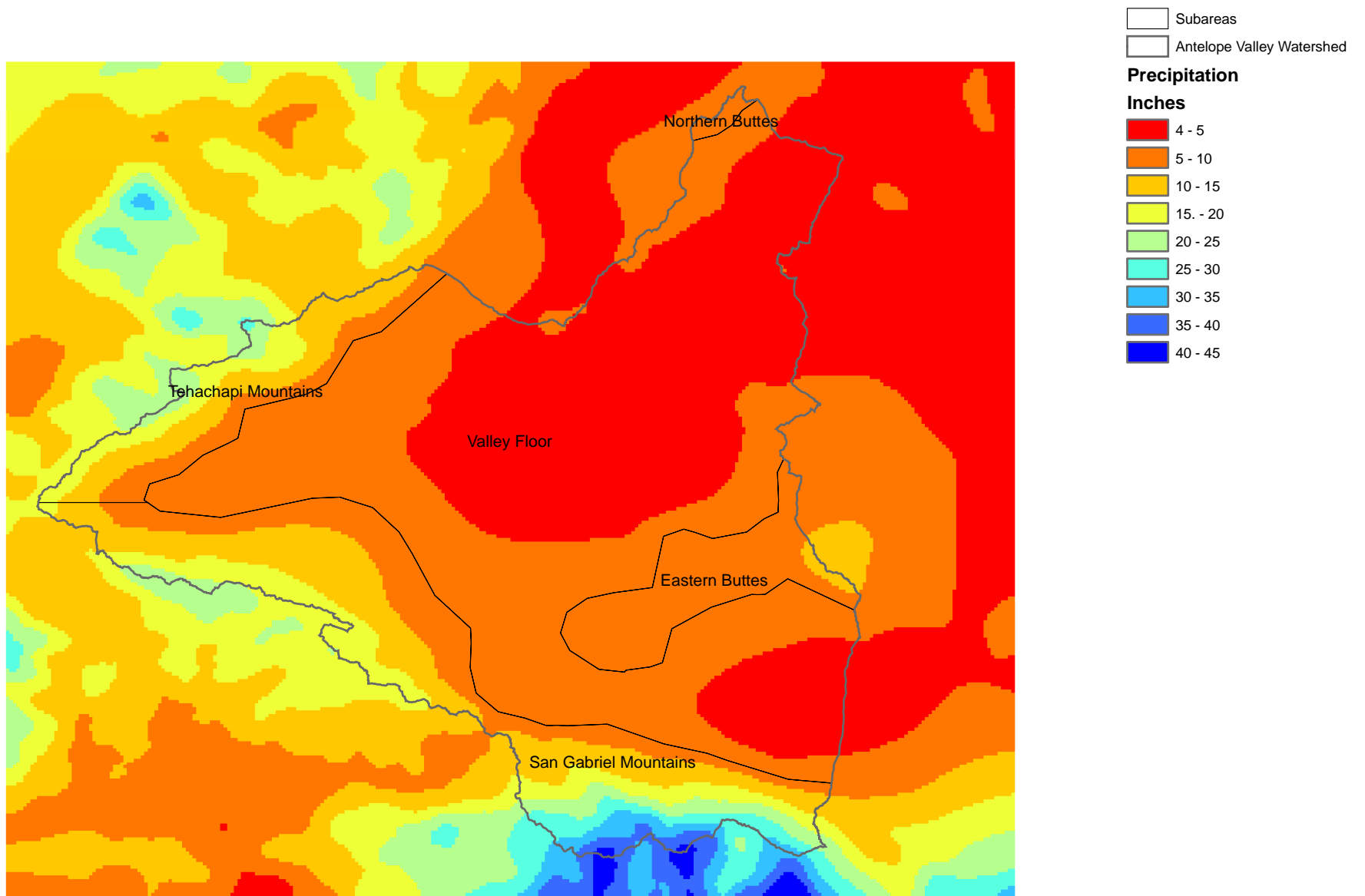
Figure C.11 Areas Where Average Annual Precipitation Exceeds 8 Inches
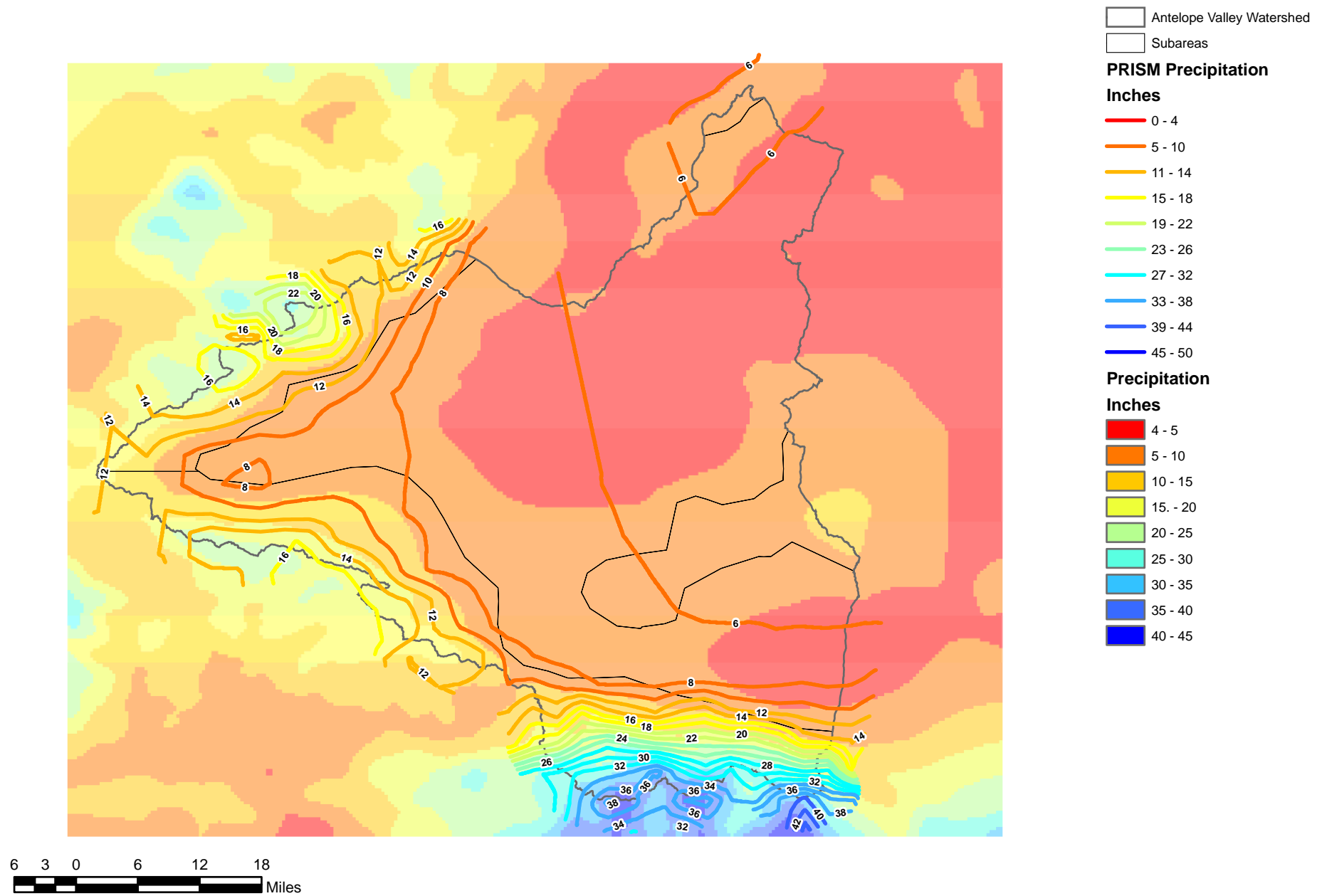
Figure C.12 Comparison of Average Annual Precipitation with PRISM
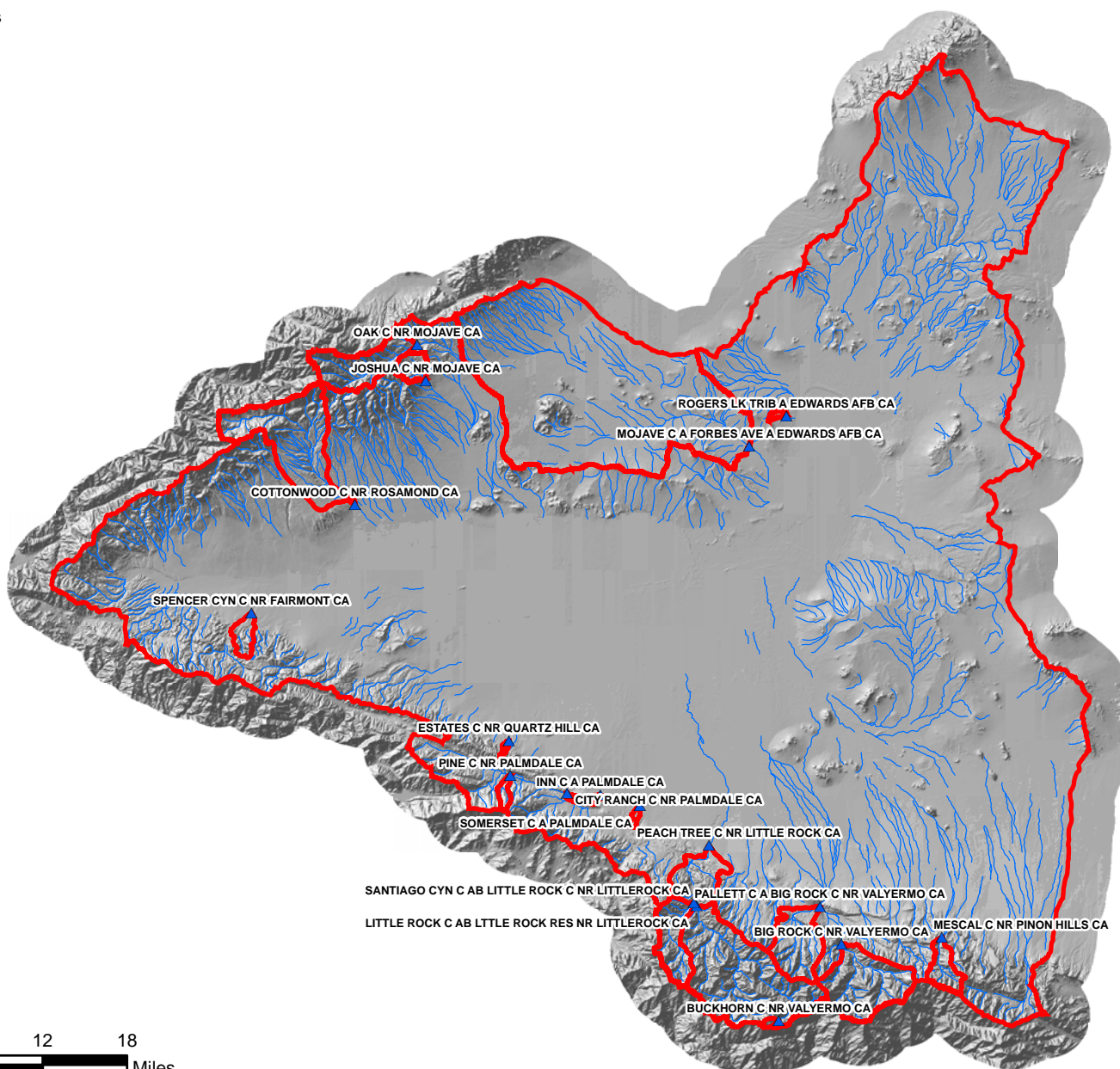
Figure C.13 Locations of Streamgaging Sites
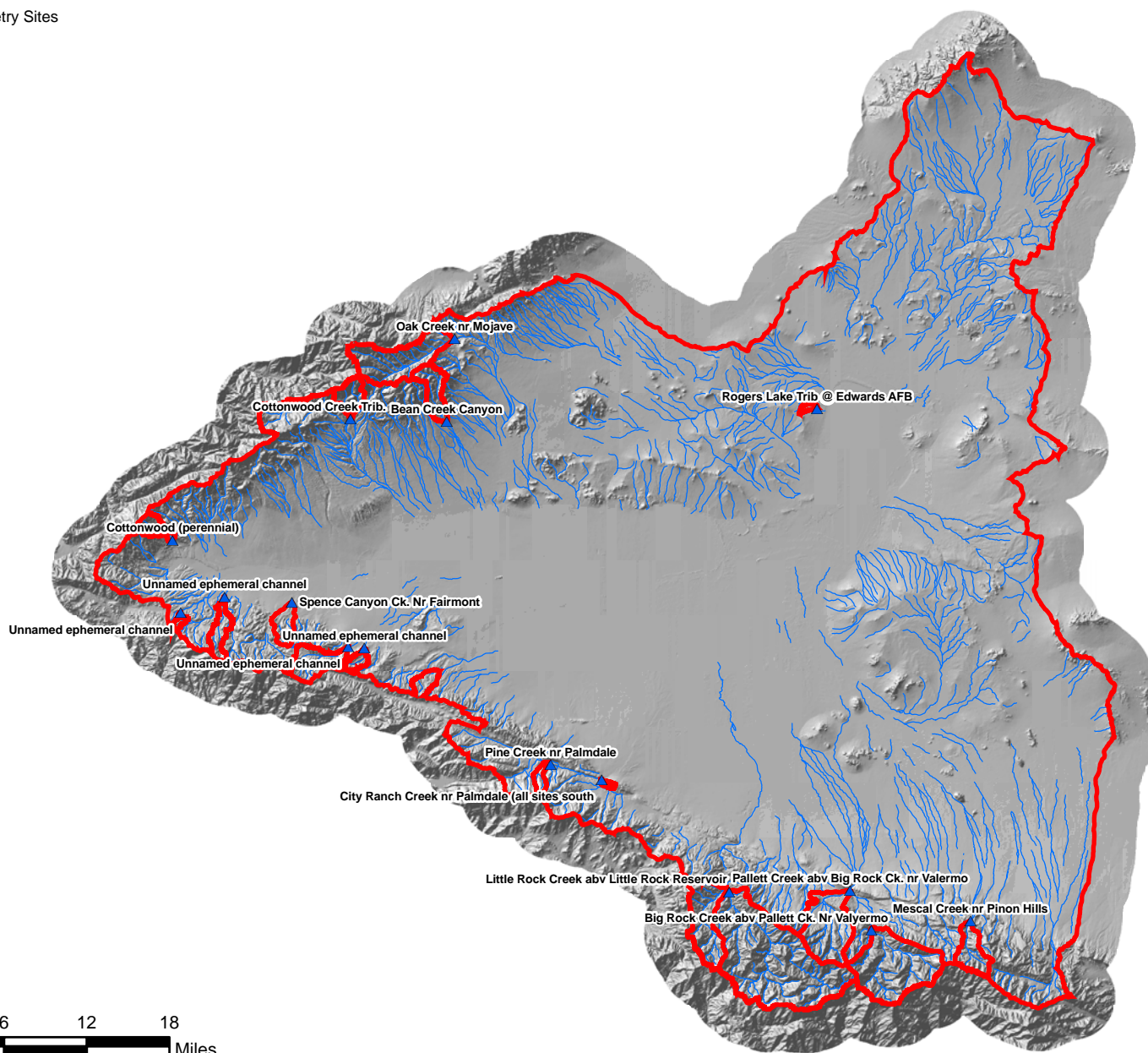
Figure C.14 Locations of Channel-Geometry Sites
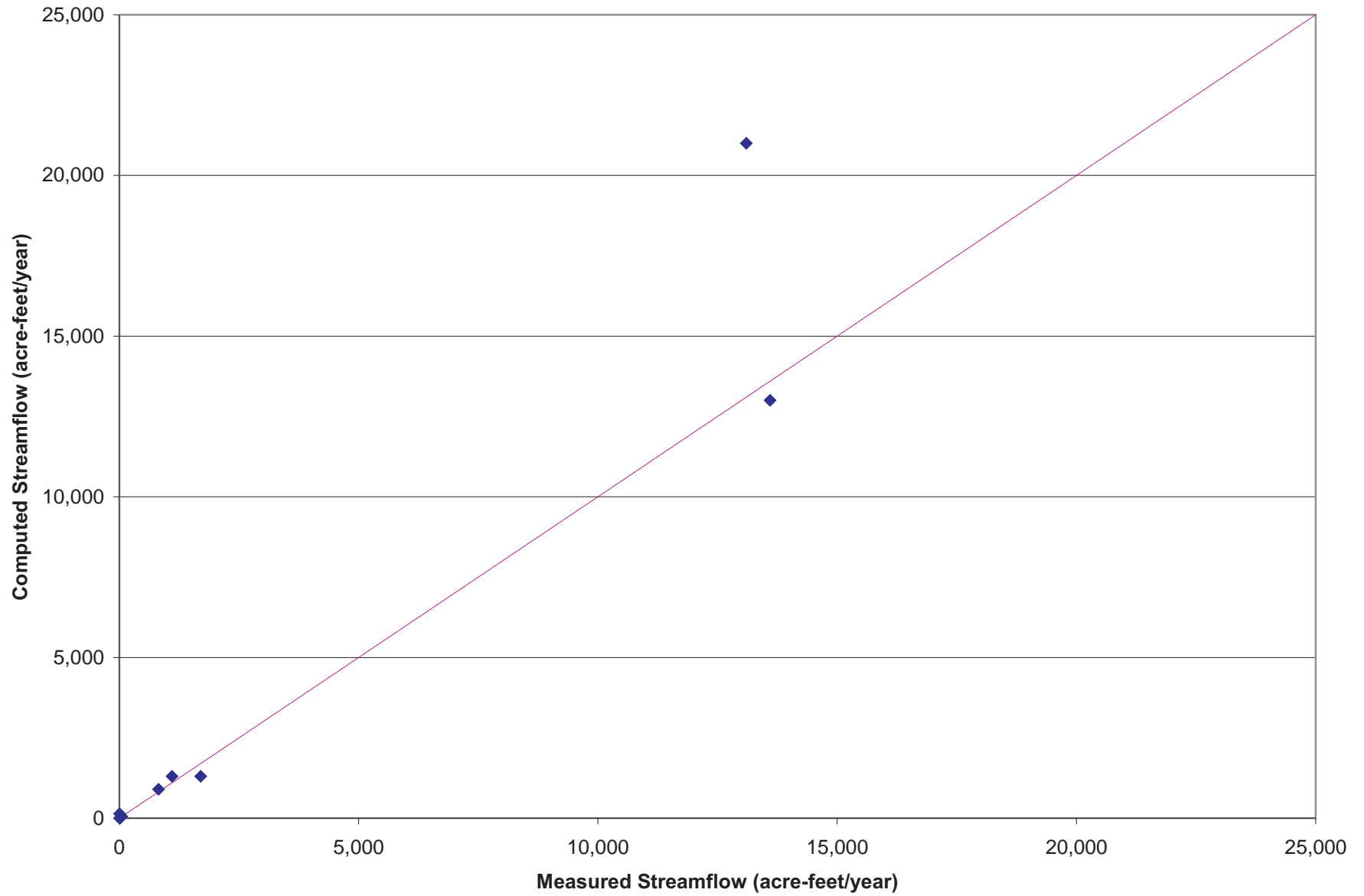
Figure C.15 Estimated and Measured Streamflow for Gaged Channel-Geometry Sites
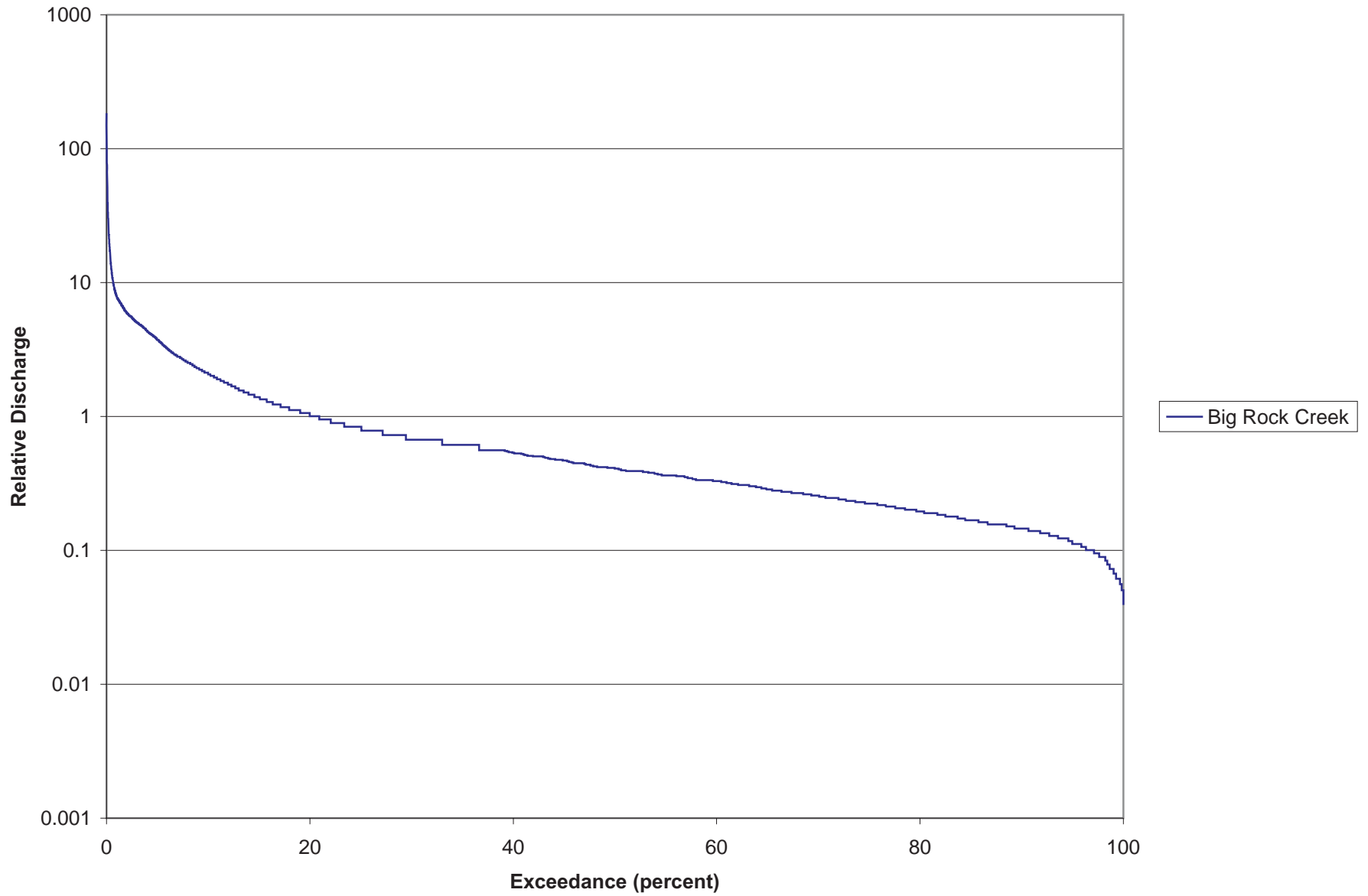
Figure C.16a Streamflow-Duration Relation for Perennial Streams
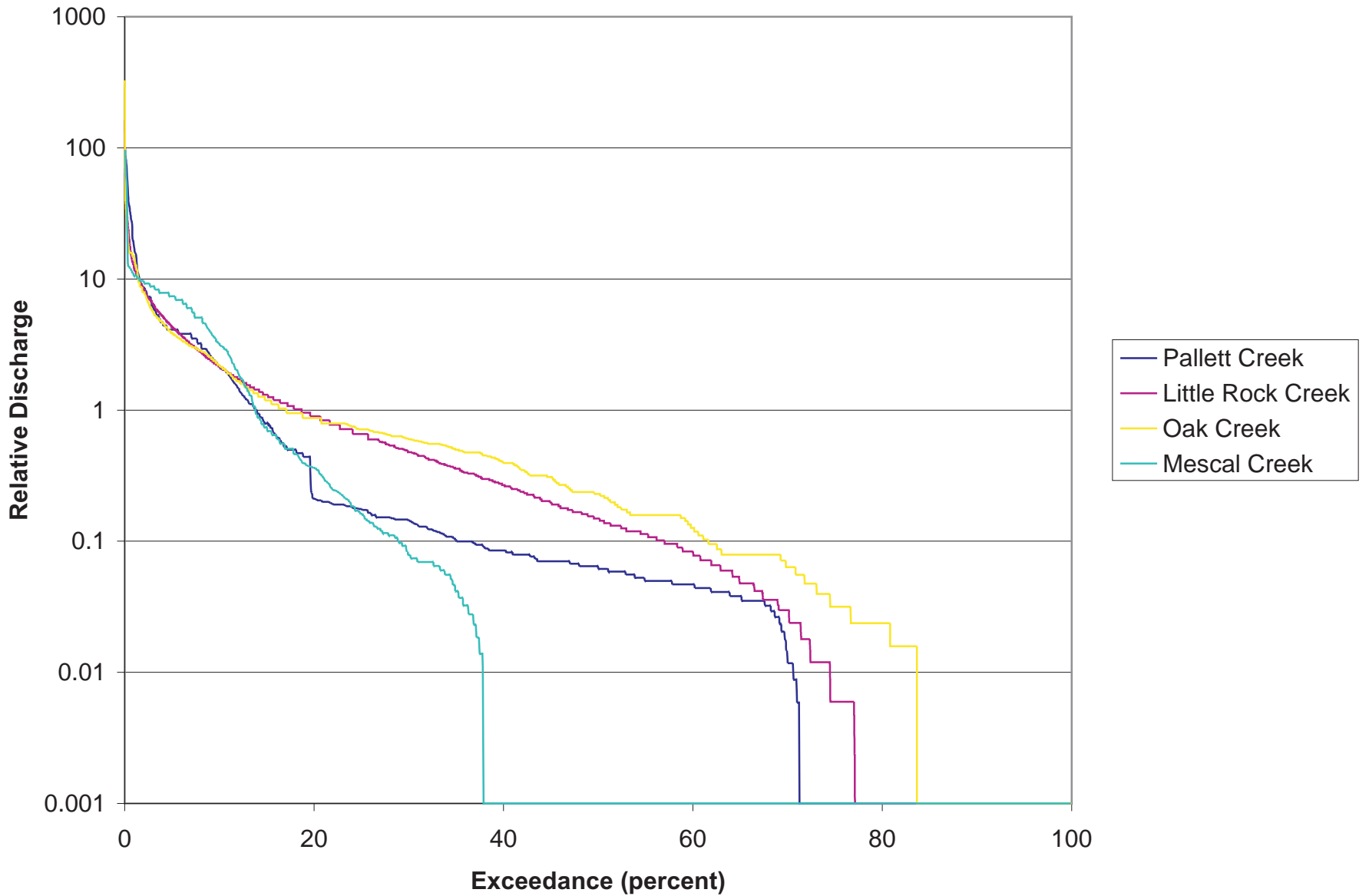
Figure C.16b Streamflow-Duration Relations for Seasonal Streams
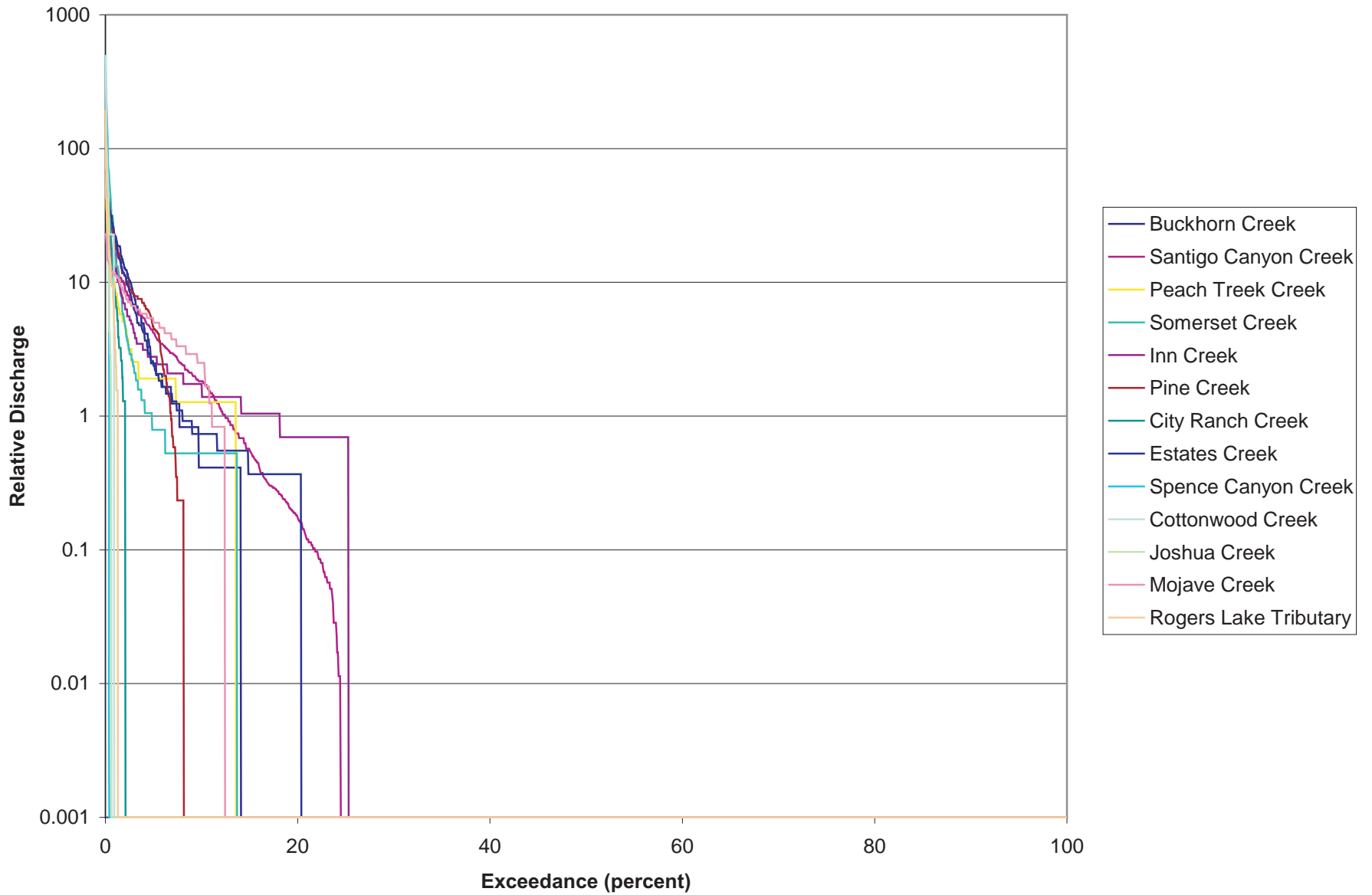
Figure C.16c Streamflow-Duration Relations for Ephemeral Streams
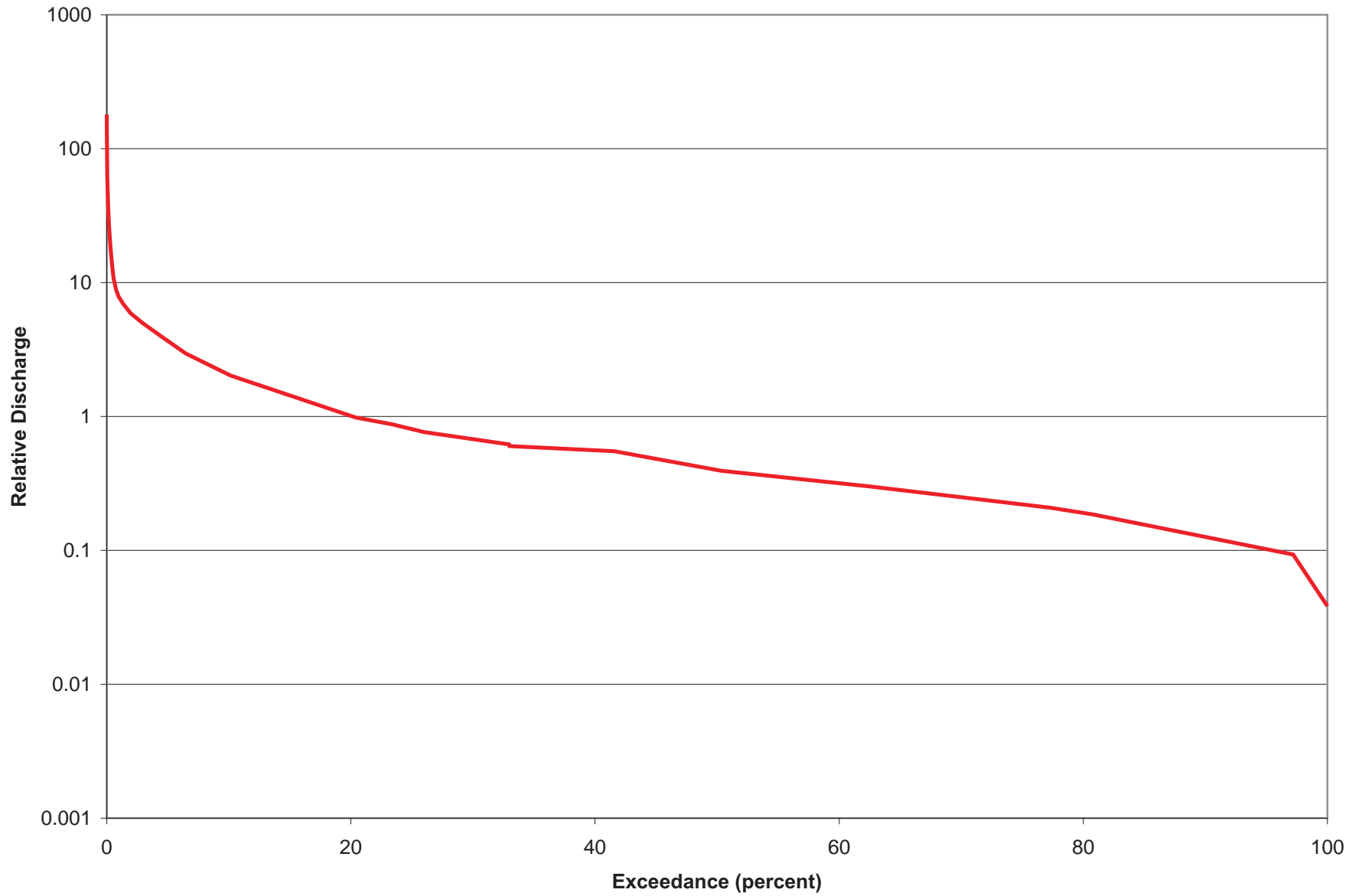
Figure C.17a Normalized Streamflow-Duration Relations for Perennial Streams
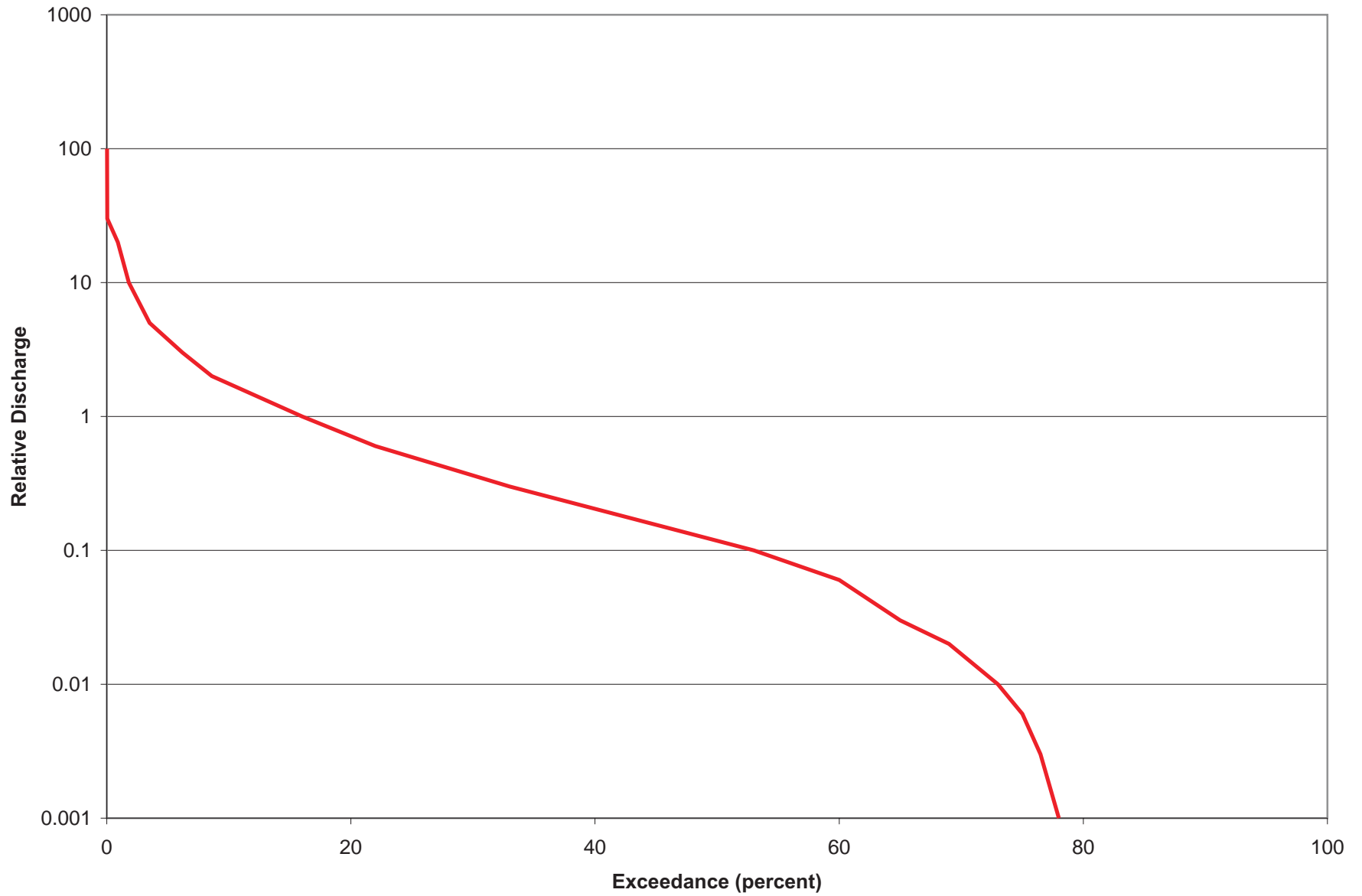
Figure C.17b Normalized Streamflow-Duration Relations for Seasonal Streams
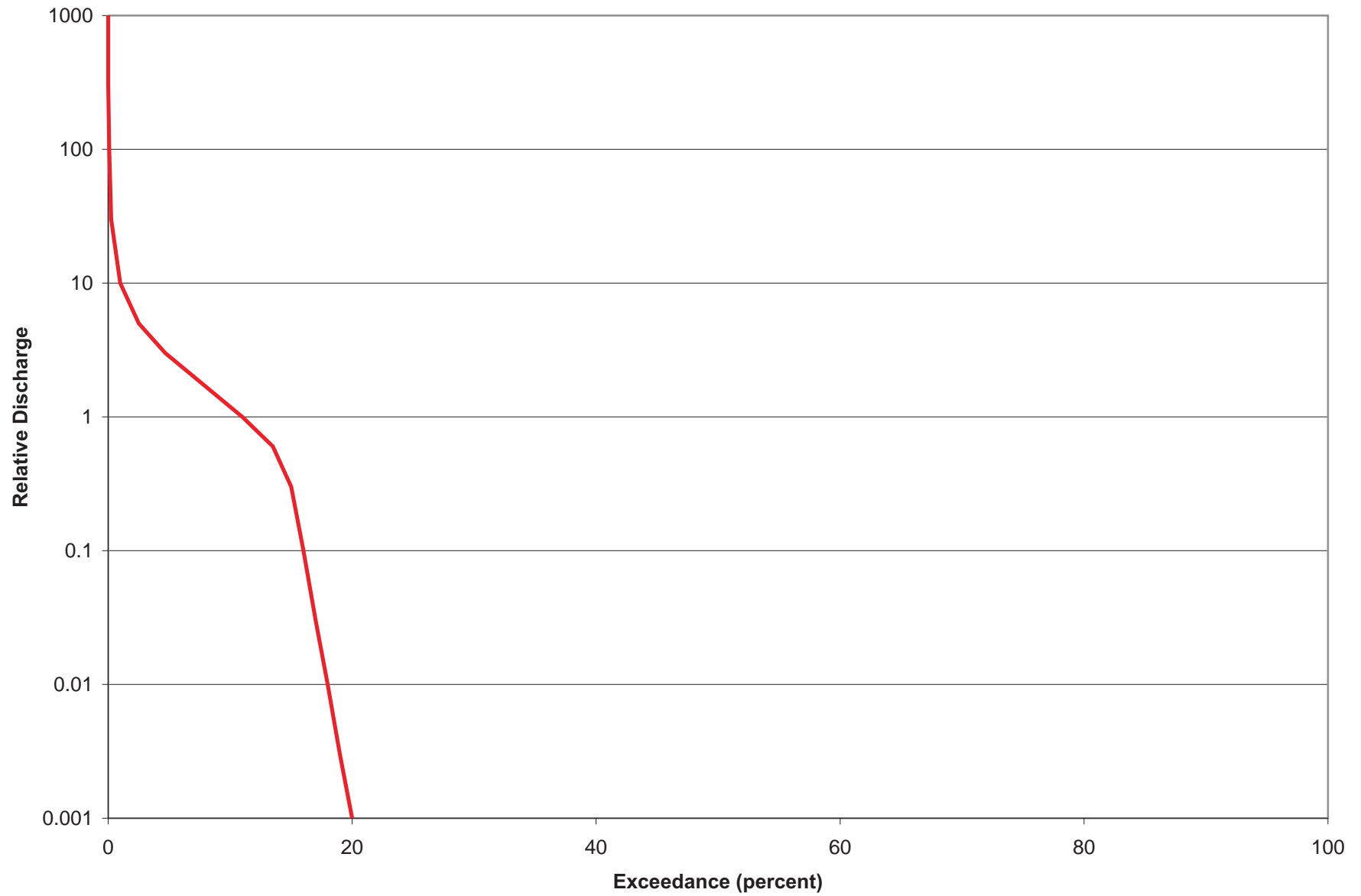
Figure C.17c Normalized Streamflow-Duration Relations for Ephemeral Streams
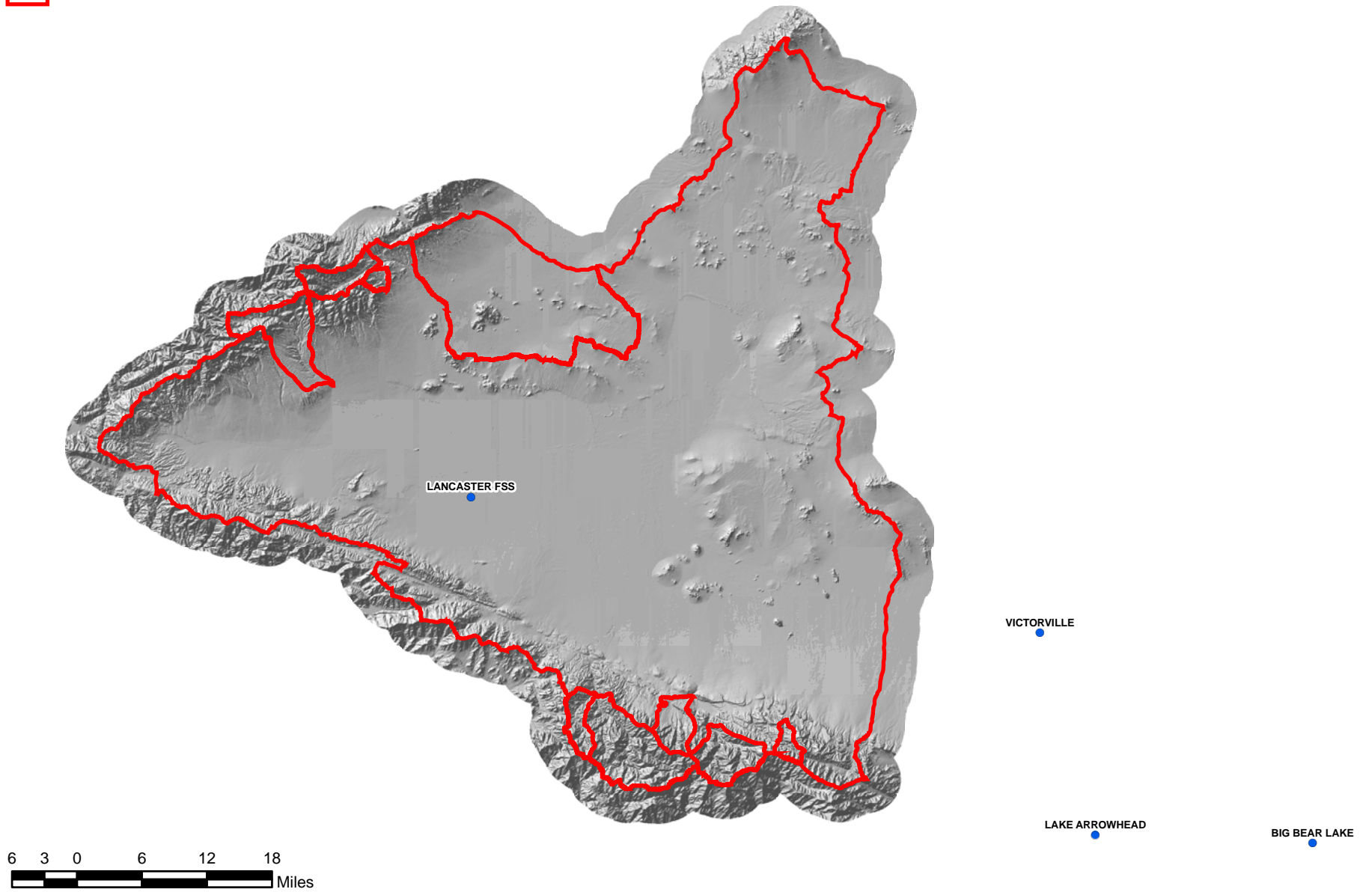
Figure C.18 Locations of CIMIS Sites
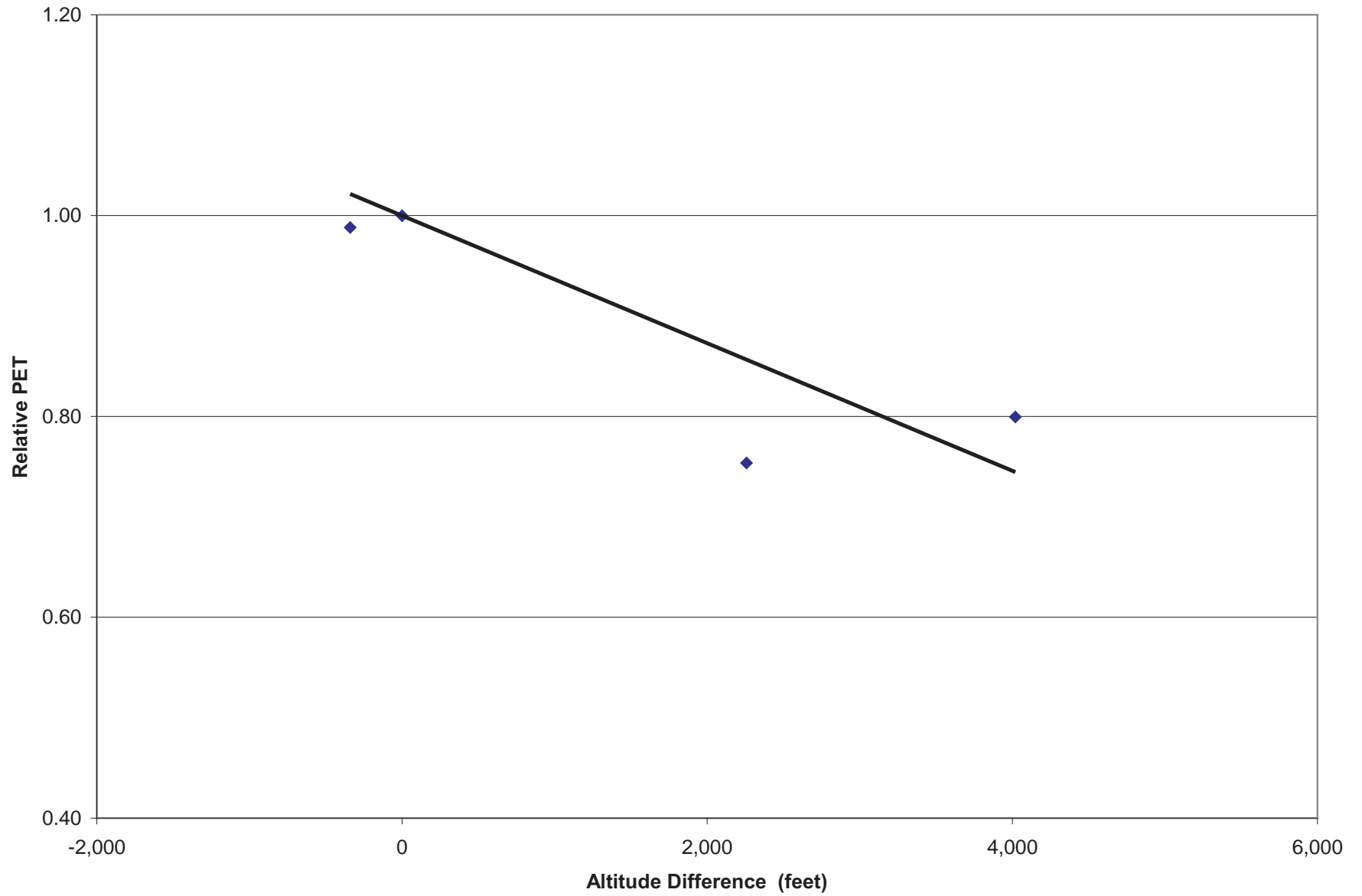
Figure C.19 PET-Altitude Relation
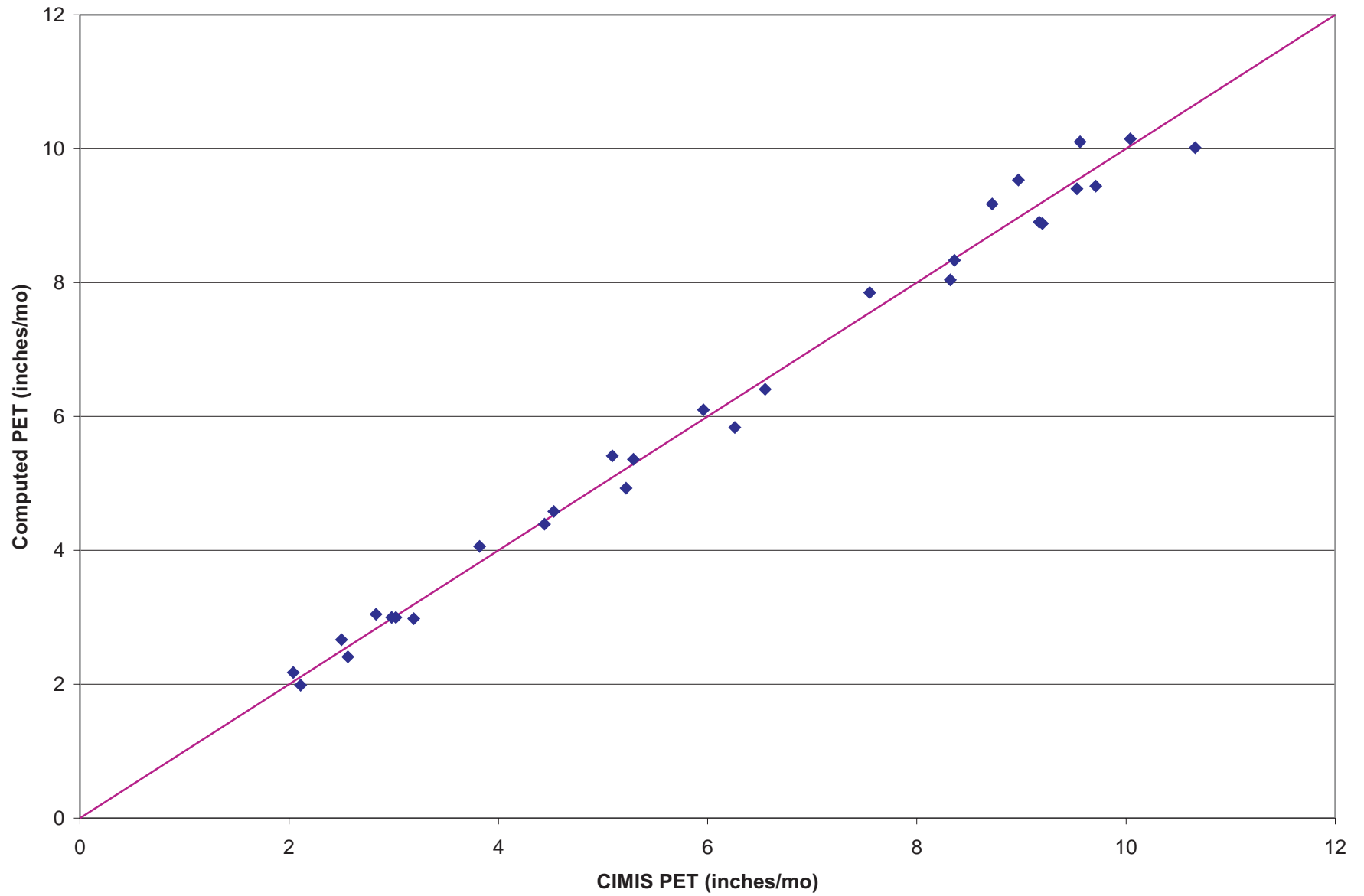
Figure C.20 Comparison of Computed and Measured PET at Palmdale
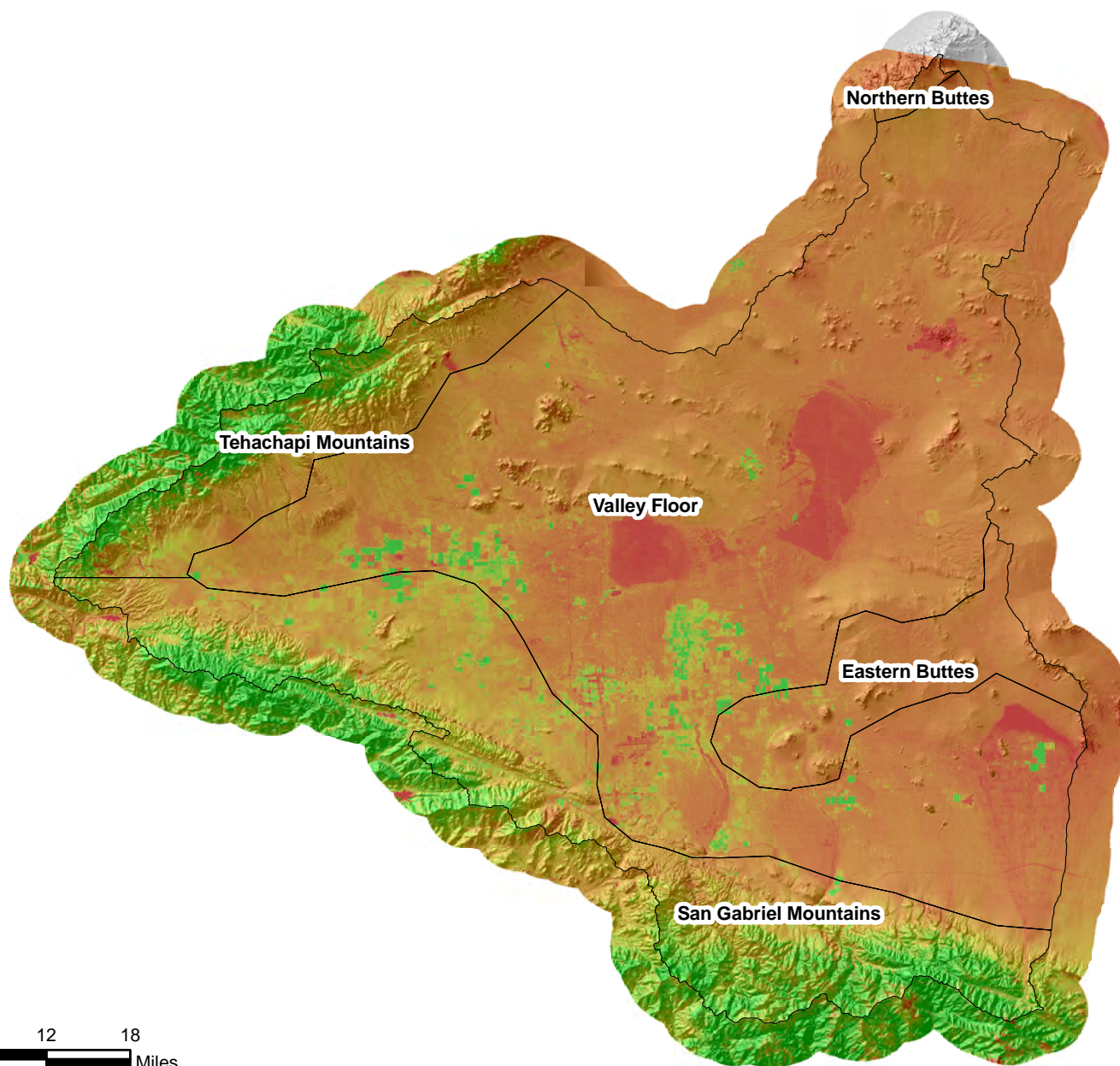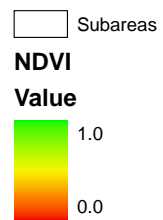
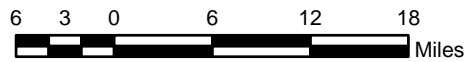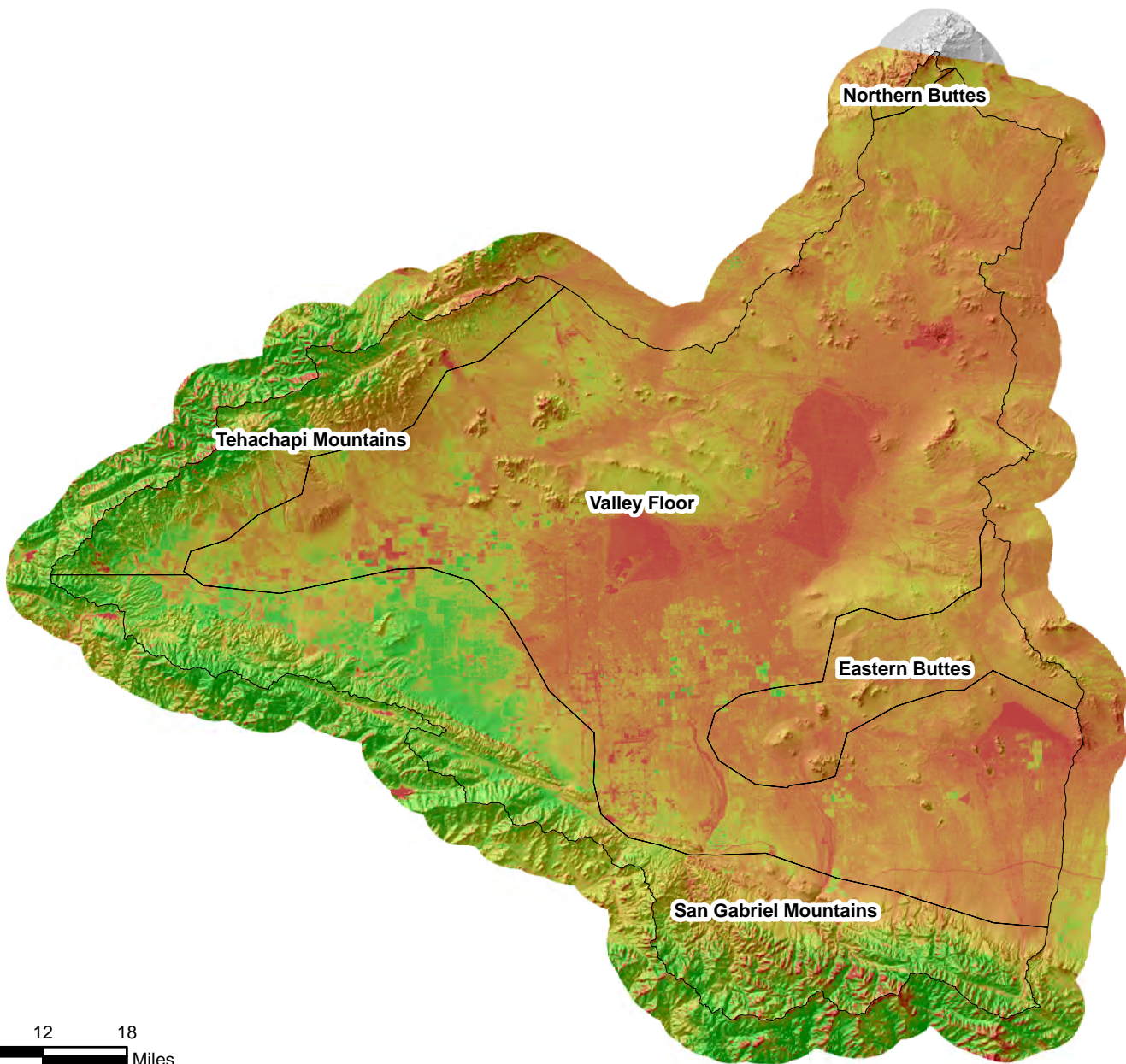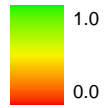**Figure C.21a Geographic Distribution of NDVI* for September 1985**

Figure C.21b Geographic Distribution of NDVI* for January 1986